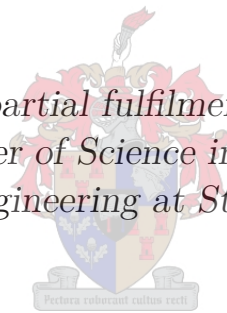


# Design of a Reluctance Synchronous Machine for an Electric Vehicle with a Multi Speed Gearbox

by

Christiaan Willem Vorster

*Thesis presented in partial fulfilment of the requirements  
for the degree of Master of Science in Electrical Engineering  
in the Faculty of Engineering at Stellenbosch University*



Department of Electrical and Electronic Engineering,  
Stellenbosch University,  
Private Bag X1, Matieland 7602, South Africa.

Supervisor: Prof M.J. Kamper

December 2014

# Declaration

By submitting this thesis electronically, I declare that the entirety of the work contained therein is my own, original work, that I am the sole author thereof (save to the extent explicitly otherwise stated), that reproduction and publication thereof by Stellenbosch University will not infringe any third party rights and that I have not previously in its entirety or in part submitted it for obtaining any qualification.

Date: .....

Copyright © 2014 Stellenbosch University  
All rights reserved.

# Abstract

## Design of a Reluctance Synchronous Machine for an Electric Vehicle with a Multi Speed Gearbox

C.W. Vorster

*Department of Electrical and Electronic Engineering,  
Stellenbosch University,  
Private Bag X1, Matieland 7602, South Africa.*

Thesis: MScEng (Elec)

December 2014

Conventional electrical vehicles (EVs) favour mostly permanent magnet machines with single speed gearboxes. This is understandable, the PM machine has a high power density making the electrical machine smaller in size. The PM machine also has a favourable field weakening capability combining this with a single speed gearbox nearly perfectly matches the required traction curve. However the dependency of rare earth metals from China and the environmental issues raised by mining these metals raise concern. Therefore alternatives should be considered. Induction -, switch reluctance - and wound rotor machines are all gaining ground as favourable traction machines to power vehicles. The reluctance synchronous machine (RSM) is known for its robustness and high efficiency, however the machine has a limited field-weakening capability. To overcome this short coming a multi gearbox from an internal combustion engine (ICE) is suggested.

By combining the RSM and multi speed gearbox it is possible to match the traction curve. There are numerous advantages offered by using this system, especially from an performance and efficiency point of view. However there are also numerous challenges faced by using the suggested powertrain, however the focus of this study is mainly on performance and efficiency of the motor and the powertrain.

As a case study a Corsa 140i is used and the design specifications is taken from the ICE. The aim is to design a RSM that meets the specifications of the ICE. The RSM structure is mathematically modelled then optimized using commercial optimization and 2D finite element software. To evaluate the

design of the RSM, the motor is then tested. The powertrain is then tested by connecting the motor onto the gearbox of the Corsa and the efficiency of the powertrain is evaluated.

The test results it shown that the RSM can be used as a traction motor. There are two motors built one with NO20 and the other with M530-65A lamination steel. Both motors perform well throughout the speed and torque spectrum. The measured efficiency at the rated condition for the motor with the NO20 steel is above 91% and the motor with the M530-65A laminations above 89%. The power train is is tested in 4<sup>th</sup> and 5<sup>th</sup> gear. The efficiency of 4<sup>th</sup> and 5<sup>th</sup> gear is approximated and the efficiency is above 90% . This high efficiency makes the multi speed gearbox a competitor for the EV power train.



# Uittreksel

## Ontwerp 'n Sinchroon Reluktansie Motor vir 'n Elektiese Voertuig met n Veranderlike Spoed Ratkas.

*(“Design of a Reluctance Synchronous Machine for an Electric Vehicle with a  
Multi Speed Gearbox”)*

C.W. Vorster

*Departement Elektriese en Elektroniese Ingenieurswese,  
Universiteit van Stellenbosch,  
Privaatsak X1, Matieland 7602, Suid Afrika.*

Tesis: MScIng (Elek)

Desember 2014

Elektriese voertuie (EVe) het meestal permanent magneet motors met 'n enkel spoed ratkas. Dit is verstaanbaar, die PMS masjien het 'n hoë krag digtheid wat die masjien kleiner maak in grote. Die PMS masjien het 'n baie goeie vloed veld verswakkings gebied en as dit gekombineer word met 'n enkel spoed ratkas, volg dit die verlangde traksie kurwe amper perfek. Die nadeel is dat die PMS motor skaars aard metale nodig het vir die magnete van China af. Die probleem is dat daar baie omgewings probleme gepaard gaan om die metale te myn en China beheer die mark. As gevolg hiervan moet ander tipe motors oorweeg word as traksie motors vir voertuie. Skakel reluktansie, induksie en 'n wikkell rotor motors is almal besig om vordering te maak as traksie motors vir EV'e. Die sinchroon reluktansie motor (RSM) is bekend as 'n robuuste en effektiewe motor. Die probleem met die RSM is dat dit nie 'n goeie vloed veld verswakkings gebied het nie. Om die probleem te oorkom, word 'n veranderlike spoed ratkas van 'n binnebrand engin voorgestel.

Deur om die RSM en die veranderlike spoed ratkas as 'n dryfstelsel te gebruik kan die verlangde traksie kurwe ook verkry word. Daar is talle voordele om 'n veranderlike spoed ratkas te gebruik, veral van af 'n draaimoment vermindering en effektiwiteits oogpunt. Daar is ongelukkig ook baie uitdagings wat gepaard gaan as 'n veranderlike spoed ratkas gebruik wil word in die dryfstelsel. Alhoewel daar baie uitdagings is kyk die studie slegs na die draaimoment

verrigting en die effektiwiteit van die dryfstelsel.

'n Corsa 140i word as 'n gevallestudie gebruik en die spesifikasies vir die elektriese motor word vanaf die spesifikasies van die binnebrand engin geneem. Die doel is om 'n motor te ontwerp wat dieselfde spesifikasies het as die binnebrand engin. Die RSM struktuur word wiskundig gemodelleer en dan geoptimeer deur gebruik te maak van kommersieel optimering en 2D eindige element sagteware. Om die ontwerp te verifieer word die motor getoets. Die dryfstelsel word dan getoets deur om die motor met die ratkas te konnekteer. Die draaimoment verrigting en die effektiwiteit word dan ge-evalueer.

Twee motors word gebou, een met NO20 laminasies en een met M530-65A laminasies. Beide motors het goeie verrigting deur die spoed en draaimoment gebied. Die gemeete effektiwiteit van die motor met die NO20 laminasies is bo 91% en die motor met die M530-65A laminasies het 'n gemeete effektiwiteit bo 89%. Die toets resultate wys dat die RSM as 'n traksie motor gebruik kan word. Die dryfstelsel word in 4<sup>de</sup> en 5<sup>de</sup> rat ge-evalueer. Die effektiwiteit van die ratkas in 4<sup>de</sup> en 5<sup>de</sup> word benader en 'n effektiwiteit bo 90% is verkry. Hierdie hoë effektiwiteit maak die veranderlike spoed ratkas 'n lewensvatbare mededinger in die EV dryfstelsel.

# Acknowledgements

I would like to express my sincere gratitude to the following people and organisations:

Professor Maarten Kamper for his help and guidance throughout the project as well as getting financial support to continue my studies and the opportunity to explore the world, what a privilege.

Mike Martin at Oceantech for his financial support for the project and his colleague Andy Meldrum who assisted in the mechanical design of the motor.

Pietro Petzer, Andre Swart and Murray Jumat with their help in the construction of the testbenches and repairs on the machines.

Wikus Villet for his help in designing a better machine and long talks regarding improvement of the sensorless control.

Albertu Prins for the collaboration with the FEM and the article for the ECCE 2013.

For the lecturers and staff at the Mechanical Engineering department at Stellenbosch University and who helped me with so many small things that put together would be a lot. Also for the opportunity to take the post graduate subjects.

Although now retired, Jakkie Blom for his knowledge, documentation and support in the mechanical design of the motor and the test benches.

David Groenewald who spent hours in fixing and programming the drive and the controller.

Eddy Howard for his superstar attitude in helping me late into night with testing, analysing and brain storming. A true champion that knows: "When the occasion demands it, the Grey boy always comes up to scratch."

Stiaan Gerber a valuable asset in the EM Lab, there is no wonder why he goes by the name "BG" or Boy-Genius. Thanks for all your help.

Daleen Kleyn who was always kind enough to help with the ordering of equipment and components.

Johannes Potgieter a great friend and colleague.

The rest of my colleagues at the EMLab for their help, support and laughter when we needed it.

Heinzmann GmbH & Co. KG for giving me an opportunity to use the skills and knowledge I have attained through my studies to prepare myself for the working environment.

My friends who encouraged me through tough times.

My Father, Mother and family who always supported me and encouraged me to finish what I started.

God the Father, who gave not only the strength but also the ability, will and character to see this through. Amen.

# Dedications

*Hierdie tesis word opgedra aan my ouers wat soveel van hulle self gegee het sodat ek myself kan kwalifiseer en my talente kon uitleef op meer as een gebied. Hulle is die ware helde.*

*This thesis is dedicated to my parents who gave so much of themselves so that I could have the opportunity to qualify and develop myself and therefore live out my talents on all spheres of life. They are the true champions.*

*The Man in the Arena: "It is not the critic who counts; not the man who points out how the strong man stumbles, or where the doer of deeds could have done them better. The credit belongs to the man who is actually in the arena, whose face is marred by dust and sweat and blood; who strives valiantly; who errs, who comes short again and again, because there is no effort without error and shortcoming; but who does actually strive to do the deeds; who knows great enthusiasms, the great devotions; who spends himself in a worthy cause; who at the best knows in the end the triumph of high achievement, and who at the worst, if he fails, at least fails while daring greatly, so that his place shall never be with those cold and timid souls who neither know victory nor defeat." Theodore Roosevelt (former President of the United States)*

# Contents

Declaration	i
Abstract	ii
Uittreksel	iv
Acknowledgements	vi
Dedications	viii
Contents	x
List of Figures	xiii
List of Tables	xv
Nomenclature	xvi
<b>1 Introduction</b>	<b>1</b>
1.1 Components of Electrical Vehicles . . . . .	1
1.2 Electrical Vehicle Powertrain . . . . .	2
1.3 The ICE vs. the Electric Motor as a Prime Mover . . . . .	4
1.4 Multi Speed Gearbox for Electrical Vehicles . . . . .	6
1.5 Single vs. Multi speed transmissions for Electrical vehicles . .	7
1.6 Problem Statement . . . . .	7
1.7 Approach to the problem . . . . .	8
1.8 Thesis Layout . . . . .	9
<b>2 Determination the design specifications</b>	<b>10</b>
2.1 Initial design specification . . . . .	10
2.2 Specifications from vehicle modelling . . . . .	11
2.3 Further comparison of single speed versus multi speed gearboxes for Electrical Vehicles . . . . .	12
2.4 Traction motor selection . . . . .	14
2.5 Design specifications for the Motor . . . . .	15

<i>CONTENTS</i>	<b>xi</b>
2.6 Summary . . . . .	16
<b>3 Performance calculations for the RSM</b>	<b>18</b>
3.1 Torque and torque ripple . . . . .	18
3.2 Power factor . . . . .	19
3.3 Windage and friction loss . . . . .	19
3.4 Copper loss . . . . .	20
3.5 Ironloss . . . . .	20
3.6 Calculating efficiency . . . . .	25
3.7 Summary . . . . .	26
<b>4 Optimization of the RSM</b>	<b>28</b>
4.1 Optimization formulation . . . . .	28
4.2 Optimization procedure . . . . .	31
4.3 Optimization Results . . . . .	32
4.4 Summary . . . . .	33
<b>5 Modifications to the optimised Rotor and the performance results of the RSM</b>	<b>35</b>
5.1 Modifications to the optimised RSM . . . . .	35
5.2 Mechanical Design of the Rotor . . . . .	36
5.3 Calculated performance results . . . . .	38
5.4 Summary . . . . .	40
<b>6 Constructed RSM and test benches for an EV</b>	<b>44</b>
6.1 Built motor . . . . .	44
6.2 Test Bench 1 . . . . .	45
6.3 Test Bench 2 . . . . .	45
<b>7 Measured results of the motors</b>	<b>50</b>
7.1 Measured weight . . . . .	50
7.2 Measured resistance . . . . .	50
7.3 Motor measurements . . . . .	51
7.4 Summary . . . . .	55
<b>8 Powertrain measured results</b>	<b>58</b>
8.1 Measured powertrain and approximated gearbox efficiency results	58
8.2 Summary . . . . .	60
<b>9 Conclusions and recommendations</b>	<b>66</b>
9.1 Conclusions . . . . .	66
9.2 Recommendations . . . . .	67
<b>Appendices</b>	<b>69</b>



<i>CONTENTS</i>	<b>xii</b>
<b>A Specifications and performance tests of the Corsa 140i.</b>	<b>70</b>
<b>B Vehicle modelling</b>	<b>77</b>
B.1 Vehicle modelling . . . . .	77
<b>C Mechanical Design for RSM with water cooled jacket.</b>	<b>80</b>
<b>Bibliography</b>	<b>93</b>

# List of Figures

1.1	Important components in an EV. . . . .	2
1.2	An example of the different torque and power outputs for an ICE (left) and an electrical motor (right). . . . .	4
1.3	Traction curve for the Corsa 140i. . . . .	5
1.4	An example of different powertrain layouts for front wheel driven electrical vehicles. . . . .	6
2.1	Traction curve of the Corsa. . . . .	11
2.2	Traction curve of the RSM for the Corsa at 70Nm. . . . .	12
2.3	Traction curve and power available at different speeds in the different gears. . . . .	14
2.4	Torque available at different speeds with different gearboxes. . . . .	15
3.1	Comparison of the ironloss determined from eq. 3.5.4 with different parameters. . . . .	23
3.2	Same as Fig. 3.1, except that it shows the large ironloss difference by using the parameters from [1]. . . . .	25
3.3	The 9.2 kW RSM used by [1]. The figure on the right shows the flux densities in the RSM when operated. . . . .	26
3.4	A schematic of how the performance calculations are done. . . . .	27
4.1	The rotor and stator of the RSM with the design variables shown. . . . .	30
4.2	The communication between the VisualDoc and JMAG is achieved via Python. . . . .	31
4.3	The optimised 35 kW RSM. . . . .	32
5.1	The different rotor structures. . . . .	36
5.2	Force diagram to calculate the forces on the rotor. . . . .	37
5.3	The displacement(exaggerated) and stresses in the rotor with the webs due to the centrifugal force. . . . .	38
5.4	The maximum stresses in the webs and the ribs. . . . .	39
5.5	The displacement(exaggerated) and stresses in the without the webs rotor due to the centrifugal force. . . . .	39
5.6	The maximum stresses in the rotor without the ribs. . . . .	40
5.7	Simulated efficiency map of the motor with NO20 stator laminations. . . . .	42

5.8	Simulated efficiency map of the motor with M530 stator laminations.	43
6.1	Photo of the RSM. The shaft has splines cut into it to fit into splines of the gearbox. . . . .	44
6.2	The power train connection of the RSM to the gearbox and differential. . . . .	45
6.3	Schematic layout of the test bench to measure the performance of the RS motor. . . . .	46
6.4	Layout of the testbench to measure the performance of the RS motor.	47
6.5	Schematic layout of the testbench to measure the performance of the drive train. . . . .	48
6.6	Layout of the testbench to measure the performance of the drive train. . . . .	48
6.7	Schematic layout of the measuring equipment of the testbench to measure the performance of the drive train. . . . .	49
6.8	Layout of the measuring equipment of the testbench to measure the performance of the drive train. . . . .	49
7.1	Contour efficiency map for motor with NO20 stator for torque versus speed. . . . .	53
7.2	Efficiency approximation error for motor with NO20 stator. . . . .	54
7.3	Contour efficiency map for the motor with the M530 stator laminations for torque versus speed. . . . .	55
7.4	Efficiency approximation error for the motor with the M530-65A stator laminations. . . . .	56
8.1	Contour efficiency map for system in 5th gear for torque over speed.	60
8.2	Error in the approximation for the system in 5th gear. . . . .	61
8.3	Contour efficiency map for the gearbox in 5th gear. . . . .	62
8.4	Contour efficiency map for system in 4th gear for torque over speed.	63
8.5	Error in the approximation for the system in 4th gear. . . . .	64
8.6	Contour efficiency map for the gearbox in 4th gear. . . . .	65
A.1	Engine speed vs. Torque and Power. . . . .	74
A.2	Engine speed vs. vehicle speed . . . . .	75
A.3	Acceleration of the vehicle vs time. . . . .	76
B.1	Forces acting on a vehicle. . . . .	78

# List of Tables

1.1	Details on different electrical vehicles in production. (SS- single speed gearbox, RWD, FWD - Rear/ Front wheel drive) . . . . .	3
2.1	Specification of the RSM . . . . .	16
3.1	Different values for the parameters to be used in eq. 3.5.4 from [1], substitution and MSE. . . . .	22
3.2	Mass and flux values obtained to calculate the iron losses. . . . .	24
3.3	Values obtained to from different loss calculation methods by simulating the RSM from [1]. . . . .	24
4.1	Design constants of the RSM traction motor. . . . .	29
4.2	Design variables of the RSM traction motor. . . . .	30
4.3	Optimum variables and performance values from the optimisation procedure. . . . .	34
5.1	Different results from chording and skewing the machine. . . . .	40
5.2	Simulation Results for the different motors at operating point S1. . . . .	41
7.1	Measured weight of the motor and the components. . . . .	50
7.2	Measured resistance of the different stators. . . . .	51
7.3	Measured results of the NO20 stator at the designed and specified point. . . . .	52
7.4	Equation parameters for eq. 7.3.1 . . . . .	52
7.5	Measured results of the M530 stator at the designed and specified point. . . . .	54
7.6	Equation parameters for eq. 7.3.2 . . . . .	54
8.1	Equation parameters for eq. 8.1.1 . . . . .	59
8.2	Equation parameters for eq. 8.1.3 . . . . .	60
A.1	Specifications of the Opel Corsa 140i 3-dr. . . . .	70
A.2	Test results for the Opel Corsa 140i 3-dr. . . . .	72

# Nomenclature

## Abbreviation

BMS	Battery Management System
CPSR	Constant Power Speed Range
EMC	Electromagnetic Compatibility
EV	Electrical Vehicle
EU	European Union
FE	Finite Element
FWD	Front Wheel Drive
HEV	Hybrid Electrical Vehicle
ICE	Internal Combustion Engine
IEC	International Electrotechnical Commission
MSE	Mean Square Error
MMFD	Modified Method of Feasible Direction
PC	Personal Computer
PM	Permanent Magnet
PMS	Permanent Magnet Synchronous
RAM	Random Access Memory
RWD	Rear Wheel Drive
RSM	Reluctance Synchronous Machine
SS	Single Speed
SQP	Sequential Quadratic Programming
TM	Traction Motor

## Constants

$$g = 9.81 \text{ m/s}^2$$

## Variables

$Re_D$	Reynolds number (diameter) . . . . .	[ ]
$Re_{air_g}$	Reynolds number (Airgap) . . . . .	[ ]

$x$	Coordinate . . . . .	[m]
$\ddot{x}$	Acceleration . . . . .	[m/s <sup>2</sup> ]
$\alpha_x$	Flux path rotor angle . . . . .	[°]
$air_g$	Airgap . . . . .	[mm]
$A$	Area . . . . .	[m <sup>2</sup> ]
$B_t$	Peak flux density in the stator teeth . . . . .	[T]
$B_{yk}$	Peak flux density in the stator yoke . . . . .	[T]
$\hat{B}$	Peak induction . . . . .	[T]
$C_f$	Coefficient of friction . . . . .	[ ]
$c_x$	Rotor center point . . . . .	[mm]
$D_r$	Rotor Outer Diameter . . . . .	[mm]
$\delta$	Current Angle . . . . .	[ <sup>circ</sup> ]
$f$	Frequency . . . . .	[Hz]
$fp_x$	Flux path width . . . . .	[mm]
$F_x$	Force . . . . .	[N]
$l$	Stack length . . . . .	[mm]
$l_e$	End winding length . . . . .	[mm]
$l_r$	Rotor length . . . . .	[mm]
$M_t$	Mass of the stator teeth . . . . .	[kg]
$M_{yk}$	Mass of the stator yoke . . . . .	[kg]
$M$	Frictional Moment . . . . .	[N·mm]
$m$	Mass . . . . .	[kg]
$n$	Rotational Speed . . . . .	[rev/min]
$n_s$	Number of position steps . . . . .	[rev/min]
$\eta$	Efficiency . . . . .	[%]
$P_{Bearing}$	Bearing losses . . . . .	[W]
$P_c$	Iron losses . . . . .	[W]
$P_{cu}$	Copper losses . . . . .	[W]
$P_{in}$	Input Power . . . . .	[W]
$P_{out}$	Output Power . . . . .	[W]
$P_v$	Time-average ironloss per unit volume . . . . .	[W/m <sup>3</sup> ]
$\rho$	Density . . . . .	[kg/m <sup>3</sup> ]
$\rho_t$	Resistivity of copper . . . . .	[Ω·m]
$\omega$	Rotational Speed . . . . .	[rad/s]
$r$	Radius . . . . .	[mm]
$R_s$	Resistance of a phase . . . . .	[Ω]

$r_{oid}$	Rotor inner diameter . . . . .	[mm]
$st_{id}$	Stator inner diameter . . . . .	[mm]
$st_{od}$	Stator outer diameter . . . . .	[mm]
$\sigma_Y$	Yield strength . . . . .	[MPa]
$\sigma_T$	Tensile strength . . . . .	[MPa]
$t_{lam}$	Lamination thickness . . . . .	[mm <sup>2</sup> ]
$t_{wid}$	Stator tooth width . . . . .	[mm]
$\theta$	Rotation angle . . . . .	[rad]
$T$	Torque . . . . .	[N·m]
$T_{ripple}$	Torque ripple . . . . .	[%]
$u$	Constant coefficient of Friction . . . . .	[ ]
$\mu$	Dynamic Viscosity . . . . .	[kg/m·s]
$W$	Number of turns in serie per phase . . . . .	[kg]
$Y_t$	Temperature constant . . . . .	[1/°C]
$yoke$	Stator yoke height . . . . .	[mm]

**Vectors and Tensors**

- U** Design constants vector, see equation 4.1.1
- X** Design variables vector, see equation 4.1.2
- F(X)** Cost Function, see equation 4.1.3

# Chapter 1

## Introduction

Electric vehicles (EVs) have gained a lot attention in recent years. Probably due to years of research and development, environmental issues, consumer demand and availability of vehicles to the public or the benefits offered by electrical vehicles. The technology is continuously improving and the search for a solution that would suit the manufacturer, the costumer and the environment is ongoing. In this Chapter the current electrical vehicle technologies are briefly explored. The torque delivered by the internal combustion engine (ICE) and the traction motor (TM) is compared and the difference discussed.

### 1.1 Components of Electrical Vehicles

Any vehicle can be seen as a moving energy converter or a power plant. The energy stored in the battery pack of an EV has to be converted to movement for the vehicle to move, converting electrochemical energy into kinetic energy. For this EVs require a wide variety of components. A selection of the most important ones can be seen in Fig. 1.1. The batteries are the main source of power. The inverter is used to convert the DC current to three-phase AC current. The supply of current to the inverter is controlled by a battery management system (BMS). The three-phase current is then used to power the traction motor. This power is then transmitted through a gearbox<sup>1</sup> to the wheels. The position sensor is required to determine the position of the rotor which is essential in the control and commutation of the traction motor. It is also possible to control the motor without a sensor. The overall performance of the the EV is depended on how well all these components function together. Therefore the design process should have clear baselines for each part to be optimised that the set criteria can be met. This would make the individual design of the components easier and when the components are put together they

---

<sup>1</sup>The meaning from the Oxford Dictionary of *gearbox* is given as "*A set of gears within a it's casing in a motor vehicle; the transmission*". The meaning of *transmission* is given as "*The mechanism by which power is transmitted from a engine to the axle in a motor vehicle*".



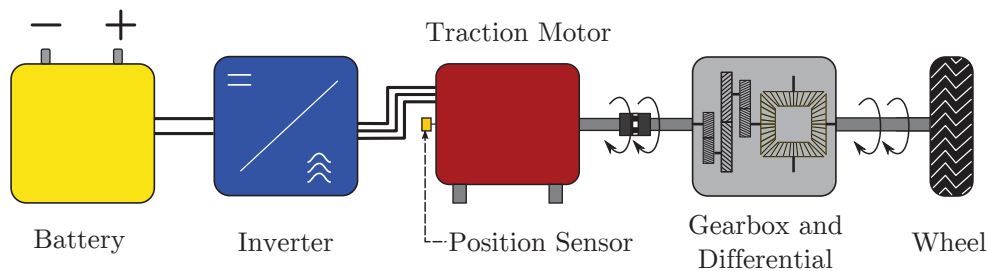


Figure 1.1: Important components in an EV.

should perform, hopefully with high efficiency and performance. The gearbox is not always necessary, it depends on the selected powertrain<sup>2</sup> configuration.

## 1.2 Electrical Vehicle Powertrain

The selection of the powertrain depends on the application the vehicle will be used for. Different powertrains offer advantages and disadvantages and the correct powertrain must be selected to meet the specific requirements for the application of use. There are two common powertrains for EVs, directly driven and geared powertrains. In directly driven vehicles the motor is directly connected to the wheel. It has the advantage that there is no gearbox and therefore the efficiency of the powertrain is only a function of the electric motor and the inverter, if all of the other losses are assumed to be negligible. The disadvantage is that there has to be at least two motors (inverters, positions sensors, etc.) in the vehicle. Typical geared powertrain EVs have the advantage that only one motor (inverter, positions sensor, etc.) can be used, however there are exceptions. The torque required by the traction motor in the gear powertrain is less than the direct drive. The disadvantages of the extra gearbox are noise, lower efficiency, extra weight and a possible decrease in reliability. There has been a wide variety of concept EVs which is either directly driven or with gearboxes. A good indicator which technology is currently preferred for sedan vehicles, is to look at which powertrain vehicle manufacturers are producing their vehicles with. Details of EVs that are currently in production, is shown in Table 1.1. Firstly, it is evident from Table 1.1 that all these vehicles have single-speed gearboxes. Secondly, most vehicles are driven by PM synchronous motors, with the exception of the Tesla model S with its induction motor and the Renault with its wound rotor synchronous motor. It seems Tesla opted to use the induction machine due to

<sup>2</sup>The meaning of *powertrain* is explained by the Oxford Dictionary as "*The mechanism that transmits the drive from the engine of a vehicle to it's axle*". The meaning of *drivetrain*, also from the Oxford Dictionary, is given as "*The system in a motor vehicle which connects the transmission to the drive axles*".

Table 1.1: Details on different electrical vehicles in production. (SS- single speed gearbox, RWD, FWD - Rear/ Front wheel drive)

Vehicle	Battery	Motor type	Motor Torque	Motor Power	Gearbox Type	Drive
Tesla Model S 60 kW Standard [3]	60 kWh	Induction	430 Nm	225 kW	SS	RWD
Tesla Model S 85 kW Standard [3]	85 kWh	Induction	440 Nm	270 kW	SS	RWD
Tesla Model S 85 kW Performance [3]	85 kWh	Induction	600 Nm	310 kW	SS	RWD
Chevy Spark EV [4]	21.3 kWh	PMS	540Nm	104 kW	SS	FWD
Nissan Leaf [5]	24 kWh	PMS	280 Nm	80 kW	SS	FWD
BMW i3 [6] [7]	18.8 kWh	PMS	250 Nm	125 kW	SS	RWD
VW e-up [8] [9]	18.7 kWh	PMS	210 Nm	82 kW	SS	FWD
Renault ZOE [10] [11]	22 kWh	Synchronous Wound-Rotor	220 Nm	63 kW	SS	FWD

cost, field weakening capabilities, inverter safety and manufacturing difficulties that can be associated with strong magnets. The possibility of controlling the magnetic flux density with a smart inverter and therefore minimising losses at lower loads, is also mentioned [2].

The torque given in the table is the traction motor torque and has to be multiplied with the gear ratio to get the wheel torque. Therefore as an example, the standard Tesla S model, with 60 kWh and 430 Nm, has a reduction gearbox with a gear ratio of 9.73:1. The torque delivered at the wheels are then 4184 Nm. To achieve this with a directly driven vehicle would be difficult and costly. If there was four motors, each motor will have to be able to deliver approximately a rated torque of 1050 Nm. Although not a sedan, Lappeenranta University of Technology (LUT) and Helsinki Metropolia University of Applied Sciences in Finland, designed and build 4 PMS motors for a 4x4 in-hub sports car[12]. The simulated nominal torque of a motor is 204 Nm at 1000 r/min and the peak torque is 751 Nm. The total peak torque at the wheels are  $\approx 3000$  Nm, which is still less than that of the standard Tesla Model S. The maximum measured efficiency of a PMS motor was 96%. If the four motors are connected to drives with an efficiency with 96% the total system will then be  $\approx 92\%$ , when neglecting all other losses in the system. Tesla reported an overall efficiency of 88% for the Roadster [13], which is also a sports car, but with a single speed gearbox.

It is not reported if the efficiency of the Tesla Roadster was determined with a field test or in-house on a bench. If determined from a field test it would make a difference in the efficiency calculation because aerodynamic losses, the friction losses from the wheels, etc. should be added to the equation. For the sake of comparing the two systems the assumptions are made that Tesla's

powertrain is  $\approx 88\%$  and was tested in-house and all the other losses are negligible. Then comparing these two sports cars, the first point that can be made is that the directly driven vehicle does have a higher powertrain efficiency compared to the single geared powertrain. The geared powertrain only has one motor and inverter compared to the 4 motors and inverters needed by the directly driven 4x4 vehicle. The higher torque motors required by these vehicles would significantly increase the cost. Therefore the second point is that the geared powertrain is way cheaper and would explain why manufacturers are implementing the single speed gearbox powertrain.

### 1.3 The ICE vs. the Electric Motor as a Prime Mover

As mentioned in Section 1.1 vehicles can be seen as energy converters. EVs and vehicles with ICE's have different energy input sources and the output torque differs significantly from each other. The torque output of the ICE is a function of a variety of things including valve timing, combustion, fuel, spark plugs, fuel and air mixture etc. making the torque output curve highly non-linear. There is however nearly a plateau range where the torque curve is relatively flat. Engine manufactures and researchers spend a significant portion of their time to improve the 'flatness' of this plateau region. On the other hand the electric motor is capable of nearly achieving maximum torque from standstill and the profile of the torque curve is for all practical reasons considered to be flat. An example comparison of the different torque and power curves can be seen in Fig. 1.2 and as mentioned the two torque and power profiles differ significantly. Vehicles need a high wheel torque at standstill to overcome the vehicle's inertia and as the vehicle speed increases the required

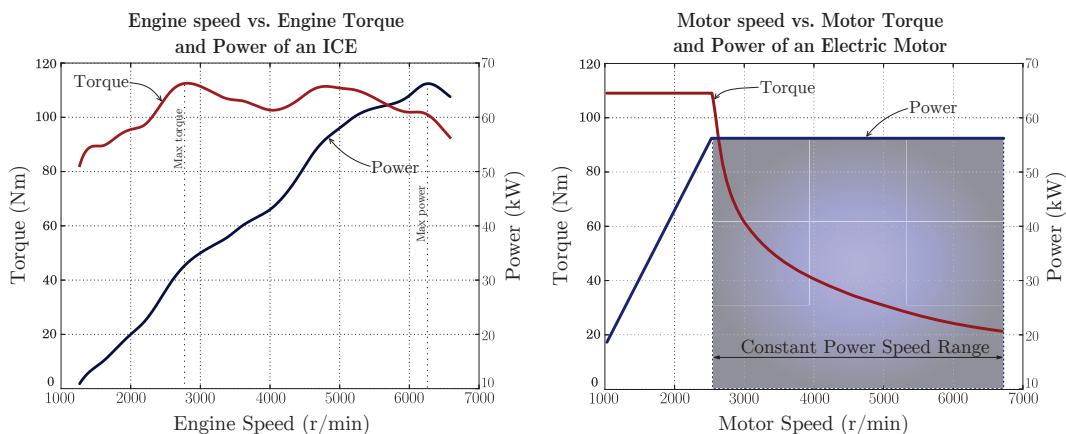


Figure 1.2: An example of the different torque and power outputs for an ICE (left) and an electrical motor (right).

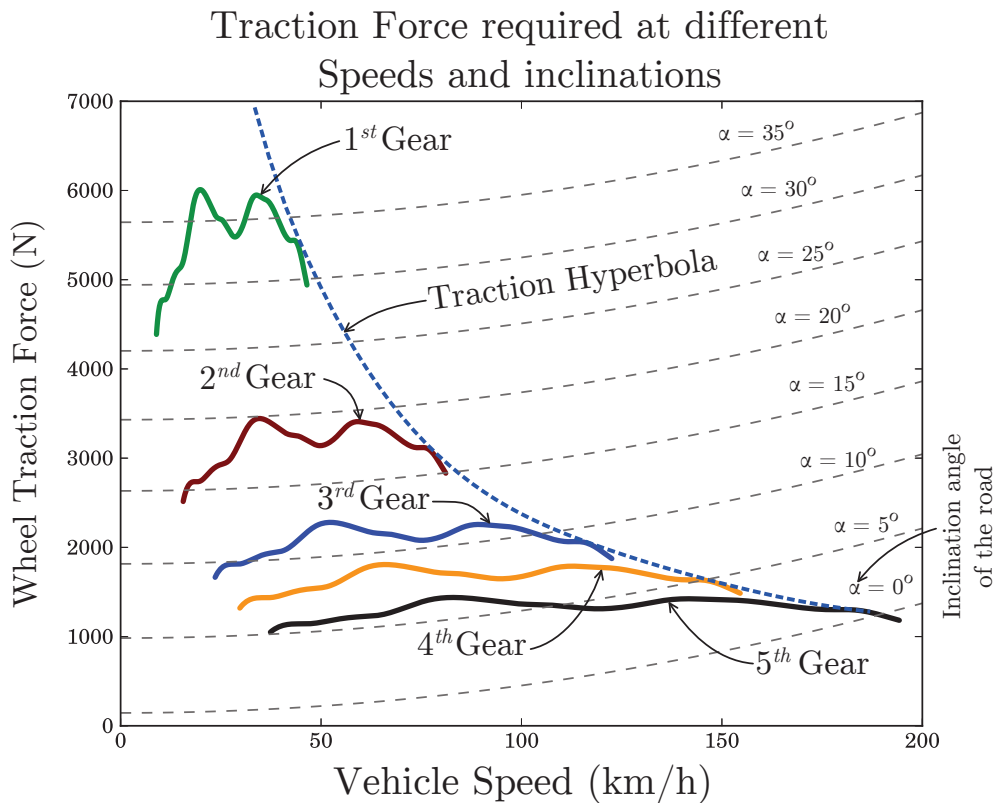


Figure 1.3: Traction curve for the Corsa 140i.

torque decreases. If gasoline powered vehicles had a gearbox with a single gear, depending on the gear ratio would either be able to have a large torque at low speed or achieve a large top speed with low torque. It is obvious that both these cases are required. Without a multi speed gearbox gasoline vehicles would not have been possible to work the way they do. The multi speed gearbox therefore enables the gasoline powered vehicle to achieve high torque at low speed, high speed at low torque and everything in between. This tractive effort versus speed is also known as a traction curve. A traction curve (hyperbola) displays the maximum force available at different speeds so that the vehicle can overcome loads and move a vehicle at different speeds and inclinations. An example of the traction curve for an gasoline powered vehicle is shown in Fig.1.3 and it is evident that the multi-speed gearbox makes it possible for gasoline vehicles to achieve the required traction. Electrical machines are capable of entering field weakening or a constant power speed range (CPSR) by using control algorithms, seen in the right of Fig. 1.2. Therefore the vehicle is capable of producing a high wheel torque at low speed and a high vehicle cruising speed with a single speed gearbox or without it. The high start up torque and the field weakening capability is two very favourable aspects of the electric motor compared to the ICE. When the curvature of the torque versus

speed plot, Fig.1.2 right, is compared to the curvature of the traction curve they nearly match perfectly. This makes the electrical motors very favourable to use for a vehicle with single-speed gearbox as seen in Table 1.1.

## 1.4 Multi Speed Gearbox for Electrical Vehicles

The functionality added and the advantages of the multi speed gearbox for gasoline vehicles are evident from Section 1.3. In Section 1.2 and 1.3 it is argued that the single speed gearbox offers advantages for EVs, such as the field weakening capability. It would seem unprecedented to add the multi speed gearbox as a powertrain option to the direct drive and single speed gearbox powertrains as shown in Fig. 1.4.

However there has been some suggestions to use EVs with multi speed gearboxes in research [14], [15],[16] and even some private companies [17], [18], [19] are mentioning benefits of a multi speed configuration. The Tesla Roadster would have been shipped with a 2 speed gearbox, however they reported to have durability, efficiency and cost challenges.[20]. Drive eO is a Latvian based company who built an electric pickup, OSCar eO, which took part and finished the 2012 Dakar. It became the first range-extended electric-drive vehicle to complete the Dakar rally. This is a remarkable feat considering the 8400 km of unforgiving terrain through Argentina, Chile and Peru. The vehicle had a 235 kW permanent magnet electric motor with 800 Nm of torque. The motor was directly coupled to a 6-speed transmission. This produced enough torque to navigate through the gruelling sand dunes and was still able to reach a maximum off-road speed of 120 km/h [21]. A multi-speed gearbox can offer benefits over it's single speed counterpart and will be discussed in the next section as well as in Chapter 2.

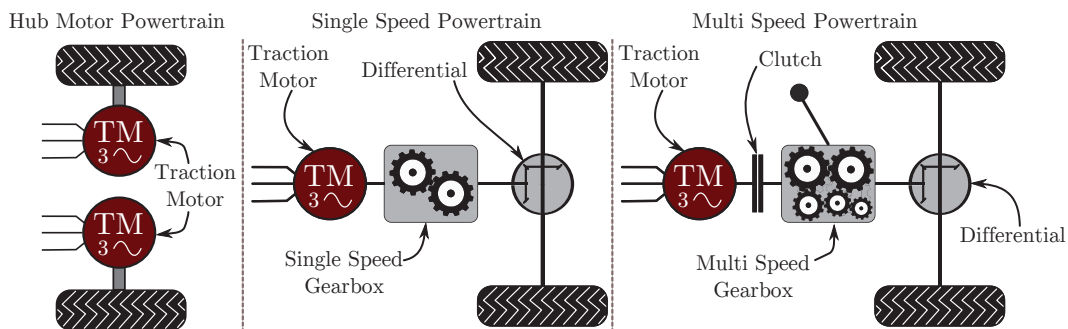


Figure 1.4: An example of different powertrain layouts for front wheel driven electrical vehicles.

## 1.5 Single vs. Multi speed transmissions for Electrical vehicles

From Section 1.3 it is evident why most companies in Table 1.1 are producing EVs with single-speed gearboxes. It could be argued that most of these vehicles torque and power performance are dependent on its CPSR performance. This requires complex field weakening control algorithms as well as advanced motor design to achieve the desired torque, power and efficiency performance at high vehicle speeds. When the required motor has to be small the torque will decrease, unless the motor is very well cooled and able to handle very high current densities. With decreased torque the gear ratio and the speed has to increase and sometimes significantly. This will leave the designer with careful design considerations with regards to the rotor bearings, iron losses and field weakening performance of the traction motor. Literature regarding electrical vehicles with a multi speed drive trains has thus far received little attention. However these studies [14]-[17] show that EVs with multi speed transmissions are able of achieving a higher efficiency on a drive-cycle compared to a single speed gearbox. This results in an increased vehicle range or a smaller battery pack with the possibility of saving weight. The other big advantage is that the overall performance of the traction motor for the vehicle is less depended on the field weakening capability. Therefore electrical machines with poor field-weakening performance such as the PM brushless DC and the reluctance synchronous machines (RSM) can be considered.

## 1.6 Problem Statement

### 1.6.1 History of the E-Corsa project

The E-Corsa project started in 2008. The aim of the project was to convert a Corsa 1.4i to a complete EV. The battery pack, drive, electronics and motor was designed to the specifications given in [22]. There were difficulties with controlling the radial-flux air-cored PM (RFPM) motor and the project was stopped.

### 1.6.2 Problem statement

- The direct drive powertrain EV has a higher efficiency than a geared drive, when the assumption is made the two different motors efficiency are the same. The drawback of the direct drive system is the higher cost with more complexity.
- With the current technology available it seems that a PMS motor with a single speed gearbox is the favourable powertrain for sedan EVs.

- There is very little literature available on the efficiencies of multi speed gearboxes. This makes it difficult to predict and make statements whether the efficiency of a multi speed gearbox would make it a viable option for an EV. However it's seems that as more research [14]-[19] are done in the development of multi speed gearboxes for EVs, the challenges and problems are overcome and benefits such as higher efficiency seems more tangible.
- One of the advantages offered by the multi speed gearbox is that the field weakening capability of the traction motor is not that important compared to traction motor used with a single speed gearbox. This make RSM's and PM brushless DC motors competitors as traction motors for EVs.
- The RSM has been suggest in literature as a traction motor in either a series [23] or parallel [24] hybrid electrical vehicle (HEV). None of these two studies looked at the efficiency of the RSM throughout the desired operation region or the efficiency of the powertrain.

## 1.7 Approach to the problem

- The same motor design specifications as for the previous E-Corsa [22] are used to design the motor for this study. The design specifications are discussed in Chapter 2.
- As a case study it was decided to design a reluctance synchronous machine (RSM) as a traction motor for the E-Corsa because of its high efficiency, robustness and durability. The multi speed gearbox offers advantages that suits the operation characteristics of the RSM. The 5-speed manual gearbox of the Corsa is used. The complete design specifications will be discussed in Chapter 2.
- Field weakening will not be implemented in the control, therefore the motor will run at a high frequency and full current. This will influence the ironlosses significantly and a simple method to predict the ironloss are also investigated in Chapter 3.
- The control was not part of the thesis but because of the self-sensing or sensorless control performance of the RSM, which was part of an other study, design changes were made to rotor to increase the saliency. These changes will be explained in Chapter 5.
- The RSM has to fit onto the bellhousing of the gearbox and has to meet the design specifications. Gradient based optimisation will be used to optimise the the machine and is discussed in Chapter 4.



- The performance and efficiency of the RSM as a traction motor has to be high to be a viable alternative to PMS motors. The performance and efficiency of the optimised machine is calculated and measured in Chapter 5 and Chapter 7 respectively.
- The efficiency of the multi speed transmission must be evaluated to determine whether it is viable from a efficiency and performance point of view for an EV powertrain and is measured and discussed in Chapter 8.

## 1.8 Thesis Layout

Chapter 2:	Design Specifications for the traction motor of the E-Corsa is determined. The single speed and the multi speed gearboxes are further compared.
Chapter 3:	The performance calculations and the losses of the RSM are discussed.
Chapter 4:	The design optimisation procedure of the RSM is discussed.
Chapter 5:	Mechanical changes to the rotor of the motor is made to increase the saliency. A mechanical strength analysis is done to determine the rotor would still be mechanically sound after these changes. After these changes the motor is simulated in JMAG to determine the motors performance.
Chapter 6:	The design of the the motor and the testbenches are discussed.
Chapter 7:	The results from the two different motors are discussed.
Chapter 8:	The system efficiency is evaluated and the gearbox efficiency is approximated.
Chapter 9:	Conclusions and recommendations.



## Chapter 2

# Determination the design specifications

This chapter describes how the initial torque design specifications were chosen and are then verified by using simple vehicle modelling. The overall design specifications of the motor is also given.

### 2.1 Initial design specification

The design specifications, as mentioned in Section 1.6.1, were determined in the previous E-Corsa project [22]. The specification sheet of the Corsa as well as test results are given in Tables A.1 and A.2 respectively, this information was published in the South African version CAR magazine in March 2000. The aim of the previous project was to design an EV that would be capable of achieving 140 km/h in 5<sup>th</sup> gear, on a straight road with no wind. The other requirement was that the Corsa should be able to have a range of at least 100 km.

From the data supplied in A.2, taking the gear ratio in 5<sup>th</sup> gear with the car at 140 km/h the engine speed was determined as 4800 r/min. The power used at 140 km/h was 35 kW, with an extra 13 kW available. This means the engine was able to deliver another 13 kW to accelerate the vehicle. From this the torque can be calculated as

$$\tau_{req} = \frac{P_{used}}{\omega_{engine}} = \frac{35}{4800 \cdot \pi/30} \approx 70 Nm \quad (2.1.1)$$

Therefore in 5<sup>th</sup> gear the output of the traction motor must be able to deliver approximately 70 Nm at 4800 Nm to achieve 140 km/h on a flat road with no wind and one passenger.

## 2.2 Specifications from vehicle modelling

To verify the design specifications, the speed engine curve of the Corsa in Fig. A.1 as well as eq. B.1.1 to B.1.6 was used to construct the traction curve in Fig. 2.1. The dashed lines ( $\alpha$  shows the inclination angle of the road) in the figures show the required force required at the wheels at different speeds and inclinations. For the design specification to be valid the wheel traction force should be above the dashed line, at  $\alpha = 0^\circ$ , that resembles the total force acting on the vehicle. From Fig. 2.2 the initial design specification is above the dashed line, it is evident that 70Nm would be sufficient to power the vehicle at the initial design specification. The IEC (International Electrotechnical Commission) uses the IEC 60034-1 [25] standard to define different duty cycles for the operation of electrical motors. The continuous duty cycle is named S1 and therefore 70 Nm is the rated torque of the continuous duty cycle. However if the motor had to compare with the ICE the maximum torque should be the same as that of the ICE, which is approximately 112 Nm. This would be the S9 duty cycle designation on the IEC standard.

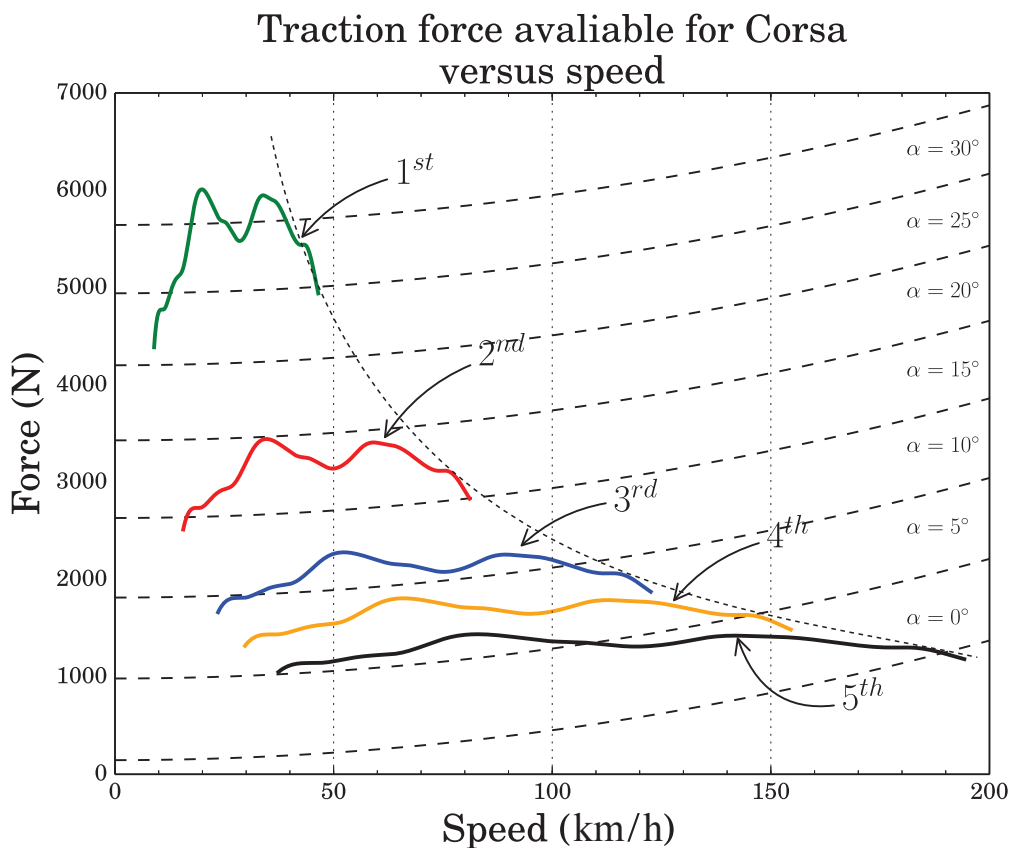


Figure 2.1: Traction curve of the Corsa.

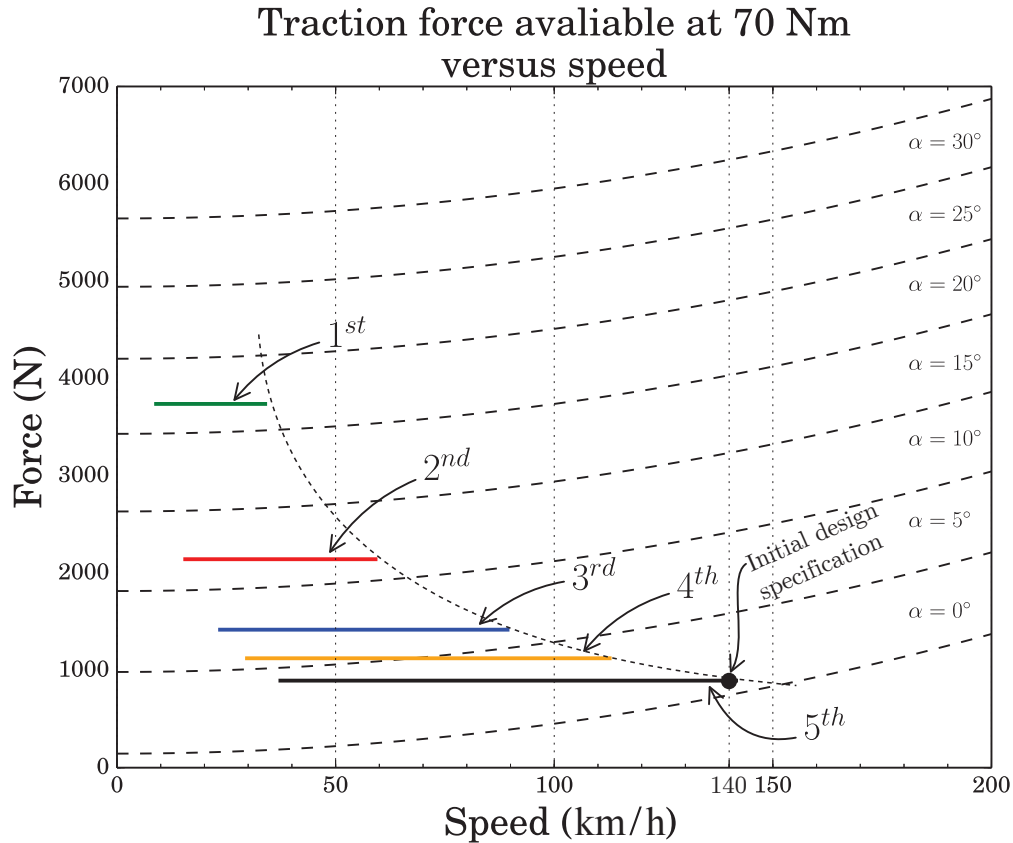


Figure 2.2: Traction curve of the RSM for the Corsa at 70Nm.

## 2.3 Further comparison of single speed versus multi speed gearboxes for Electrical Vehicles

In Section 1.5 the possible advantages of using a multi speed gearbox are discussed. This section follows on the previous discussion.

### 2.3.1 Possible difficulties and efficiency of using a multi speed gearbox.

A manual multi speed gearbox would require a clutch. However it is mentioned by [17] that a clutch is, per se, not necessary, because it is possible to synchronise the motor and the gearbox speeds when the gear is shifted. The effect of this is unknown, is it possible that the system might have a shock when a gear is shifted? Another thing to take into account is the complexity of the control algorithm that would control and synchronise the motor and the gear shifter. The assumption is made that these are negligible problems.

The construction and the components of single speed and multi speed gearboxes are different and therefore the efficiencies would also differ. There is much difficulty in finding proper literature regarding the efficiency of multi speed gearboxes, especially an efficiency map. Either it has not been important to publish information regarding the efficiency or the efficiency is difficult to measure, because of the numerous factors that contribute to the efficiency. BorgWarner a company who manufactures single speed gearboxes reports a tested efficiency of more than 97% for their eGearDrive [26]. The book Automotive Transmissions [27] deals with the fundamentals, selection, design and application of gearboxes/transmissions, they report an efficiency of between 92-97% for a manual mechanical transmission of a passenger vehicle. These values are comparable and if true it would make the multi speed gearbox a viable competitor whilst offering other benefits.

### 2.3.2 Traction and speed comparison

The traction and power curve that would result in using a variable speed gearbox is seen in Fig. 2.3. The torque is very similar to the torque shown in Fig. 2.2. What is important is the vehicle power shown in Fig. 2.3. The power has a saw tooth form and this means that the drive cannot be utilised at its full capacity. To be able to utilise the drive to its full potential the motor could be run in field weakening for a short time. This would however be contradicting to the initial choice of choosing a RSM with a multi speed gearbox that would not go into field weakening. The argument can also be given that no vehicle would run its motor at its rated power the whole time and therefore the drive would not be utilised to its full potential in any case.

Because the overall mass of the vehicle has an effect on the required traction, the required traction can be assumed so stay at least the same. This is based on the assumption that the mass of the batteries and the motor will be similar to that of the internal combustion engine. From Fig. 2.2 it is evident that the vehicle is able to ascend a hill of approximately  $20^\circ$  in 1<sup>st</sup> gear, while being able to achieve a speed of approximately 140 km/h in 5<sup>th</sup> gear. This is for the rated torque and speed. The maximum torque and power is also shown in Fig. 2.2.

A comparison of the multi speed and single speed gearboxes is seen in Fig. 2.4. This figure shows the torque versus speed for different gearboxes. The first is the motor for the variable speed gearbox, as seen the Figure the torque required is 70 Nm at a speed of 4800 rev/min. If the required torque, or volumetric size, from the motor is kept the same but a single speed gearbox is used the gear ratio would be 14.68:1 and the motor would operate at more than 20 000 r/min. If the gear ratio is halved to 7.34:1, the maximum speed would also decrease to 10 000 r/min and the torque would need to double to 140 Nm, this would also more or less double the volumetric size. This motor

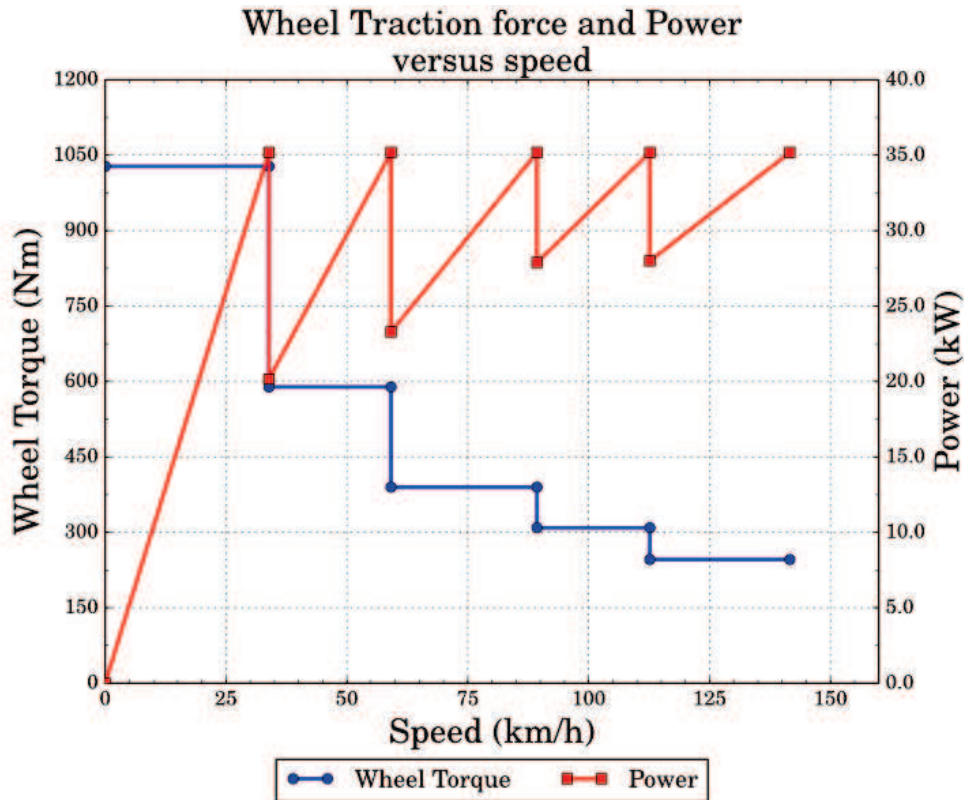


Figure 2.3: Traction curve and power available at different speeds in the different gears.

is double the rated torque and speed required from the motor compared to a motor with multispeed gearbox.

Therefore the advantage from a multi speed gearbox is that a smaller motor can be used. Smaller meaning the rated power stays the same but the rated torque is less. The development of multi speed gearboxes have been in production for nearly a century and the assumption is made that it is cheap, reliable and well developed. The advantage that neutral can be selected for safe towing is favourable especially for permanent magnet motors. The vehicle can be geared down while stopping or slowing down and would result in maximum tractive effort braking.

## 2.4 Traction motor selection

There are a wide variety of electrical machines that can be selected for this specific application. IPM or PMS motors are used by most vehicle manufactures. The IPM is dependent on permanent magnets which is expensive and can be demagnetized. The induction and field-wound rotor motors are also used by Tesla and Renault respectively, both with their pro's and con's.

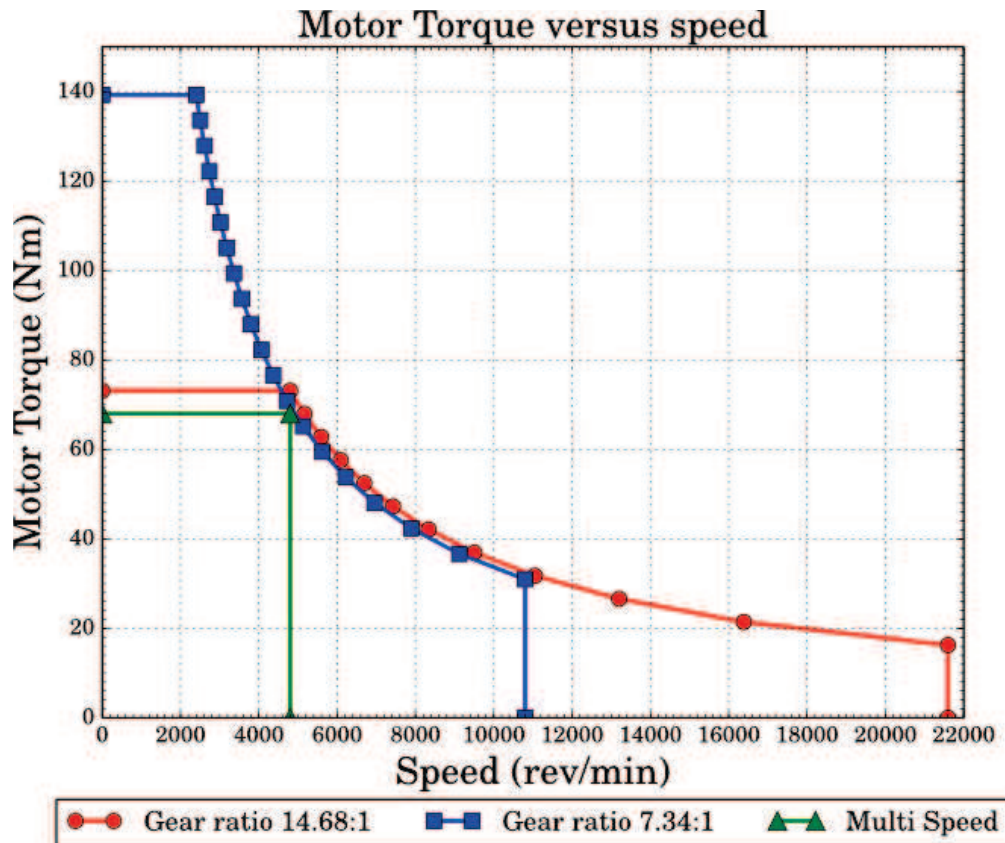


Figure 2.4: Torque available at different speeds with different gearboxes.

The synchronous reluctance machine is not commonly used as a traction motor. Most recently it started making news for being very efficient and are used for fan and pump applications. ABB [28] and KSB [29] are currently producing these machines as alternatives to induction machines. An European Union (EU) funded project MotorBrain [30] is working on a EV project to use a RSM in their EVs powertrain. The advantage that the synchronous reluctance motor offer is it's high efficiency and high energy density while it needs no brushes, magnets or coils on its rotor. The RSM is also a very robust machine and is chosen as the desired traction motor.

## 2.5 Design specifications for the Motor

There are a number of physical design constraints the machine has to conform to. The motor has to fit onto the bellhousing of the gearbox and in the engine compartment. The absolute maximum diameter available is 274 mm. The possibility of adding a water-cooled housing is considered and the maximum stator diameter is chosen as 230 mm. The length of the machine must be kept to a minimum to fit into the available space, the maximum length is 530

mm. Overlap windings are used in the machine and the end winding length is chosen as 60 mm on each side and the stator length is chosen at 110 mm. Due to the possibility to use water cooling the current density is chosen as 8 A/mm<sup>2</sup>. To keep the ironloss to a minimum the lamination steel for the stator and rotor is chosen as NO20 and the thickness of a lamination is 0.2 mm.

The following design specifications are chosen for the RSM:

Table 2.1: Specification of the RSM

Specification	Value	Unit
Rated torque	70	Nm
Rated power	35	kW
Peak torque	112	Nm
Peak power	55	kW
Maximum speed	4800	rev/min
Battery pack voltage	350	V
Stator outer diameter	230	mm
Stator stacklength	110	mm
Shaft diameter	43	mm
Air-gap length	0.4	mm
Current density	8.0	A/mm <sup>2</sup>
Number of poles	4	
Number of stator slots	36	
Lamination steel	NO20	
Cooling	Water	

## 2.6 Summary

- For the vehicle to run at 140 km/h in 5<sup>th</sup> gear on a flat road would require 70 Nm at 4800 r/min from the traction motor. This was also verified by using vehicle modelling techniques.
- From [27] the efficiency of the multi speed gearbox is comparable to a single speed gearbox [26] but should be verified through testing to determine how well they compare.
- The power profile of multi speed drive train has a sawtooth form, this implies that the inverter cannot be fully utilised.

- The multi speed power train offers the benefit of a smaller motor and lower speed compared to a single speed gearbox.
- The RSM has high efficiency, simple construction, robust and no copper or magnets on the rotor. The RSM doesn't have a good field weakening capability, but when combining the strengths and weaknesses the RSM is a suitable candidate for the multi speed power train.



## Chapter 3

# Performance calculations for the RSM

This chapter discusses the methods used to determine the performance of the machine by calculations and simulations. Methods to calculate the efficiency, the windage and friction losses, copper losses and iron losses in the RS machine are discussed. The aim is to explore what techniques can be used that would not be too computationally expensive, yet still produce accurate results.

### 3.1 Torque and torque ripple

The torque in the airgap is calculated by JMAG FE software [31] as shown in eq. 3.1.2. The average torque is calculated from this in eq. 3.1.1. To reduce the torque ripple the rotor of the machine is skewed by using 5 sub-machines as in [1] and [32]. The simulation is run through a torque periodicity to calculate the torque and torque ripple accurately.

$$T_{avg} = \frac{1}{n_s} \sum_{i=0}^n \frac{1}{k_s} \sum_{j=1}^{k_s} \tau(\theta_i \pm \alpha_j) \quad , \quad (3.1.1)$$

where  $n_s$  is the number of position steps,  $k_s$  is the number of skewed sub motors and  $\tau(\theta \pm \alpha)$  is the FE torque at position  $\theta_i$  and  $\alpha_j$  the skew angle of the sub motor.  $\tau$  is the instantaneous torque and is calculated by the FE program using Maxwell's Stress Tensor method [33] as

$$\tau(\theta_i \pm \alpha_j) = \frac{1}{\mu_0} \oint_{\Gamma} r B_t B_n \cdot d\Gamma \times l \quad , \quad (3.1.2)$$

where  $\mu_0$  is the permeability of a vacuum or free space,  $r$  is the radius of the contour  $\Gamma$  in the centre of the airgap,  $B_t$  and  $B_n$  the normal and tangential flux densities in the air-gap respectively and  $l$  is the stack length of the machine. The torque ripple is calculated by

$$T_{ripple} = \left( \frac{T_{max} - T_{min}}{T_{avg}} \right) . \quad (3.1.3)$$

## 3.2 Power factor

It is shown by [1] that the power factor can be calculated, by ignoring the stator resistance and the ironloss, as

$$PF = \cos \left( \tan^{-1} \left( \frac{\frac{\sigma_{SR}}{v_{CR}} + v_{CR}}{\sigma_{SR} - 1} \right) \right), \quad (3.2.1)$$

where PF is the power factor,  $\sigma_{SR} = L_d/L_q$  and  $v_{CR} = I_q/I_d$ .

## 3.3 Windage and friction loss

The bearing friction loss [34] can be calculated as

$$P_{Bearing} = 1,05 \times 10^{-4} \cdot M \cdot n, \quad (3.3.1)$$

$P_{Bearing}$  is the bearing power loss,  $M$  is the frictional moment,  $n$  is the rotational speed.

The frictional moment can be calculated with the assumptions that:

- bearing load  $P \approx 0,1 C$
- good lubrication
- normal operating conditions

$$M = \frac{u \cdot P_{load} \cdot d_{bearing}}{2}, \quad (3.3.2)$$

$u$  is the constant coefficient of friction for the bearing,  $P_{load}$  is the equivalent bearing load,  $d$  is the bearing bore diameter [35].

If the motor has no external fan fixed to the shaft the windage can be calculated as [36] [? ]:

$$P_{windage} = \frac{\pi}{32} \cdot k \cdot C_f \cdot \rho \cdot \omega^3 \cdot D_r^4 \cdot l_r, \quad (3.3.3)$$

$k$  is the roughness coefficient,  $\rho$  is the density of the coolant,  $\omega$  is the angular velocity,  $D_r$  is the rotor outer diameter,  $l_r$  length of the rotor,  $C_f$  is the friction coefficient and is dependent on the Couette Reynolds number,

$$Re_{air_g} = \frac{\rho \cdot \omega \cdot D_r \cdot air_g}{2\mu}, \quad (3.3.4)$$

where  $air_g$  is the air-gap length and  $\mu$  the dynamic viscosity of the coolant.

$$C_f = 10 \frac{(2air_g/D_r)^{0.3}}{Re_{air_g}}, Re_{air_g} < 64, \quad (3.3.5)$$

$$C_f = 2 \frac{(2air_g/D_r)^{0.3}}{Re_{air_g}^{0.6}}, 64 < Re_{air_g} < 5 \times 10^2, \quad (3.3.6)$$

$$C_f = 1.03 \frac{(2air_g/D_r)^{0.3}}{Re_{air_g}^{0.5}}, 5 \times 10^2 < Re_{air_g} < 10^4, \quad (3.3.7)$$

$$C_f = 0.065 \frac{(2air_g/D_r)^{0.3}}{Re_{air_g}^{0.2}}, 10^4 < Re_{air_g}. \quad (3.3.8)$$

### 3.4 Copper loss

The copper loss is calculated as

$$P_{cu} = 3I^2 R_{st}, \quad (3.4.1)$$

where  $P_{cu}$  is the copper loss for the stator windings,  $I$  is the current and  $R_{st}$  is the resistance of the coils. When ignoring the skin effect the resistance of the coils can be calculated as,

$$R_s = \frac{2W\rho_t(l+l_e)}{n_a A_{cu}/z}, \quad (3.4.2)$$

where  $W$  is the number of turns per phase,  $l$  is the stack length,  $l_e$  is the average end winding length,  $n_a$  is the number of parallel circuits of the stator windings and  $A_{cu}/z$  is the active copper area of a stator conductor. The resistivity of copper,  $\rho_t$  at a certain temperature,  $t_c$ , can be calculated as

$$\rho_t = \rho_{20}(1 + Y_t(t_c - 20)), \quad (3.4.3)$$

where  $\rho_{20} = 17 \times 10^{-9}$  ohm·m and  $Y_t = 0.0039/^\circ\text{C}$ . The resistance of the coils are calculated at a temperature of  $75^\circ\text{C}$ .

### 3.5 Ironloss

There is difficulty in modelling and calculating an accurate ironloss values for electrical machines, even with a lot of methods and literature available. Some methods are complex and computationally expensive or difficult to implement and therefore are not considered, because it goes beyond the scope of this thesis.

### 3.5.1 Steinmetz equation

The first method to determine the ironloss was proposed by Charles Proteus Steinmetz. He found that the ironloss is a function of the frequency and the flux density as in eq. 3.5.1.

$$P_v = kf\hat{B}^\beta \quad (3.5.1)$$

where  $P_v$  is the time-average ironloss per unit volume,  $k$  and  $\beta$  are material properties,  $\hat{B}$  is the peak induction of a sinusoidal excitation with a frequency of  $f$ .

### 3.5.2 Measuring ironlosses

To determine the parameters for the equation the loss curves has to be determined. There are two devices available to determine the ironloss of electrical steel namely the Epstein frame or the Soken tester. The Epstein frame is used to determine the magnetic properties of soft magnetic steels. The test are done under the IEC 60404-2 and BS EN 60404-2 standards. The Soken is a hand held device used to determine the iron loss at 50 and 60 Hz and at a magnetic flux densities of 1 T, 1.5 T and 1.7 T. The manufacturer claims that the measurement uncertainty is less than 5%. Because of the difficulty to have a standard that would suit the every machine and transformer, it wouldn't be unrealistic to say that the losses should be adjusted to suit different geometries and frequencies. This can be simulated but would require accurate modelling and can then only be verified by measurement.

### 3.5.3 FE ironloss equation

The JMAG FE analysis calculates the hysteresis and eddy current losses as in eq. 3.5.2 and 3.5.3 respectively [37], the motor is stepped through a full electrical period to obtain an accurate value for the ironloss

*Hysteresis loss:*

$$P_h = \sum_{e=1}^E \left\{ \sum_{k=1}^N \alpha(|B_k|) \cdot f_k \right\} V_e, \quad (3.5.2)$$

where  $\alpha$  is the coefficient of the magnetic flux density  $|B_k|$  for harmonic order  $k$  determined by the frequency separation method,  $f_k$  is the frequency for harmonic order  $k$ ,  $V_e$  is the volume of each element,  $N$  is the maximum frequency order and  $E$  is the number of elements.

Eddy current loss:

$$P_e = \sum_{e=1}^E \left\{ \sum_{k=1}^N \beta (|B_k|, f_k) \cdot f_k^2 \right\} V_e , \quad (3.5.3)$$

where  $\beta$  is the coefficient of the magnetic flux density  $|B_k|$  and frequency  $f_k$  for harmonic order  $k$  determined by the frequency separation method.

### 3.5.4 Alternative ironloss equation

A modified ironloss equation 3.5.4 that can be implemented, as used by [1], it is attractive because of it's simplicity,

$$P_c = c f^x (\hat{B}_t^y M_t + \hat{B}_{y_k}^y M_{y_k}) \quad (3.5.4)$$

where  $\hat{B}_t$  and  $\hat{B}_{y_k}$  are the maximum flux densities in the teeth and yoke respectively at a supply frequency  $f$ .  $M_t$  and  $M_{y_k}$  is the iron mass of the teeth and yoke respectively. The constants  $c, x$  and  $y$  can be determined from the loss tables from the suppliers. Because this method uses maximum flux density at any given instant, it is a method to include in a 2D geometric FE optimization process, if possible to get the areas for the geometries from the FE software. Even though it has some error it will take into account the flux densities and the shape of the teeth and the yoke. This error is constant in the optimization processes and will have a minor effect on the end result from the optimization.

### 3.5.5 Ironloss case study

The simulation results vs. the measured results from [1] show good correlation with a small error in the efficiency. Eq. 3.5.4 was used to determine the ironloss in the study. The assumption is then made that this method accurately approximates the ironloss without being computationally expensive. It is important to calculate the constants  $c, x$  and  $y$  correctly. In [1] the lamination material for the stator and rotor is M36-26 Ga, the thickness of the steel is

Table 3.1: Different values for the parameters to be used in eq. 3.5.4 from [1], substitution and MSE.

Variables	c	x	y
[1]	0.0337	1.32	2
Substitution	0.00396	1.4866	1.98
MSE	0.014	1.171	1.91

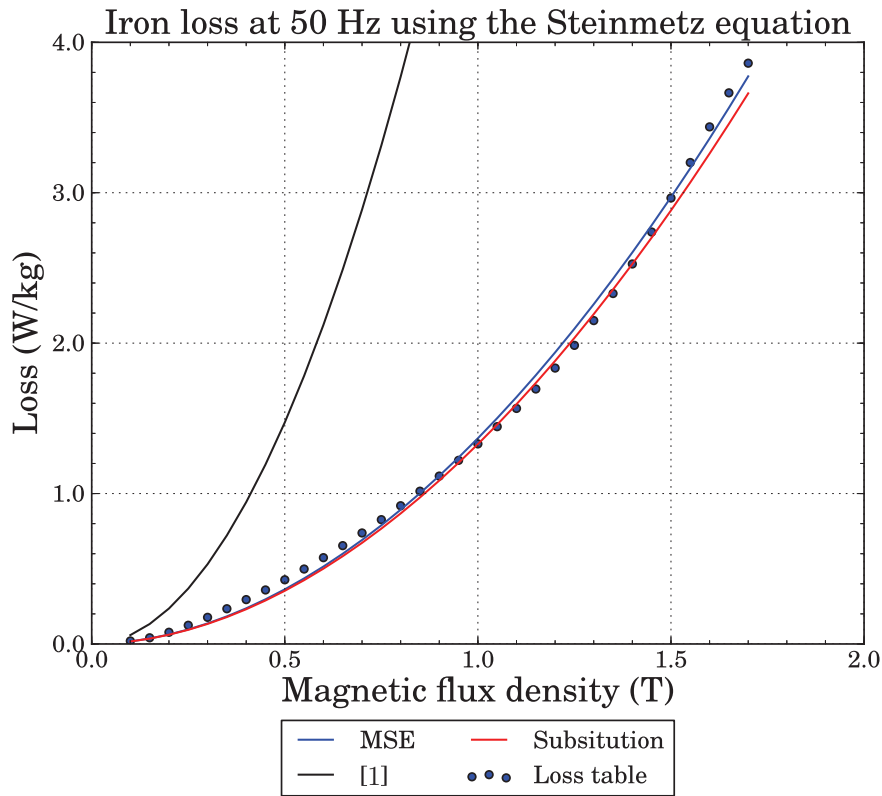


Figure 3.1: Comparison of the ironloss determined from eq. 3.5.4 with different parameters.

0.47 mm.

To calculate the constants substitution and mean square error (MSE) is used. The M36-26 Ga ironloss data is taken from AK Steel [38]. To determine the parameters with the substitution method, the flux and frequency is substituted in eq. 3.5.4 and the parameters calculated. To calculate these parameters with the MSE method, initial values are chosen and then a solver is used to optimise these parameters until the squared error difference in values calculated from eq. 3.5.4 and the loss table is a minimum. In both cases the accuracy is dependant on the available data from steel suppliers. For the MSE the initial values are also important. When proper data for all the frequencies are not available interpolation and extrapolation should be used, extreme caution using extrapolation. The values for the constants from the study [1] and these two methods are shown in Table 3.1.

The obtained values differ and to compare the values from this table, the values are substituted into eq. 3.5.1 and plotted against the data from the loss tables, the result is seen in Fig. 3.1 and Fig. 3.2. From these graphs the values

Table 3.2: Mass and flux values obtained to calculate the iron losses.

Variables	$M_y$	$M_t$	$B_y$	$B_t$
Values (unit)	11.08 (kg)	6.583 (kg)	1.78 (T)	1.84 (T)

Table 3.3: Values obtained to from different loss calculation methods by simulating the RSM from [1].

Method	Stator (W)	Rotor (W)	Total (W)
Original Ironloss from [1]	291	0	291
Values from [1] to calculate Ironloss	331	0	331
MSE	74.56	0	74.56
Substitution	75.36	0	75.35
JMAG	80.75	20.79	101.5

from the substitution and MSE methods closely follows the data values from the loss tables. The values from [1] are much larger and overestimates the ironloss. It is important to remember that even though the steel used in the study for [1] and the steel from AK Steel is the same type, the iron loss has been improved since these parameters were first calculated. This would also cause a difference.

To further investigate eq. 3.5.4 the 2-D RSM model from [1] is redrawn and re-simulated in JMAG FE software. The previous ironloss values from [1], the ironloss from JMAG and calculating the ironloss with eq. 3.5.4 with the values from Table 3.1 is compared. It is not possible to get the geometric information such as area or mass from JMAG, therefore the RSM is redrawn in Autodesk Inventor [39] to get the masses of the stator yoke ( $M_y$ ) and the stator teeth ( $M_t$ ). The peak flux density in the yoke and teeth was taken from the simulation done in JMAG, as shown in Fig. 3.3. These values are tabulated in Table 3.2.

The different losses are shown in Table 3.3. The stator ironloss from JMAG and calculated methods using the values from MSE and substitution show a good comparison. However the values from the previously determined study differs greatly. The calculated ironloss with the previously determined parameters also differs if the masses and flux densities are substituted into eq. 3.5.4. This may be due to the fact that the steel B-H curve differs and the simulation programs are also different. The results are inconclusive and without proper testing data the accuracy of this method is not sufficient.

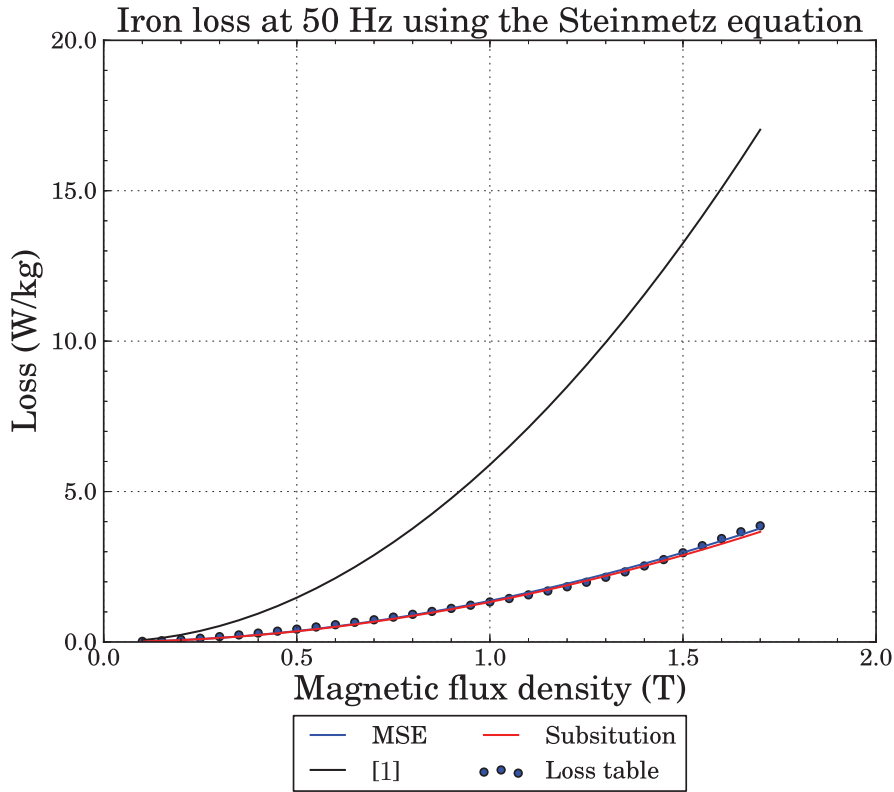


Figure 3.2: Same as Fig. 3.1, except that it shows the large ironloss difference by using the parameters from [1].

### 3.6 Calculating efficiency

The efficiency is calculated as

$$\eta = \frac{P_{out}}{P_{in}} \cdot 100 \quad (3.6.1)$$

where

$$P_{in} = 3V_{\phi}I_{\phi}\cos(\theta) = 3V_{\phi}I_{\phi}PF \quad (3.6.2)$$

and

$$P_{out} = (T_{avg} \cdot \omega) - P_{bearing} - P_{windage} - P_c. \quad (3.6.3)$$

$\eta$  is the efficiency of the motor,  $P_{in}$  is the input power,  $P_{out}$  is the output power,  $V_{\phi}$  and  $I_{\phi}$  is the phase voltage and phase current respectively as determined from the FE software,  $\omega$  is the output speed of the shaft and  $P_c$  is determined from the FE software. A schematic of how the calculations are done is shown in Fig. 3.4



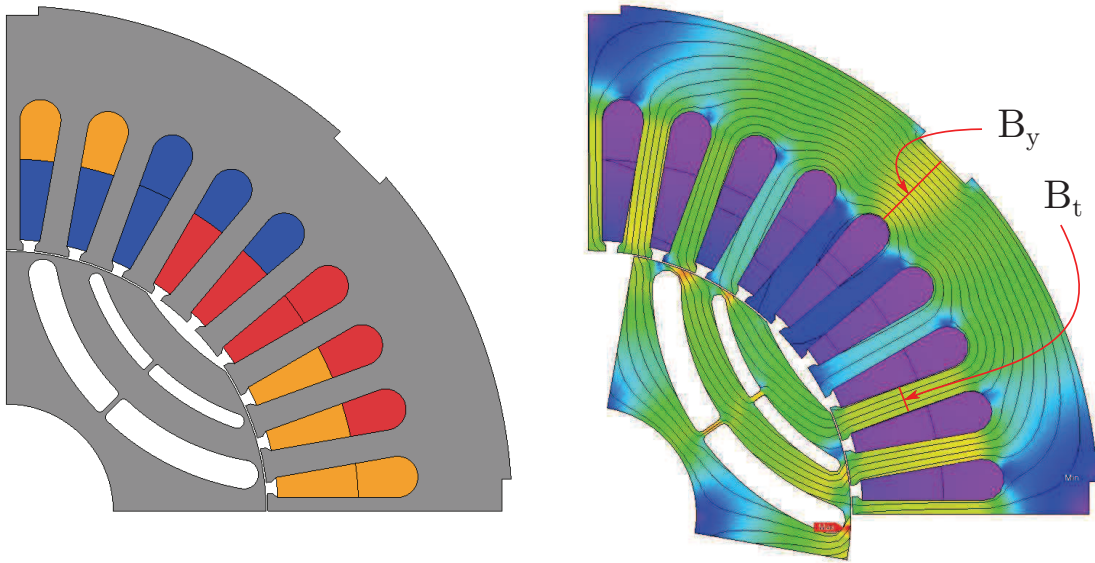


Figure 3.3: The 9.2 kW RSM used by [1]. The figure on the right shows the flux densities in the RSM when operated.

### 3.7 Summary

- The methods proposed to calculate the windage and friction and copper losses are simple and are not computationally expensive.
- The proposed method to calculate the ironloss is simple and not computationally expensive. It has been used with success in the past [1]. It requires however the peak flux densities and masses from the structure. This makes it difficult when using commercial software, especially when there is no option to get the area or mass. This method however doesn't take into account the ironloss in the rotor.
- From the case study it is interesting to observe that the stator ironloss from JMAG and the ironloss calculated using eq. 3.5.4 with the constants from the substitution and MSE methods are not much different.
- The values of the constants  $c_x$  and  $y$  from the previous study and the values determined from substitution and MSE methods are different. It seems that to accurately use this method the values should be adjusted using measured values.

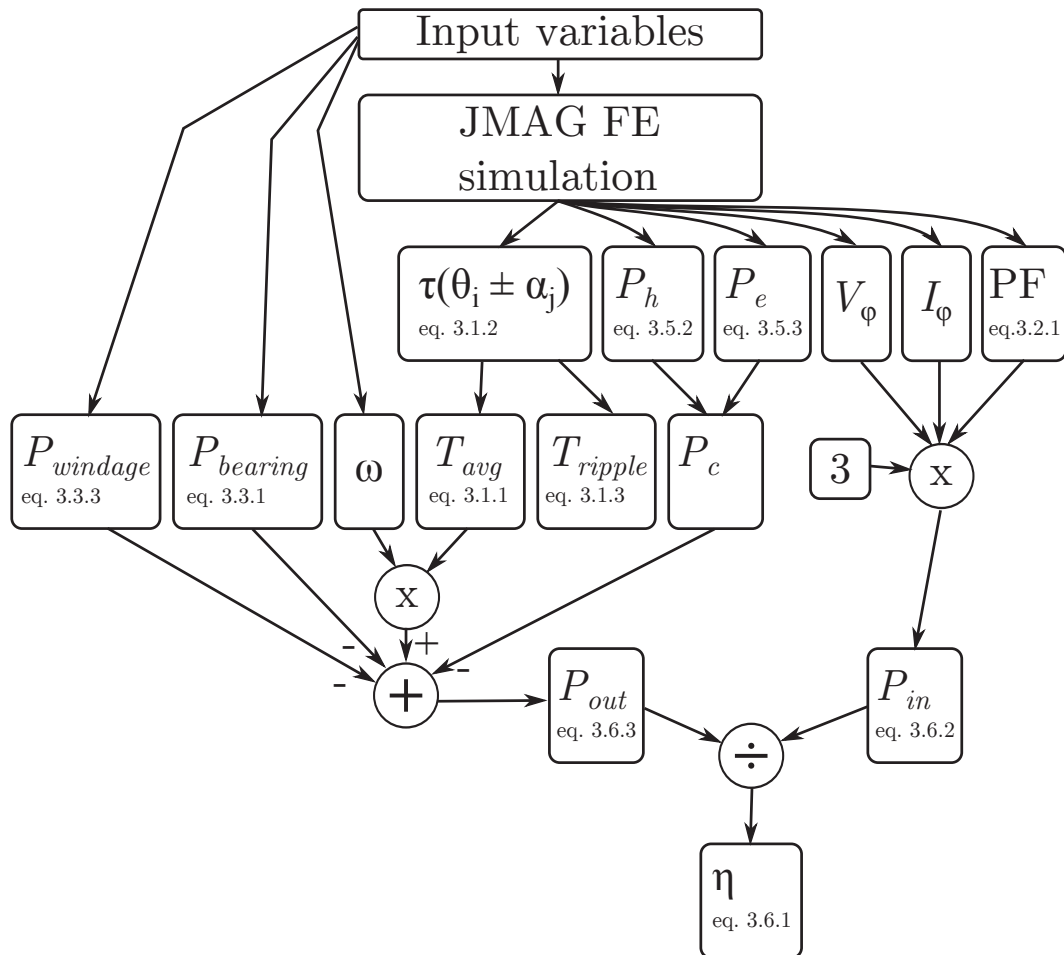


Figure 3.4: A schematic of how the performance calculations are done.

# Chapter 4

## Optimization of the RSM

The design optimization is explained in this chapter. The aim of the optimization was to find a machine that would suit the design specification.

### 4.1 Optimization formulation

The proper definition and formulation of optimization design problems are important and can take up to 50% of the overall effort to solve it [40]. It is important to formulate a proper optimization problem and therefore a five-step formulation procedure is followed as in [40]. The steps are:

1. Project/ problem description
2. Data and information collection
3. Definition of design variables
4. Optimization criterion
5. Formulation of constraints

#### 4.1.1 Problem Description

The problem description is done in Chapter 2. To quickly recap the design specifications for the optimization procedure. The traction motor of choice is a RSM. The performance required from the motor is 70 Nm at 4800 rev/min and the maximum efficiency and a torque ripple as low as possible. The RSM must be able to fit onto the bellhousing of the gearbox and in the engine compartment of a Corsa 140i. This limits the overall diameter of the motor to 274 mm and the stator to 230 mm. The RSM has to run from an inverter connected to a battery pack with a voltage of 350 V. The design specifications are shown in Table 2.1.

Table 4.1: Design constants of the RSM traction motor.

Variable	Abbreviation	Initial Design value
Stator OD	$st_{od}$	230 mm
Rotor ID	$ro_{id}$	43.0 mm
Airgap	$air_g$	0.4 mm
Current Angle	$\delta$	$67^\circ$

### 4.1.2 Data and information collection

The analysis of the RSM motor is done with commercial finite element (FE) software JMAG. The design variables are written to the FE software from the optimisation software VisualDoc [41] via a Python script. The simulation is then run to calculate the torque and torque ripple. The torque and torque ripple are then read back also via a script. From these values the performance is calculated and sent back to the optimization program.

### 4.1.3 Definition of design variables

The 2D structure of the rotor and the stator is modelled mathematically. Most of the variables are geometric variables and are shown in Fig. 4.1. As is seen Fig. 4.1 a half of the rotor and a quarter of the stator is shown. This is only for illustration purposes to clearly show all the design variables. Only a quarter of the machine is run in the FE simulation. There are a total of 13 geometric variables, 10 on the rotor and 3 on the stator. The variables are chosen in such a way that the steel is optimized and not the air. This meaning, as shown in Fig. 4.1, the width and the angles of the magnetic flux paths are changed instead of the widths and angles of the flux barriers. The flux paths are drawn using circle equations, this is sufficient for this 4-pole RSM. The design variables are shown in Fig. 4.1. The meaning of the constants and variables is explained in Tables 4.1 and 4.2 respectively. The geometric constants are the rotor inner diameter, the air gap and the stator outer diameter. The current angle,  $\delta$  was chosen as a design constant at  $67^\circ$ .  $\mathbf{U}$  is the design constants and are given in eq. 4.1.1 and  $\mathbf{X}$  is the design variables and are given in eq. 4.1.2.

$$\mathbf{U}^T = [ro_{id} \quad st_{od} \quad air_g \quad \delta] \quad (4.1.1)$$

$$\mathbf{X}^T = \begin{bmatrix} t_{wid} & st_{id} & fp_1 & fp_2 & c_1 & c_2 & \dots \\ \dots & c_3 & c_4 & \alpha_1 & \alpha_2 & \alpha_3 & \alpha_4 & yoke \end{bmatrix} \quad (4.1.2)$$

### 4.1.4 Optimization criteria

The machine was optimised using a multi-objective cost function given as

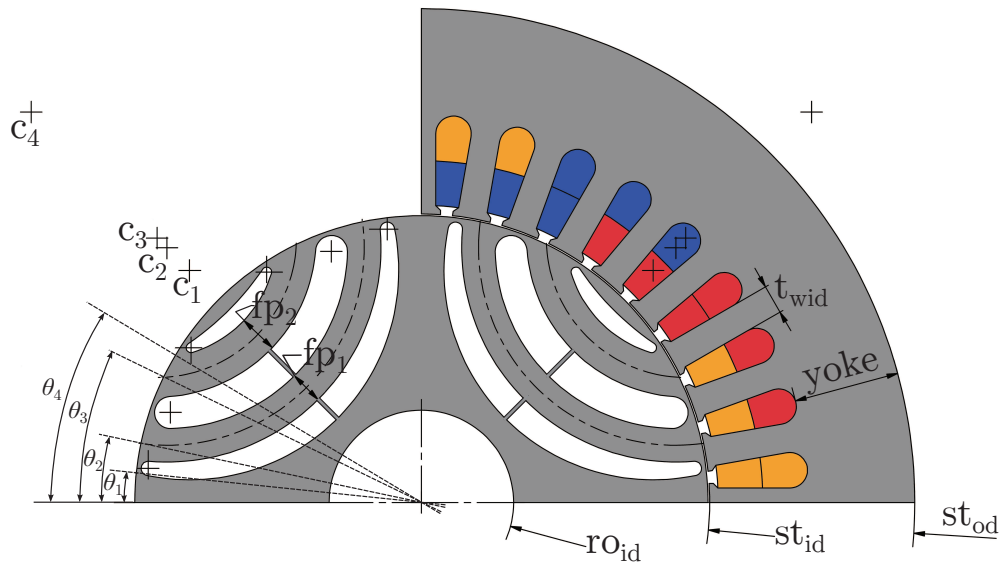


Figure 4.1: The rotor and stator of the RSM with the design variables shown.

Table 4.2: Design variables of the RSM traction motor.

Variable	Abbreviation	Initial Design value
Yoke height	yoke	20 mm
Tooth Width	$t_{wid}$	6.1 mm
Stator ID	$st_{id}$	120.1 mm
Flux path 1 width	$fp_1$	6 mm
Flux path 2 width	$fp_2$	7 mm
Circle center point 1	$c_1$	52.4 mm
Circle center point 2	$c_2$	56.4 mm
Circle center point 3	$c_3$	62.8 mm
Circle center point 4	$c_4$	90 mm
Bottom flux path angle	$\alpha_1$	4.5°
Flux path 1 angle	$\alpha_2$	12.5°
Flux path 2 angle	$\alpha_3$	23.5°
Top flux path angle	$\alpha_4$	33.5°

$$F(\mathbf{X}) = (F_1(\mathbf{X}), F_2(\mathbf{X})), \quad (4.1.3)$$

where

$$F_1(\mathbf{X}) = \frac{P_{cu}}{T_{avg}} \quad (4.1.4)$$

and

$$F_2(\mathbf{X}) = T_{ripple} \quad (4.1.5)$$

the cost function is minimised.

#### 4.1.5 Formulation of constraints

There are explicit bounds put on the all the the design variables. Therefore each variable had a maximum and minimum value to limit it to go into an infeasible direction.

### 4.2 Optimization procedure

The next step of the optimisation was to incorporate the design variables in a meaning full way with optimisation software VisualDoc [41]. VisualDoc is a commercial optimization software package. It is a general purpose multidisciplinary design, optimization and process integration software. The design modules such as optimization and design of experiments can be added to almost any analysis software [42]. The FE was run in JMAG [31], another commercial program. JMAG is electromagnetic field analysis software that makes it easy to run electromagnetic field simulations. The software can run 2D and 3D electromagnetic simulations. To communicate between the 2 programs, Python 2.7 is used, with the modules NumPy and SciPy [43]. The process is illustrated in Fig. 4.2. There are a variety of algorithms available to be used for the gradient based optimization the namely: Modified method of feasible direction (MMFD), Sequential Quadratic programming (SQP), Sequential Linear Programming (SLP) and sequential unconstrained optimisation (BIGDOT). These methods search for the minimum of the objective function in the design space and within the constraints. More information regarding these methods can be found in [40], [41] and [44]. To calculate the gradient the central difference method was used. To get an accurate indication of the torque ripple the FE had to be stepped through a torque period, which in this case was  $30^\circ$  mechanical. The stator was not chorded nor the rotor skewed in the optimisation.

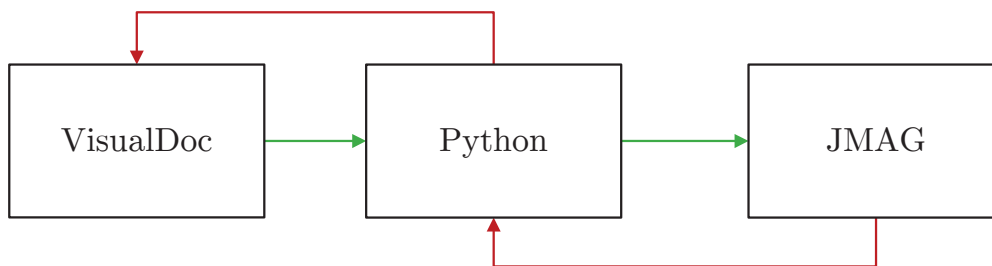


Figure 4.2: The communication between the VisualDoc and JMAG is achieved via Python.

### 4.3 Optimization Results

The optimisation was run several times and the initial values were changed at the start of each run. The MMFD, SQP and BIGDOT gradient based methods were all used to see whether it was possible to improve the design with each optimisation run. The simulations were run on a Pentium i7 with 8 gigabytes of RAM on 64-bit Windows 7. The time it took for one simulation in JMAG differed, however the average time was approximately 1:30 min. The average time for the optimization was approximately 5 hours. The results from the optimisation is tabulated in Table 4.3 and the optimised machine can be seen in Fig. 4.3. The torque ripple is still high, however this is the minimum value that was reached in the all of the optimisation iterations. This high torque ripple is overcome by skewing and chording the machine and is shown in the following Chapter.

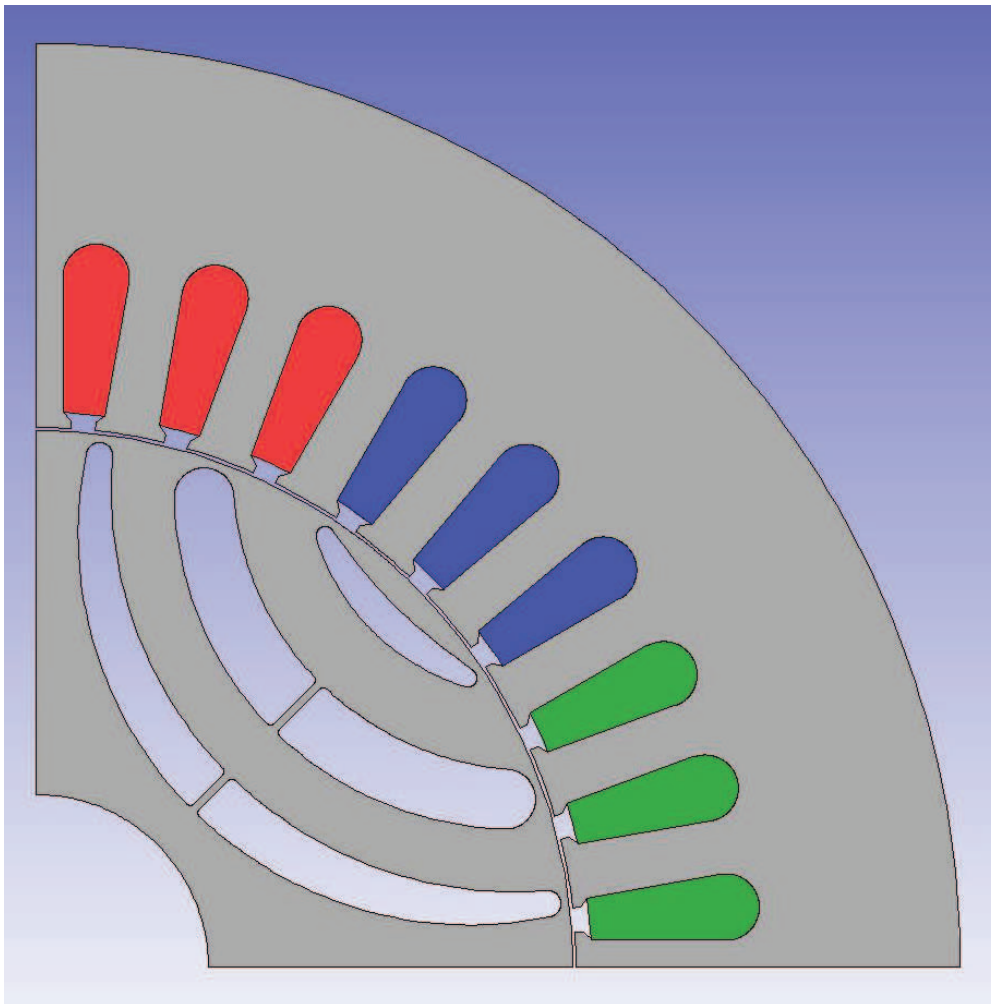


Figure 4.3: The optimised 35 kW RSM.

## 4.4 Summary

- The optimisation decreased the initial stator inner diameter and increased the tooth width and yoke height of the stator. This decreased the slot area of the coils. Due to the decrease in stator inner diameter the rotor outer diameter increased. Both the rotor flux paths increased in size. This is probably due to the high current density of  $8 \text{ A/mm}^2$  that is specified in the design specifications. It seems that the optimisation increased the active flux paths in the machine to keep the machine out of saturation at the specified operation point.
- The RSM was successfully optimised to reach the set requirements. The torque ripple is still high but it is shown in the following Chapter that by skewing the rotor and chording the stator effectively reduces the torque ripple.



Table 4.3: Optimum variables and performance values from the optimisation procedure.

Variable	Initial Value	Optimum Value	Unit
$st_{od}$	230	230	mm
$st_{id}$	120.1	134.4	mm
$air_g$	0.4	0.4	mm
yoke	20.0	24.67	mm
$t_{wid}$	6.1	6.76	mm
stacklength	110	110	mm
$ro_{id}$	43	43	mm
$c_1$	52.4	54.03	mm
$c_2$	56.4	59.3	mm
$c_3$	62.8	61.58	mm
$c_4$	90.0	90.94	mm
$\alpha_1$	4.5	5.9	°
$\alpha_2$	12.5	11.85	°
$\alpha_3$	23.5	25.88	°
$\alpha_4$	33.5	32.14	°
$fp_1$	6.0	7.81	mm
$fp_2$	7.0	9.16	mm
Torque	-	72.3	Nm
$I_{s_{RMS}}$	-	138.6	A
$R_{phase}$	-	0.02	$\Omega$
f	-	160	Hz
$P_{cu}$	-	1266	W
$T_{ripple}$	-	17.3	%
$\delta$	-	67	°
Number of turns per slot	-	8	
Number of slots	-	36	
Number of poles	-	4	

## Chapter 5

# Modifications to the optimised Rotor and the performance results of the RSM

There are design and construction changes made to the initial design specifications and the optimised motor. This section discusses the design changes and evaluates the performance of the RSM.

### 5.1 Modifications to the optimised RSM

There had to be changes made to the initial design specifications and the optimised motor. There are geometric, material and cooling changes made to the RSM, the changes are as follow:

- The initial motor was designed to be water-cooled. However due to high cost it was decided to rather use an air-cooled casing for the motor. The initial water-cooled RSM design is shown in Appendix C.
- The RSM motor was optimised with lamination steel NO20. However it was decided to change the rotor steel to M530-65A. This was done to save costs. From the FE the ironloss in the rotor increased with the M530-65A laminations steel, however the increase was still acceptable.
- It was decided to build another air-cooled motor with lamination steel M530-65A, the rotor and stator. This was done to compare the performance between the two different motors. The motor with the M530-65A laminations costs less, however the ironloss would be higher and therefore the efficiency would be lower. It was also done to determine whether it would be possible to approximate the ironloss with the same geometry but different lamination steels.

- To increase the saliency the rotor was changed by removing the webs. This will be discussed in the next section.
- The material and geometric changes are taking into account in the FE software. However the cooling change from water to air is not taken into account in the FE software.

### 5.1.1 Design Changes to optimised Rotor

The motor designed in this thesis was part of a larger study [45] that looked at the saliency performance of the RSM. As mentioned earlier (Chapter 1) the control was not part of the research project. The research showed that the saliency ratio would increase if the the inner webs would be removed. The different structures can be seen in Fig. 5.1. The effect by removing this webs on the torque and torque ripple performance was insignificant. However this would also change the mechanical strength, the next section deals with the mechanical strength analysis of the rotor.

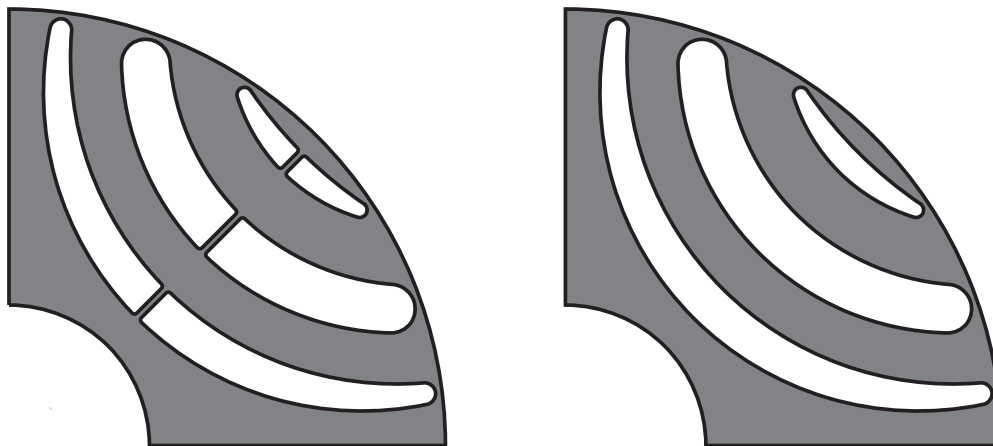


Figure 5.1: The different rotor structures.

## 5.2 Mechanical Design of the Rotor

Due to the rotor change for the saliency requirement, the mechanical strength of the structure was checked. A simple force diagram is shown in Fig. 5.2. Only the forces due to the centrifugal forces is shown. The forces due to the magnetic field or the acceleration is not taken into account. The assumption is made that these forces are negligible in steady operation. This can not be verified and is beyond the scope of the this study.

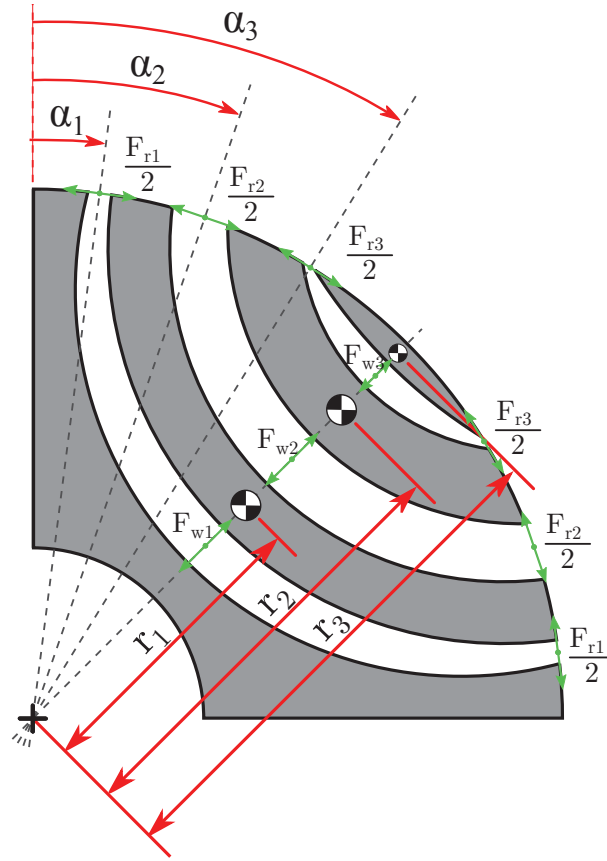


Figure 5.2: Force diagram to calculate the forces on the rotor.

To analytically calculate the the forces in the rotor ribs without the webs eq.5.2.1 to 5.2.3 can be used. Both rotors are made from M530-65A, the thickness of a lamination is 0.65 mm. The tensile strength is,  $\sigma_T = 450$  MPa and the yield strength is,  $\sigma_Y = 315$  MPa. The breadth of the rib is 1.2 mm. The density of the material is,  $\rho = 7700$  kg/m<sup>3</sup>. The mass of a flux path can be calculated as

$$m_n = \rho \cdot A_n \cdot t, \quad (5.2.1)$$

where  $m_n$  is the mass of a flux path,  $\rho$  is the density of the material,  $A_n$  is the area of a flux path and  $t$  is the thickness of the lamination. The centrifugal force due to the mass can be calculated as

$$F_{c_n} = r_n \cdot m_n \cdot \omega^2 \quad (5.2.2)$$

where  $F_{c_n}$  is the centrifugal force of a flux path,  $r_n$  is the distance to the center of gravity from the center point and  $\omega$  is the rotational speed. The total centrifugal force can be calculated as

$$F_T = \sum_{k=1}^n F_{c_n} \quad (5.2.3)$$

where  $F_T$  is the total centrifugal force. It is difficult to accurately determine the stresses and displacements with this method due to the assumptions and simplifications.

To determine the stresses and displacements more accurately mechanical FEM was used. Only the centrifugal force was taken into account. The rotor speed was the rated speed of 4800 r/min. The FE was run in SimXpert, a commercial FE software. The results from this analysis is shown from Fig.5.3 to Fig.5.6. By removing the webs in the rotor increases the stresses in the ribs significantly, up 2.7 times and the maximum displacement of the rotor also increase up 2 times. The maximum stress in the barrier is still less than the yield strength and the the displacement of the rotor is so small it would not have an effect on the airgap. Therefore the rotor without the ribs can be used with confidence.

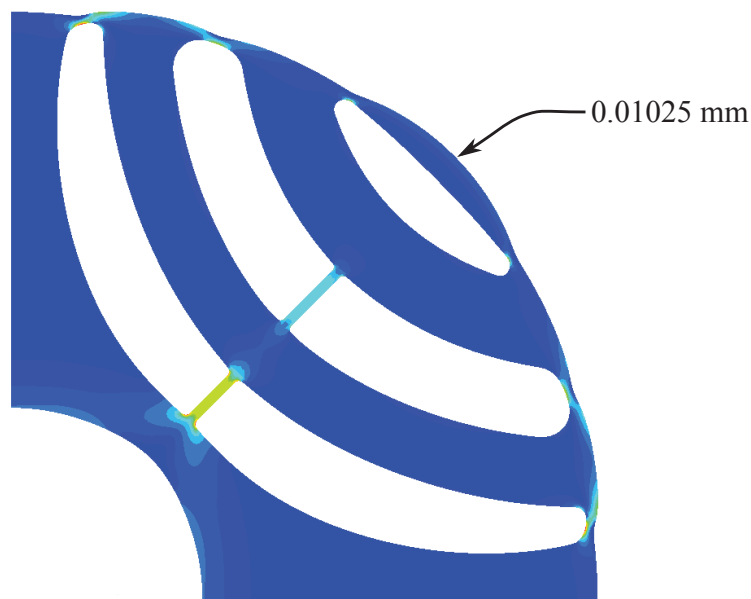


Figure 5.3: The displacement(exaggerated) and stresses in the rotor with the webs due to the centrifugal force.

## 5.3 Calculated performance results

### 5.3.1 Chording the stator and skewing the rotor

The effect by chording and skewing the machine with the NO20 stator laminations is shown in Table 5.1. The rotor is skewed by one slot pitch and the stator is chorded 7/9. The torque and torque ripple reduced when the machine

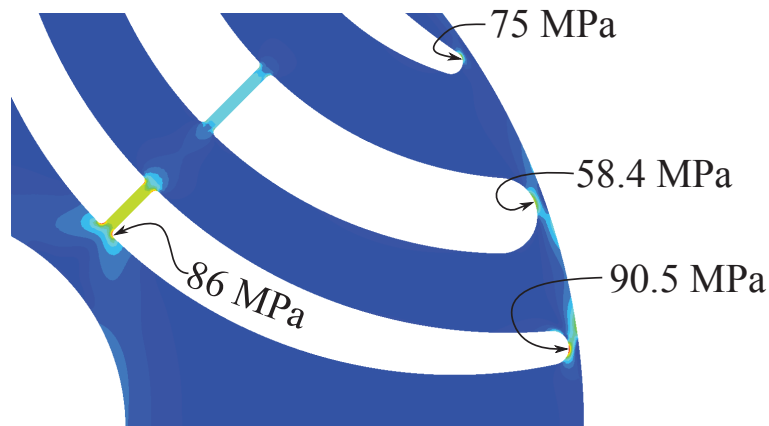


Figure 5.4: The maximum stresses in the webs and the ribs.

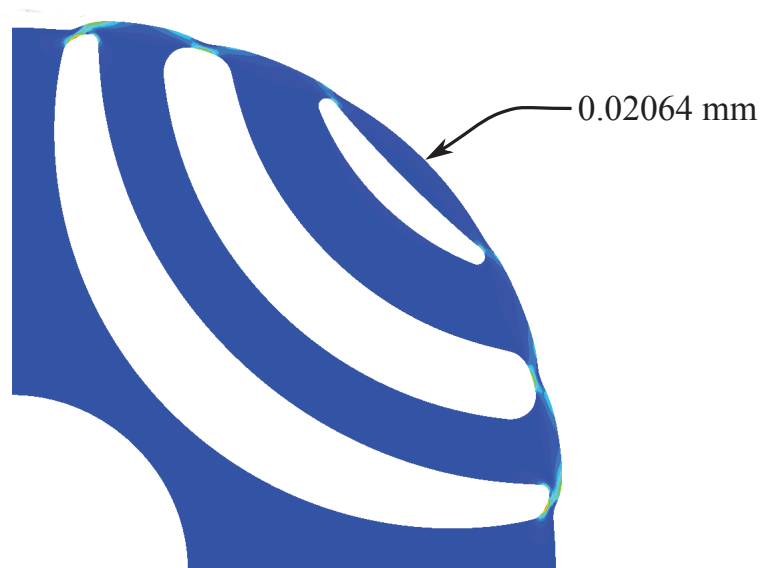


Figure 5.5: The displacement(exaggerated) and stresses in the without the webs rotor due to the centrifugal force.

was skewed and chorded, even though the torque fell it is still in the design specification. The torque ripple is low enough for practical purposes.

### 5.3.2 Comparison between different motors at the rated conditions (S1)

The stacking factor in the stack of the stator with the NO20 laminations are calculated as 93% and the stator with the M530-65A laminations as 98%. The stacking factor for the rotors are calculated as 98%. The simulation results for

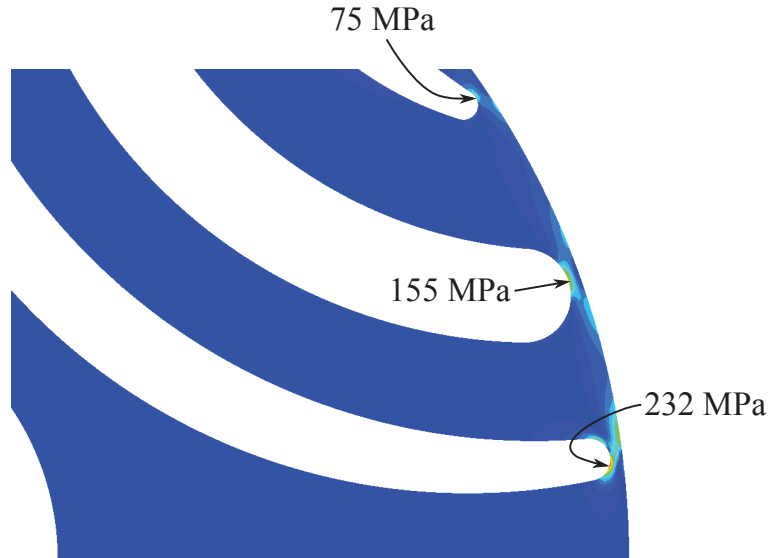


Figure 5.6: The maximum stresses in the rotor without the ribs.

Table 5.1: Different results from chording and skewing the machine.

	Unskewed Unchorded	Skewed Unchorded	Unskewed Chorded	Skewed Chorded
Torque(Nm)	74.71	72.68	71.02	69.35
$T_{ripple}$ (p2p)	16.96	10.51	13.19	6.49

the rated condition (S1) are given in Table 5.2.

### 5.3.3 Efficiency maps of the different motors

The machines were simulated at different operation points to calculate the efficiency maps of the two different motors using the methods discussed in Chapter 3. The points on the graphs show the simulated points and the results are shown in Fig's 5.7 and 5.8. Both motors have high efficiencies above 90% at the rated condition.

## 5.4 Summary

- The cooling of the motor was changed to reduce the cost of the machine.
- The webs in the rotor was removed to increase the saliency of the motor. This change effected the mechanical strength of the motor, however the rotor is still mechanically strong enough to operate at the rated speed.

Table 5.2: Simulation Results for the different motors at operating point S1.

Variable	NO20	M530	Unit
Lamination Thickness	0.2	0.65	mm
$T_{avg}$	69.35	71.49	N·m
$T_{ripple}$	6.49	6.62	%
n	4800	4800	rev/min
$I_{RMS}$	138.6	138.6	A
$V_{ph}$	125.7	138.8	V
$R_s$	0.02	0.02	$\Omega$
f	160	160	Hz
$P_{in}$	37.33	39.14	kW
$P_{out}$	34.82	35.93	kW
$P_{cu}$	1728	1728	W
$P_c$	596	1291	W
PF	0.71	0.7	-
$\delta$	67	67	$^\circ$
$\eta$	93.4	92.0	%

- The lamination steel of the rotor is changed from NO20 to M530-65A to reduce the cost of the machine. This increases the ironloss of the RSM.
- Another motor is built with M530-65A laminations. This is done to compare the ironloss and the efficiency between the two different motors.
- The skewing and chording reduced the torque and torque ripple, however they are both in the design specification.
- The RSM with the NO20 motor has a higher efficiency as the motor with the M530-65A laminations at the rated condition. This is expected because the NO20 laminations has a lower ironloss. The performance of the M530-65A motor is however still acceptable and a large part of the efficiency is above 90%.



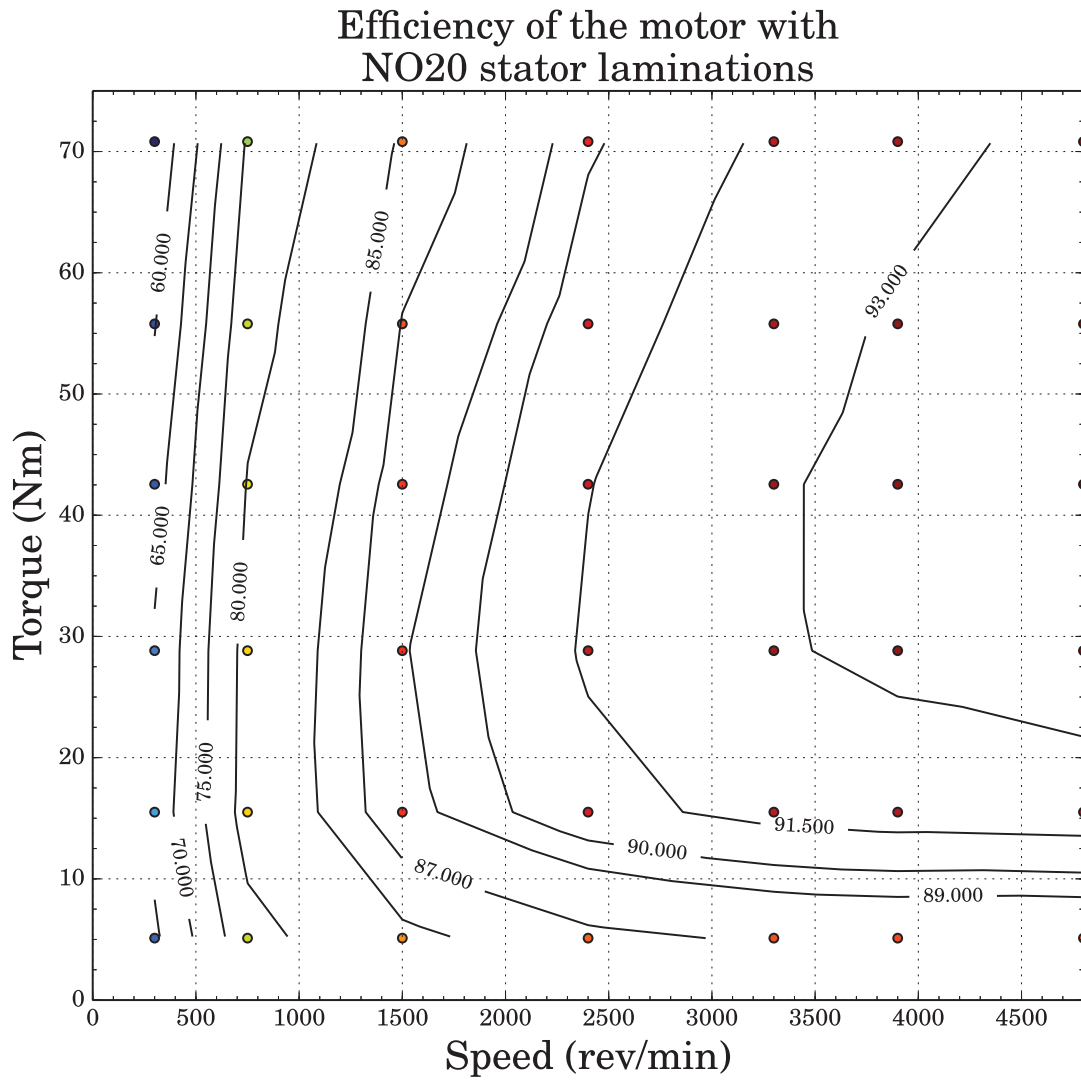


Figure 5.7: Simulated efficiency map of the motor with NO20 stator laminations.

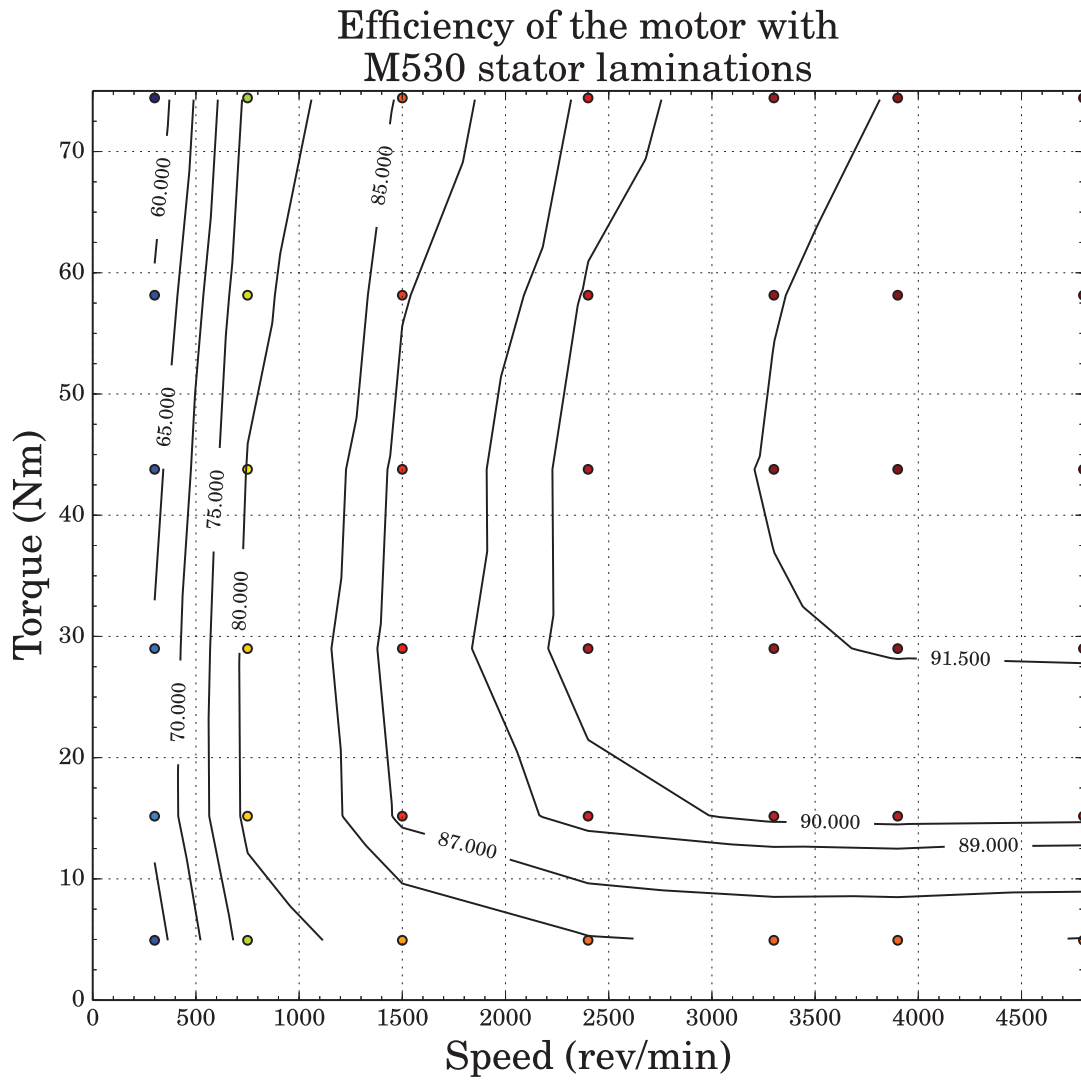


Figure 5.8: Simulated efficiency map of the motor with M530 stator laminations.

## Chapter 6

# Constructed RSM and test benches for an EV

The following section describes constructed RSM and the two test bench designs and construction.

### 6.1 Built motor

The motor is shown in Fig. 6.1. Both motors look the same only the laminations of the stators differ. To connect the RSM to the gearbox, splines were cut into the shaft. The splines are visible in Fig. 6.1. The connected motor and gearbox are shown in Fig. 6.2.



Figure 6.1: Photo of the RSM. The shaft has splines cut into it to fit into splines of the gearbox.

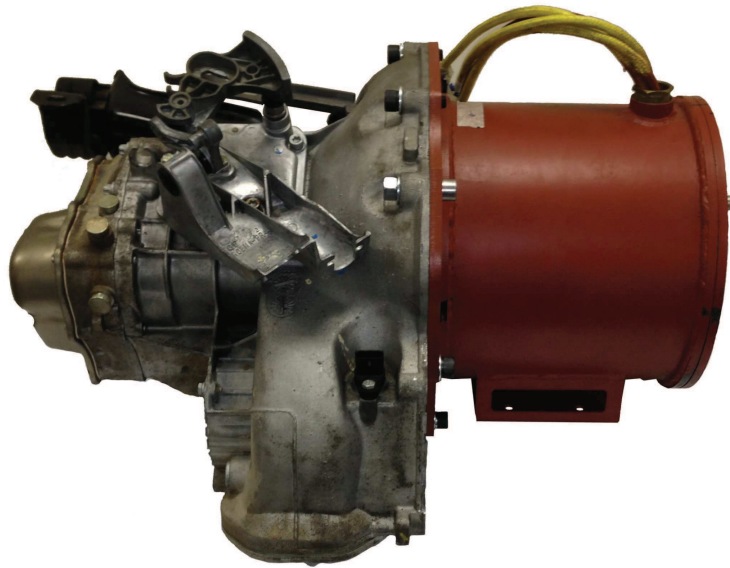


Figure 6.2: The power train connection of the RSM to the gearbox and differential.

## 6.2 Test Bench 1

The first testbench that was designed and built to measure the performance of the physical motor with the simulated motor. A layout schematic of the testbench can be seen in Fig. 6.3. The constructed test bench can be seen in Fig. 6.4. The motor is connected to an eddy-current dynamometer via propshafts. The torque and speed sensor is between the two propshafts.

To measure the input power, a Norma 5000 power analyser is used. The torque and speed is measured with a Lorenz messtechnik 500 Nm torque sensor. The digital torque sensor is connected to a PC via a USB cable. Lorenz supplies the necessary software for the measurement. The load is supplied by the eddy current dynamometer. The eddy current dynamometer is water cooled.

## 6.3 Test Bench 2

The aim of the second test bench is to be able to measure a drive cycle on the test bench while measuring the efficiency of the whole system. The motor is connected to the gearbox of the Corsa as in Fig. 6.2.

The design is also implemented to move the power train seamlessly between the vehicle and the test bench. In Fig. 6.5 the three stands show where the drive train is mounted in the engine compartment of the vehicle. This makes it easier to test different battery packs and different control techniques and algorithms. As with most first iterations the design is not ready to test a

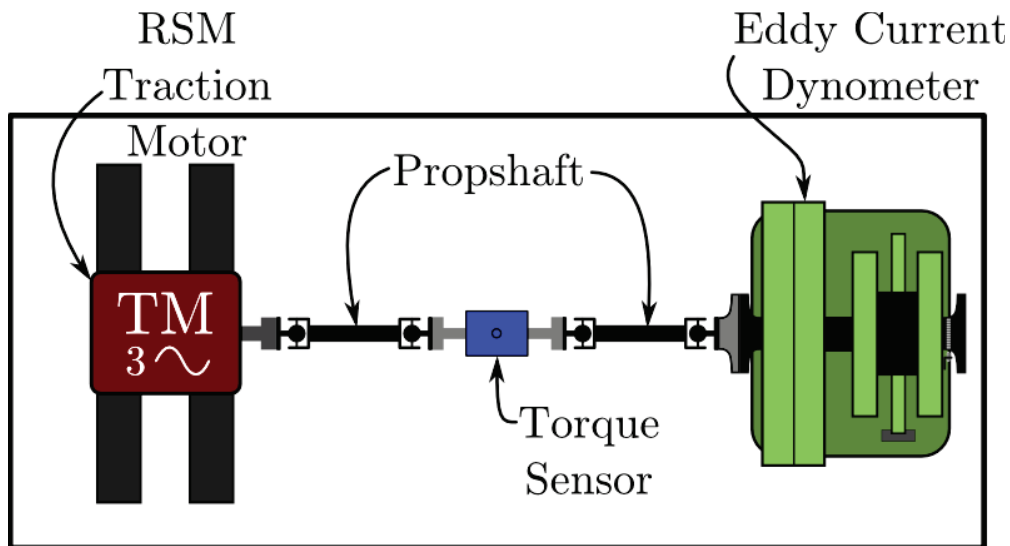


Figure 6.3: Schematic layout of the test bench to measure the performance of the RS motor.

drive cycle, only the efficiency of the power train. There are still a few design alterations to be made to properly measure a drive cycle. However, the upside is that before investing a lot of money into the concept it is possible to measure the efficiency of the variable gear speed gearbox. The constructed test bench can be seen in Fig. 6.6.

The input power is measured with the Norma 5000 power analyser. The Norma 5000 is connected to PC with a RS232 to USB cable. The information is fed into National Instruments Labview. The torque is determined from 500kg loadcells. The loadcell is connected to a torque arm on the dynamometer. The speed is measured with a magnetic pulse-pickup. These signals are sent to National Instruments CompactDAQ. The DAQ is connected to PC via a USB cable, here the information is sent to Labview. The load supplied by the dynamometer can either be controlled manually or via the CompactDAQ. A schematic of the measuring layout and the measuring equipment can be seen in Figs. 6.7 and 6.8.

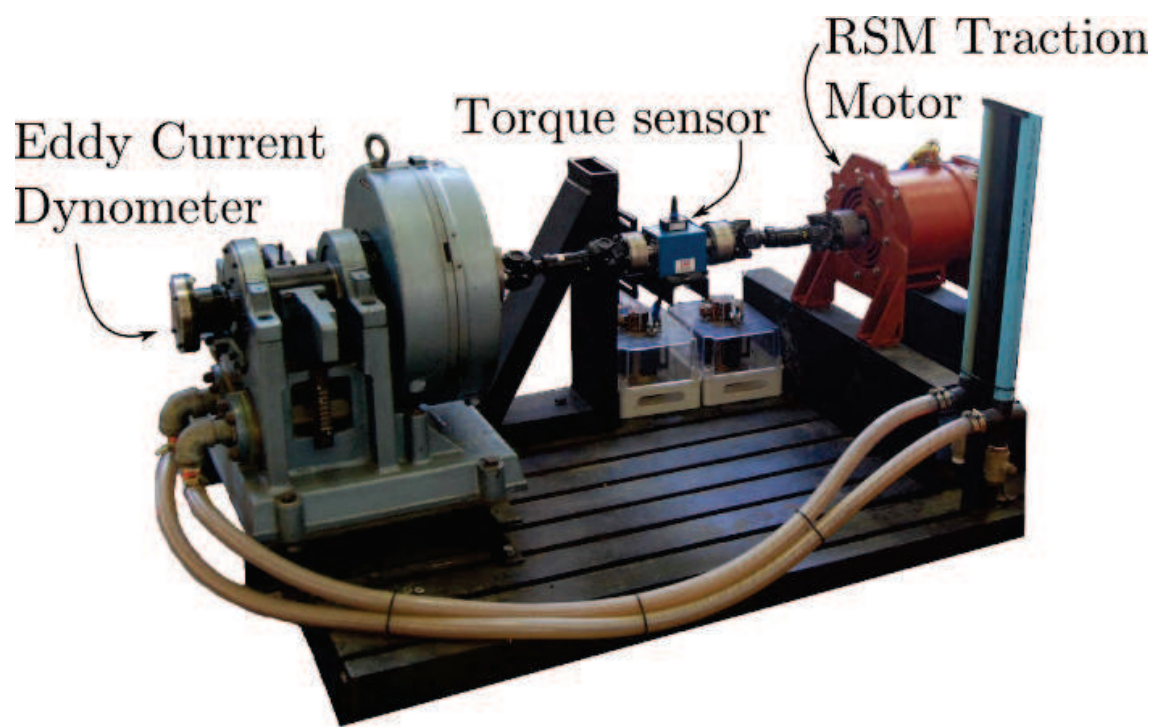


Figure 6.4: Layout of the testbench to measure the performance of the RS motor.



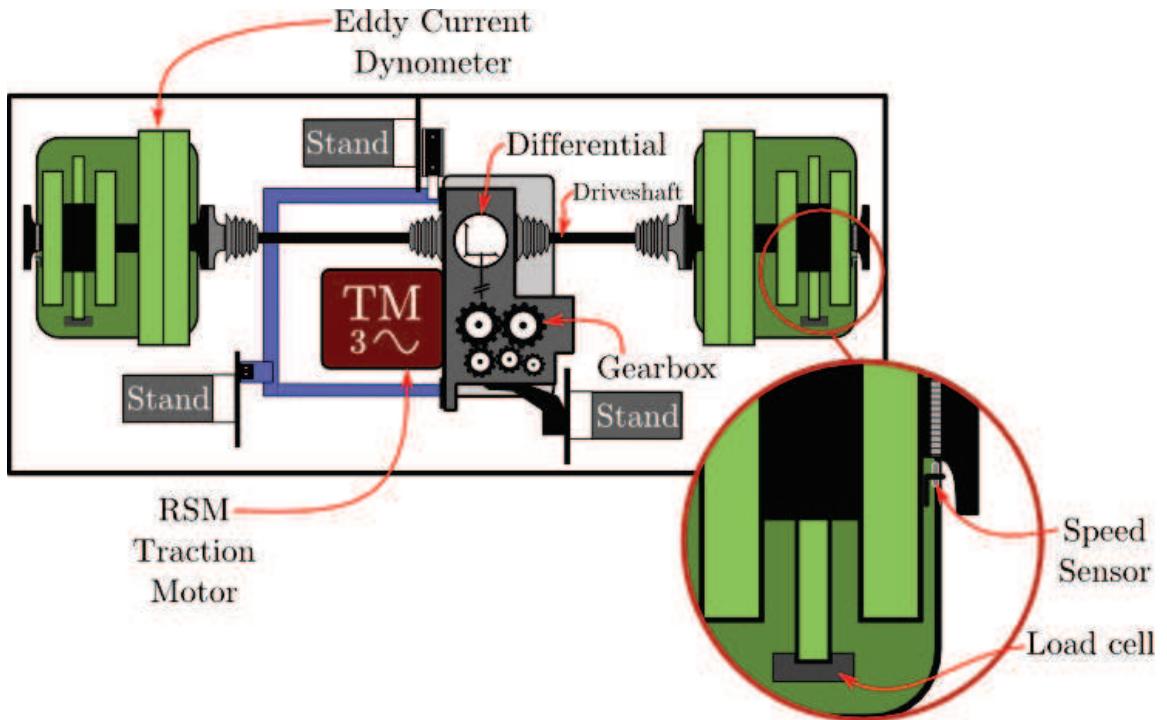


Figure 6.5: Schematic layout of the testbench to measure the performance of the drive train.

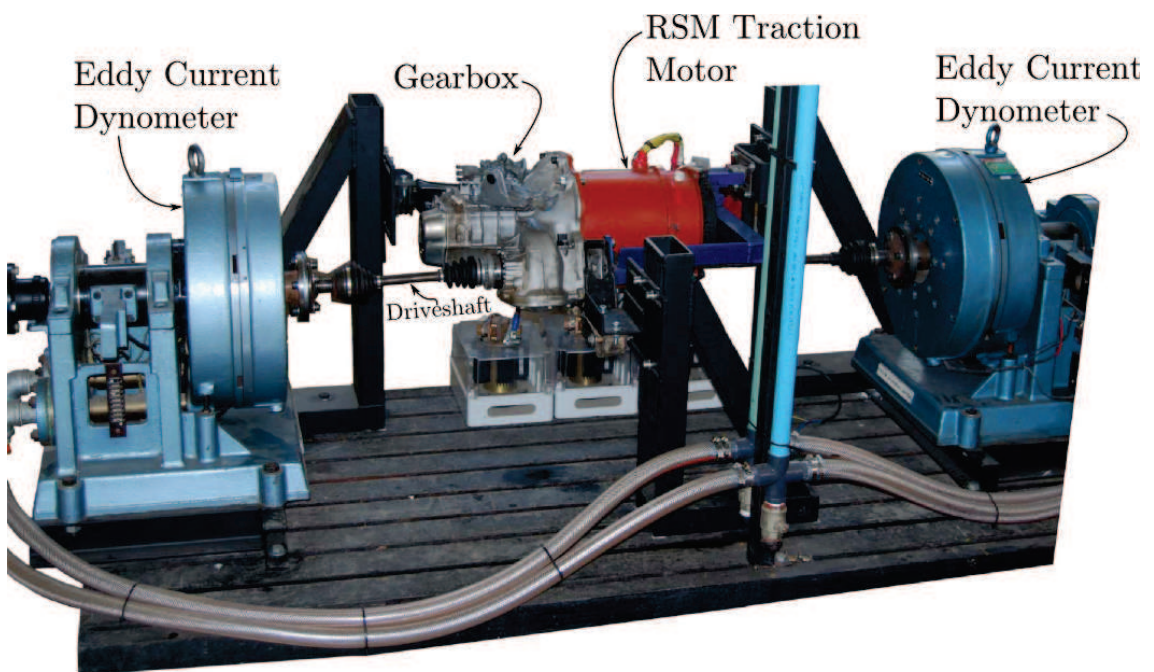


Figure 6.6: Layout of the testbench to measure the performance of the drive train.

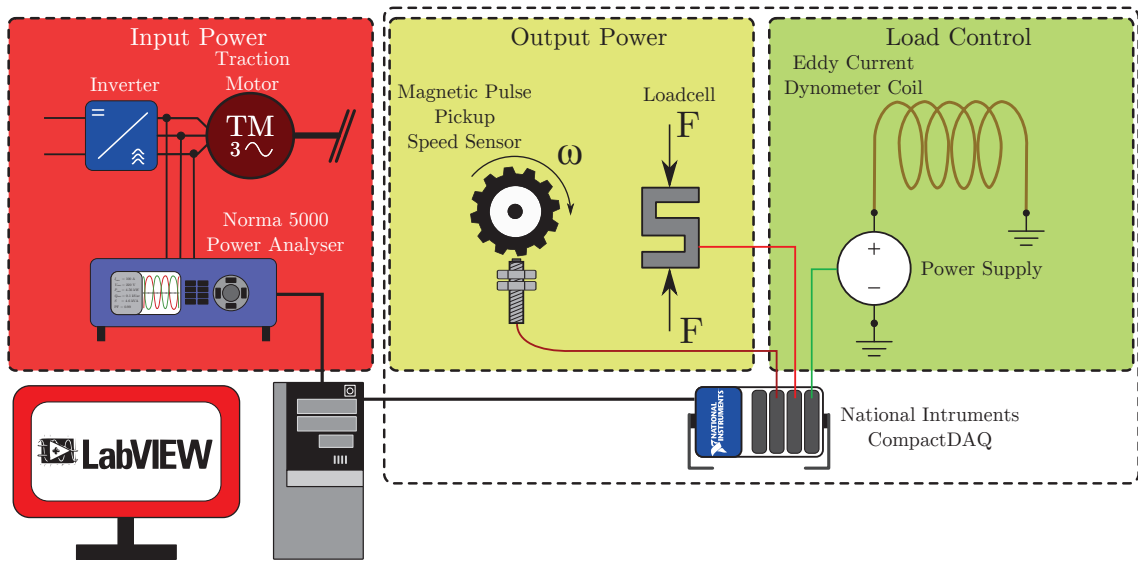


Figure 6.7: Schematic layout of the measuring equipment of the testbench to measure the performance of the drive train.

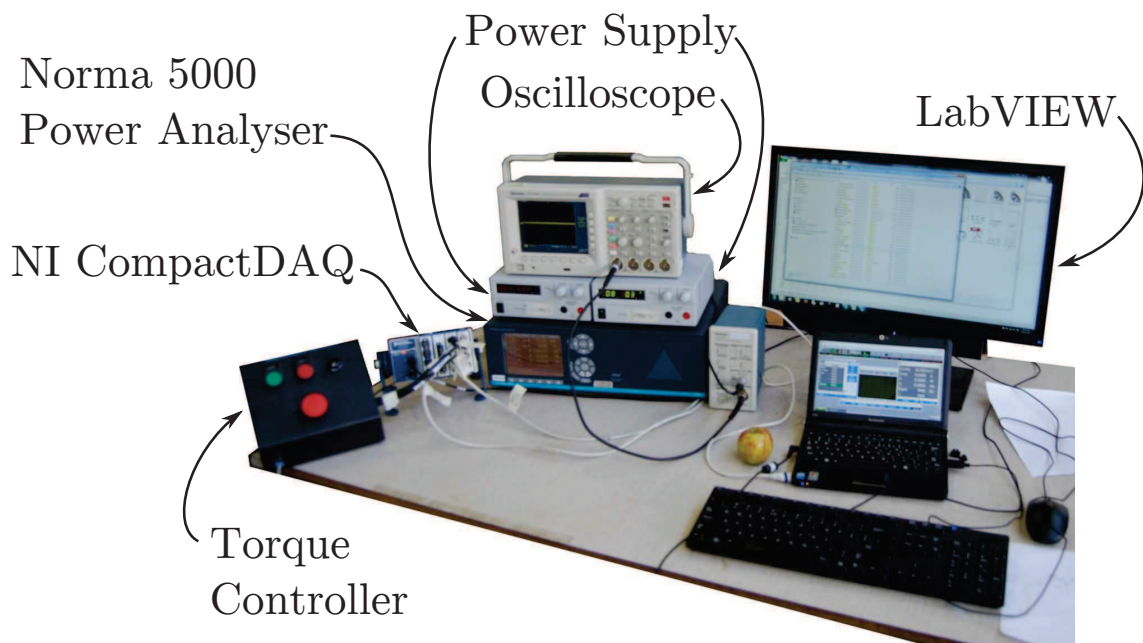


Figure 6.8: Layout of the measuring equipment of the testbench to measure the performance of the drive train.



# Chapter 7

## Measured results of the motors

This Chapter discusses all the measured results. The weight, resistance and performance of the motor is measured.

### 7.1 Measured weight

The weight of all the components can be found in Table 7.1.

### 7.2 Measured resistance

The motor is connected in star(Y-connection).The calculated resistance is 20 m $\Omega$  at 75°C and the calculated resistance is 16.5 m $\Omega$  at 20°C. The measurements were done from phase to neutral at a room temperature of 20 °C with a micro-Ohmmeter and are shown in Table 7.2. The measured values of the two stators differ. The resistance of the stator with M530-65A laminations is

Table 7.1: Measured weight of the motor and the components.

Part	Weight(kg)
Front plate	7
Back plate	4
Rotor with bearings	11
Stator and housing	34
RSM Total	56
Gearbox	35
Motor and Gearbox	91
Fan (Optional)	1.5
Clutch and Flywheel (Optional)	19
Total	111.5

7.65% higher than the stator with the NO20 laminations. Therefore if the coil temperature and the current is the same the copperloss will be 7.65% higher for the stator with the M530-65A laminations. This error is due to the quality control of the manufacturer, as the difference is very large. The calculated value is lower than both of the measured resistances, this is due an error in approximating the the end-winding length and the fill factor.

Table 7.2: Measured resistance of the different stators.

Phase	A	B	C	Average
NO20	18.875 m $\Omega$	18.875 m $\Omega$	18.85 m $\Omega$	18.867 m $\Omega$
M530-65A	20.19 m $\Omega$	20.47 m $\Omega$	20.26 m $\Omega$	20.31 m $\Omega$

### 7.3 Motor measurements

The motor was designed to operate at the rated condition (S1) and is tested from zero speed and torque to S1. The motors can't be tested at higher torques or speeds, the inverter and the test benches are not designed for this.

There was much difficulty in configuring the drive for the application. The drive was built and designed in-house.

It is decided to measure an efficiency map for the two motors. This would show the performance difference between the the two laminations and would make it possible to determine a method to approximate the ironloss. However this would not be so easy as there was much difficulty experienced with the measurements. Due to the inherent characteristics of the motor and the test bench there was problems with vibrations. This caused much difficulty as these oscillations had an effect on the control of the motor. At 100-105Hz and 150-160Hz electrically these vibrations and oscillations was the worst. A difference in the resistance makes an comparison between the stators difficult and the system would require temperature measurement to determine the resistance and copper loss more accurately. There was also problems with EMC that was caused from the drives and equipment surrounding the test environment. This caused the communication between the Norma 5000 power analyser and the PC Labview system to fail. After several attempts to re-establish communication it was decided to record the measurements manually. The complexity in solving these EMC problems are beyond the scope of this study. The coil temperature was only checked with a thermal gun at different intervals. The windage and friction losses for the motor was also not tested and the loss will therefore must be approximated by analytical equations. The propshafts used in the

system makes it difficult to measure the torque ripple as they also cause speed oscillations.

The motor was in torque or current control mode and the speed was controlled with the dynamometer.

### 7.3.1 Measured results NO20

The result from the rated condition (S1) test is seen in Table 7.3. The required speed could not be reached due to a natural frequency resonance in the system. However the results are close to the simulated results.

Table 7.3: Measured results of the NO20 stator at the designed and specified point.

	$I_\phi$ (A)	$V_\phi$ (V)	PF	$S_{in}$ (kVA)	$P_{in}$ (kW)	n (r/min)	T (Nm)	$\eta$
Measured	142.28	116.01	0.71	49.52	34.8	4375	69.5	91.6

The machine was tested at different points to determine an efficiency map for the motor. Each dot on the graph is a measured point. It took much time to measure all the desired points. The ambient temperatures differed and the temperatures of the coils also differed at different points. The temperature was checked at non regular intervals with a thermal image gun, the coil temperature could only be checked at the drive end of the motor through a opening in the front flange. A fan is mounted to the back of the motor and the temperature distribution through the motor is non-regular, the non-drive end is much cooler than the drive-end. The measured temperatures differed, the average temperature was approximately 95°C. Due to the natural frequencies and the measurements error it was decided to fit the data to an equation. An online equation fitting tool that can fit a whole variety of 2D and 3D equations to data [46] is used. The fitting errors are shown and the user can then select the best fit according to his opinion with multiple options. To get a good fit to the data, the data was scaled to between 0 and 1, by dividing the speed by 4800 r/min and the torque by 75 Nm. The resulting equation is given in eq. 7.3.1, where  $x$  is the speed (pu) and  $y$  is the torque (pu). The parameters of the equation are given in Table 7.4. The resulting contour plot is shown in Fig. 7.1.

$$\eta = a + b \cdot \ln(x) + c \cdot \ln(y) + d \cdot \ln(x)^{2.0} + f \cdot \ln(y)^{2.0} + g \cdot \ln(x) \cdot \ln(y) \quad (7.3.1)$$

Table 7.4: Equation parameters for eq. 7.3.1

Parameter	a	b	c	d	f	g
Value	9.0723e-1	1.2062e-2	-1.7306e-2	-2.5995e-2	-2.8559e-2	6.605e-3

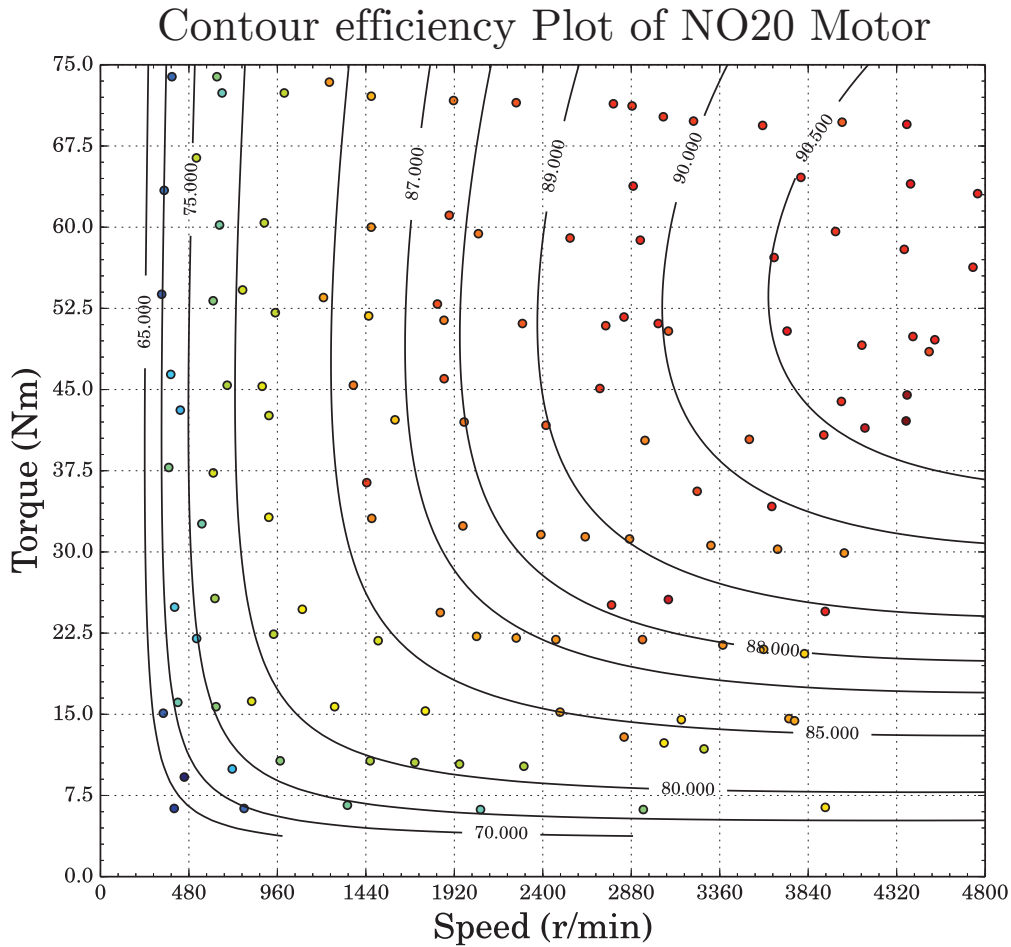


Figure 7.1: Contour efficiency map for motor with NO20 stator for torque versus speed.

### 7.3.2 Measured results M530-65A

It was possible to reach the rated condition with the M530-65A motor. The efficiency of the motor was below 90% at the rated condition the result is shown in Table 7.5. Due to the difficulty experienced in the measurement of the NO20 motor a thermocouple was attached to a coil at the drive end of the motor. This made it easier to monitor the temperature and the operating temperature was kept between 60-70 °C. To draw the efficiency map the same method was used as in the previous section. To get a good fit to the data, the data was scaled to between 0 and 1, by dividing the speed by 4800 r/min and the torque by 75 Nm. The resulting equation is given in eq. 7.3.2, where  $x$  is the speed (pu) and  $y$  is the torque (pu). The parameters of the equation are given in Table 7.6. An efficiency map of the machine is shown in Fig 7.3. The approximation error due to using this eq. 7.3.2 is shown in Fig. 7.4. The efficiency of the motor is high throughout the speed and torque spectrum. The

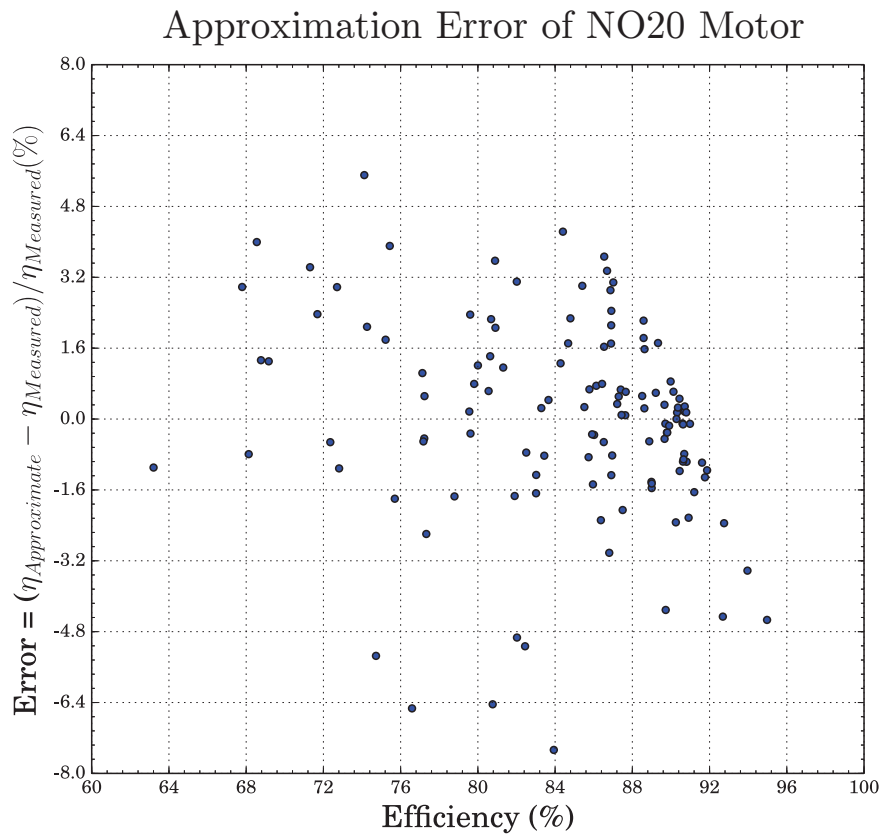


Figure 7.2: Efficiency approximation error for motor with NO20 stator.

high efficiency region at low torque is different from the simulated values. This is possibly due to the higher ironloss at higher torque and is underestimated with the FE software.

Table 7.5: Measured results of the M530 stator at the designed and specified point.

	$I_\phi$ (A)	$V_\phi$ (V)	PF	$S_{in}$ (kVA)	$P_{in}$ (kW)	n (r/min)	T (Nm)	$\eta$
Measured	137.00	124.00	0.705	50.95	35.93	4811	63.55	89.2

$$\eta = a + b \cdot \ln(x) + \frac{c}{y} + d \cdot \ln(x)^2 + \frac{f}{y^2} + g \cdot \frac{\ln(x)}{y} \quad (7.3.2)$$

Table 7.6: Equation parameters for eq. 7.3.2

Parameter	a	b	c	d	f	g
Value	8.694e-01	1.4798e-03	1.2444e-02	-3.0804e-2	-1.27453e-03	-6.1271e-03

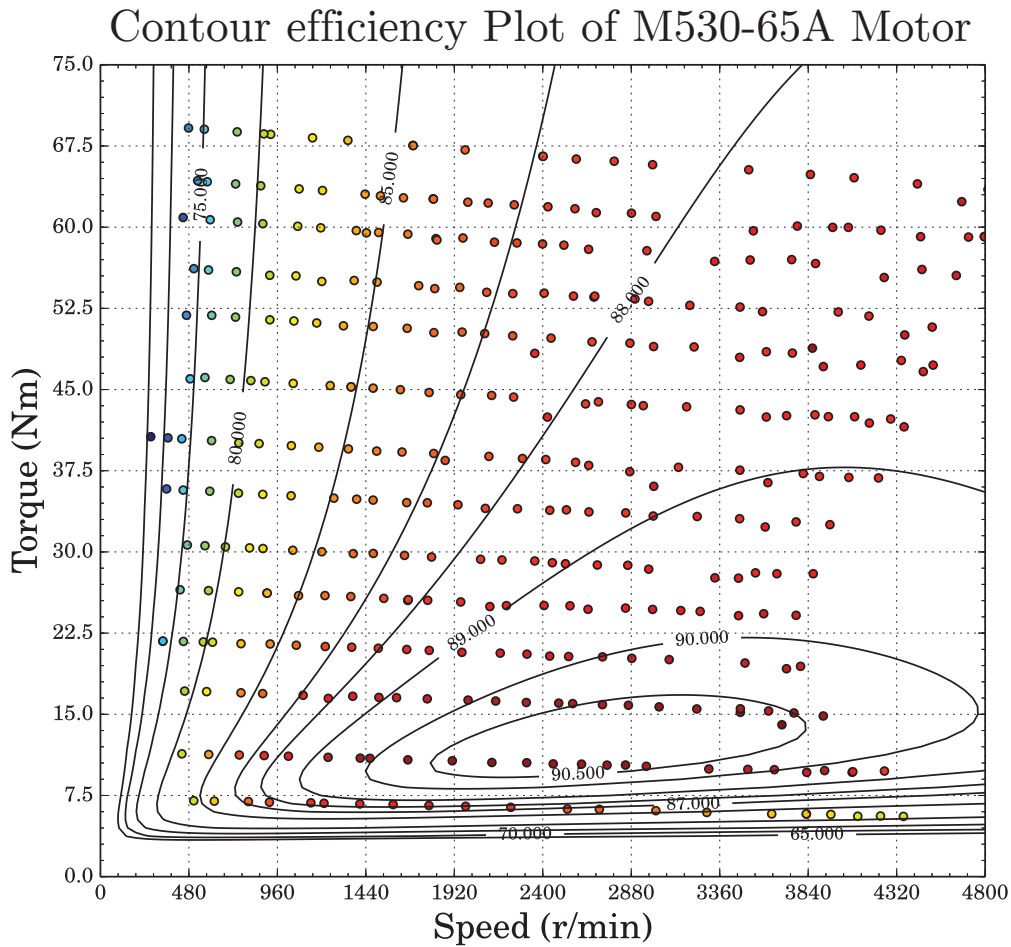


Figure 7.3: Contour efficiency map for the motor with the M530 stator laminations for torque versus speed.

## 7.4 Summary

- The calculated and measured resistance values differ this is due to an approximation error of the end-winding length and the fill factor that is used in the calculation.
- The resistances of the two built motors differ, this is due to manufacturing differences.
- The motors can only be tested up to the rated condition (S1). There are problems with mechanical vibrations and EMC, this had an influence on the measurements.
- The two different motors were not tested at the same ambient and coil temperatures.

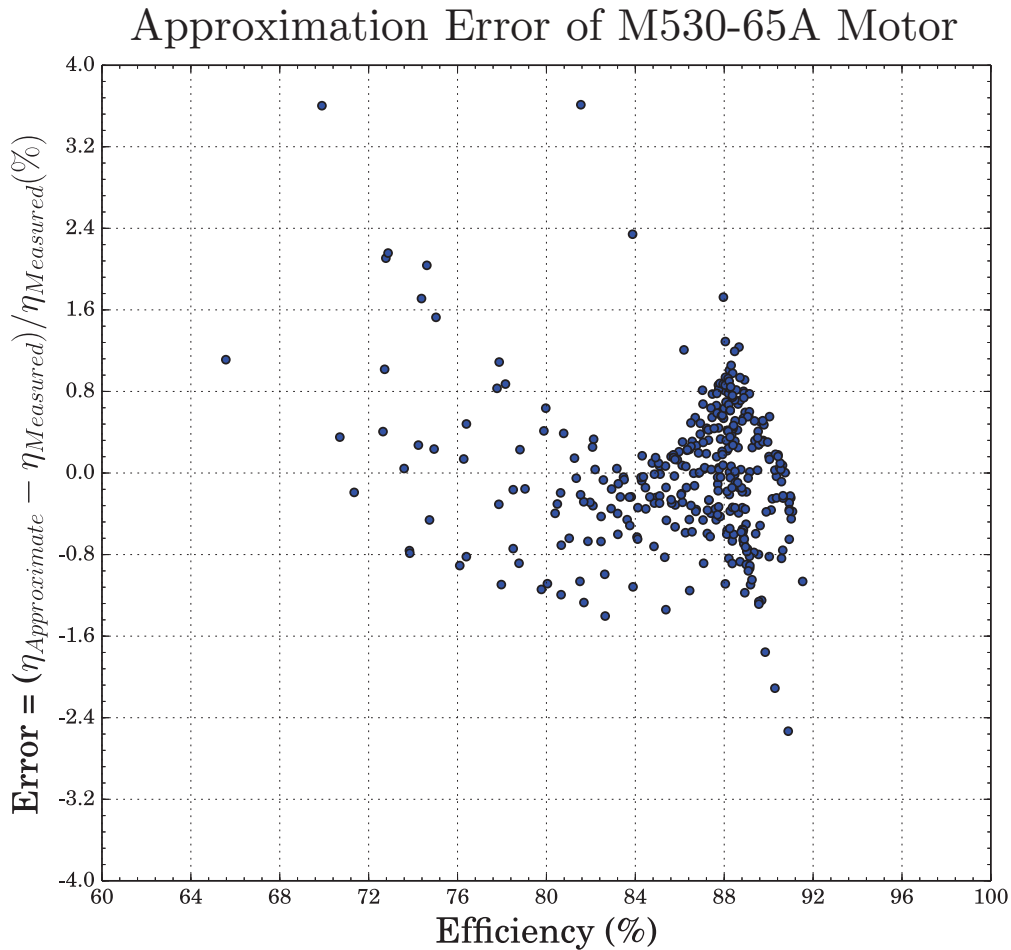


Figure 7.4: Efficiency approximation error for the motor with the M530-65A stator laminations.

- The test bench was not designed to measure the windage and friction losses and due to time constraints there was not a possibility to measure the losses on a different test bench.
- The cooling of the motor was not regular and the the non-drive end was cooler than the drive end.
- The equations used to determine the efficiencies of the motors are accurate and the error in using these equations are small. The extrapolated region should be used with caution.
- The simulated and measured efficiency maps of the stator with the NO20 laminations show resemblances and the biggest difference is the efficiency that is over estimated in the FE simulation.

- The simulated and measured efficiency maps of the stator with the M530-65A laminations differ. The measured efficiency is much higher at low torque than at the rated condition, this is due to the ironloss that is predicted lower in the FE simulation.



# Chapter 8

## Powertrain measured results

The section discusses the system, motor and gearbox efficiency in 4<sup>th</sup> and 5<sup>th</sup> gear. Due to the limitations on the eddy current dynamometers, not all the gears could be tested.

### 8.1 Measured powertrain and approximated gearbox efficiency results

The motor with the NO20 laminations is connected to the bellhousing of the gearbox to form the drive train. The same communication error was experienced between the Norma 5000 and Labview on the PC. Therefore the results were recorded manually. All the gears were tested, however the dynamometers can't handle high torque at low speed and the results from these measurements are inconclusive. The vibration on the system was much better compared to the vibration when only the motor was tested. This is because the motor was flange mounted on the bellhousing and the vibration mounting couplings helped to damp these oscillations.

The gearbox was run until the oil and the motor was warm. Because the motor was mounted on the gearbox the coil temperature could not be measured with the thermal image gun. There was also no sensors on the coils and the temperature could therefore not be measured. The cooling of the system was not optimised as the fan is blowing all the hot air to the gearbox and the gearbox is also generating heat. It is not clear at what temperature the motor was operating.

The results from these tests were also fitted to equations using an equation fitter. Therefore it is possible to calculate the efficiency of the gearbox. It is observed that even though the torque at the wheels was the same the speed might differ at times. The differential acts as a speed divider and the speed is summed together and halved to get an average value. The torque is summed together. The output power was then calculated from these averages. The input to the motor is measured but not to the inverter.

### 8.1.1 5<sup>th</sup> Gear

Most of the spectrum in 5<sup>th</sup> gear could be measured, the dots on the graph show a measured point, with most of the measurements possible and the rated speed and nearly the torque of the RSM was achieved in the measurements. The results were then fitted to eq. 8.1.1, where  $x$  is the speed (pu) and  $y$  is the torque (pu). The parameters for the equation are given in Table 8.1. The approximated efficiency plot is shown in Fig. 8.1.

$$\eta = a + b \cdot \ln(x) + \frac{c}{y} + d \cdot \ln(x)^2 + \frac{f}{y^2} + g \cdot \frac{\ln(x)}{y} \quad (8.1.1)$$

Table 8.1: Equation parameters for eq. 8.1.1

Parameter	a	b	c	d	f	g
Value	8.4832e-01	-6.4386e-02	-9.919e-03	-4.8934e-02	-8.6938e-04	-4.3625e-03

This result should be used with caution were there is no measured data. Where there is data available, the values would yield accurate results and the efficiency of the system could be approximated accurately. The error is shown in Fig. 8.2. Most of the error lies between -4 to 4 %, there are however points with larger error.

With the equations known to approximate the efficiencies of the motor and the power train, the gearbox efficiency can be calculated with eq. 8.1.2. The result should be used with caution as there are a lot of uncertainty and error from the motor efficiency and the power train efficiency. What is promising from these results is the approximated efficiency that is above 90% at speeds and torques where there are data available.

$$\eta_{Gearbox} = \frac{\eta_{System}}{\eta_{Motor}} \quad (8.1.2)$$

### 8.1.2 4<sup>th</sup> Gear

The same methodology as with approximating 5<sup>th</sup> gear was used in calculating and approximating 4<sup>th</sup> gear. Equation 8.1.3 approximates the efficiency of the system, where  $x$  is the speed (pu) and  $y$  is the torque (pu). The parameters of the equation are given in Table 8.2. The approximation of the system efficiency is shown in Fig. 8.4. As mentioned earlier the areas with no data points should be used with extreme caution.

$$\eta = a + b \cdot \ln(x) + c \cdot \ln(y) + d \cdot \ln(x)^2 + f \cdot y^2 + g \cdot \ln(x)\ln(y) \quad (8.1.3)$$

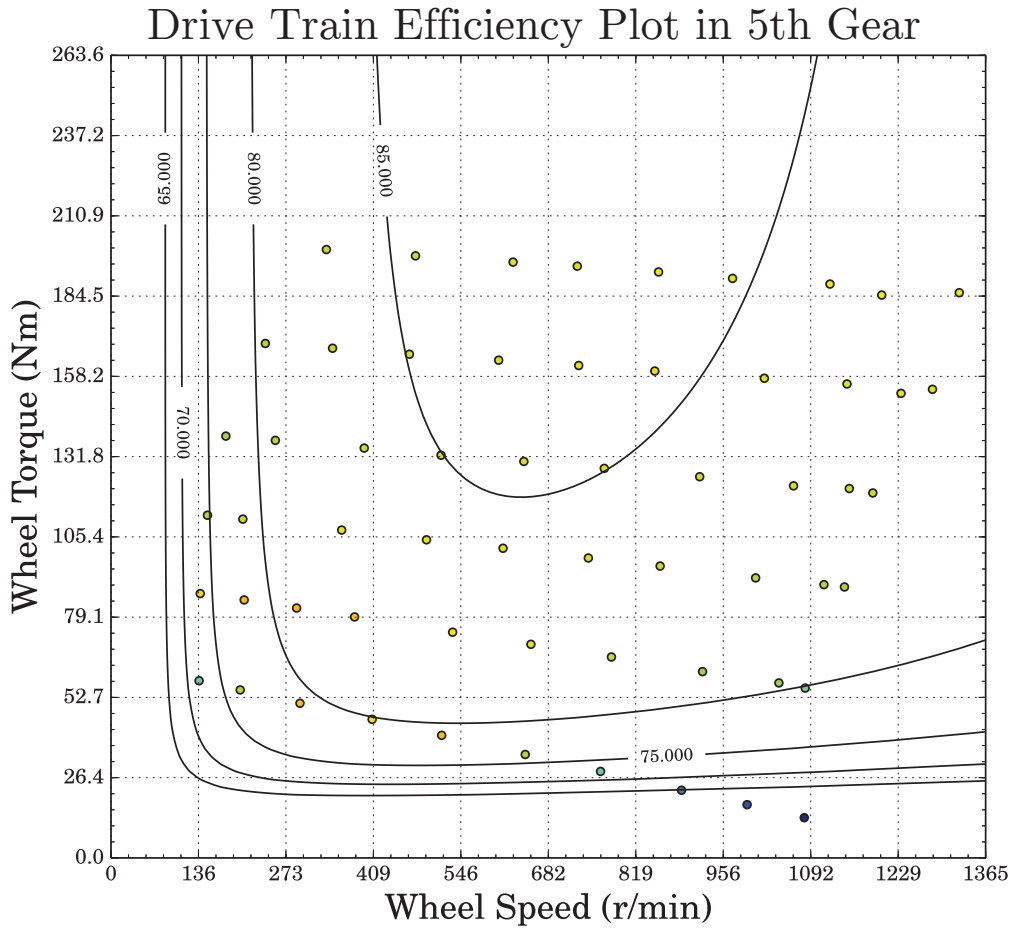


Figure 8.1: Contour efficiency map for system in 5th gear for torque over speed.

Table 8.2: Equation parameters for eq. 8.1.3

Parameter	a	b	c	d	f	g
Value	8.3808e-01	-1.0907e-01	1.9527e-02	-4.844e-02	-1.9538e-02	2.0756e-02

The error in approximating the efficiency is very small and within  $\pm 2\%$  of the measured values.

If eq. 8.1.1 is used to calculate the efficiency of the gearbox in 4<sup>th</sup> gear the result is shown in Fig. 8.6. The approximated efficiency is above 90% in most of the spectrum.

## 8.2 Summary

- Only 4<sup>th</sup> and 5<sup>th</sup> gear can effectively be measured, the rest of the test results for the gears are inconclusive.

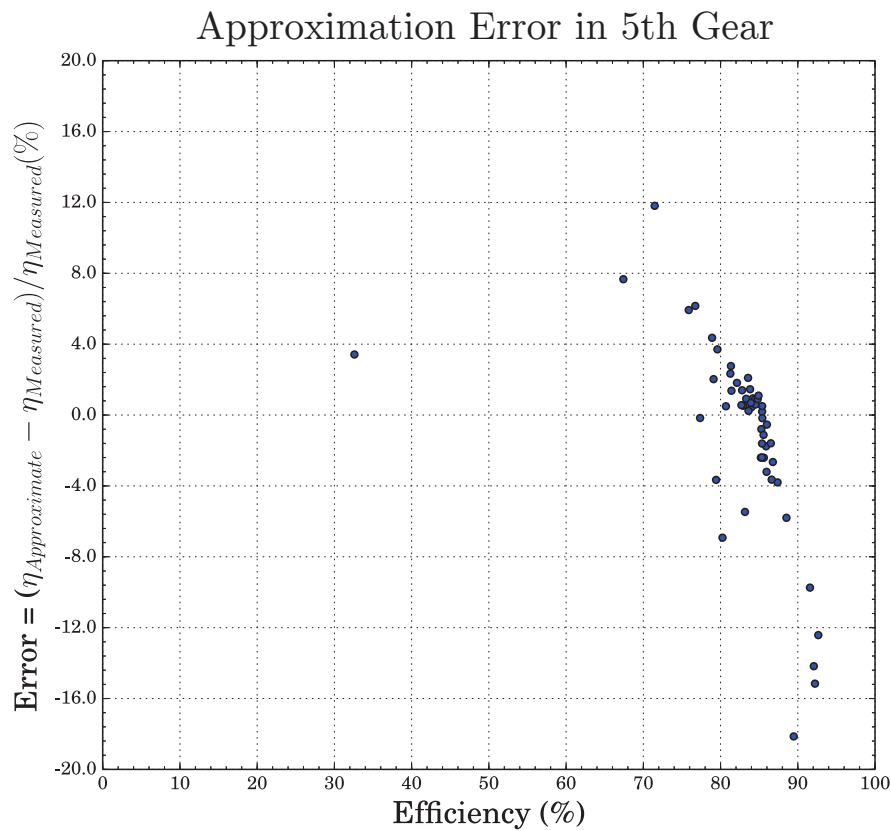


Figure 8.2: Error in the approximation for the system in 5th gear.

- The vibrations are less on test bench 2 than when only the motor is tested. This is due to the flange mounting of the motor and the vibration rubbers from the Corsa.
- It was not possible to measure the temperature of the coils in the motor and makes it difficult know how much the efficiencies of the motor differs in the different tests and how it compares to the test done only on the motor.
- The drive train efficiency in both gears are high, above 80% in most of the spectrum. This includes the motor and gearbox (gears and differential), the efficiency of the inverter is not included.
- The approximated efficiency of 5<sup>th</sup> and 4<sup>th</sup> gear is 90 - 96%, making the multi gear a competitor for the single speed gearbox in the EV power train.

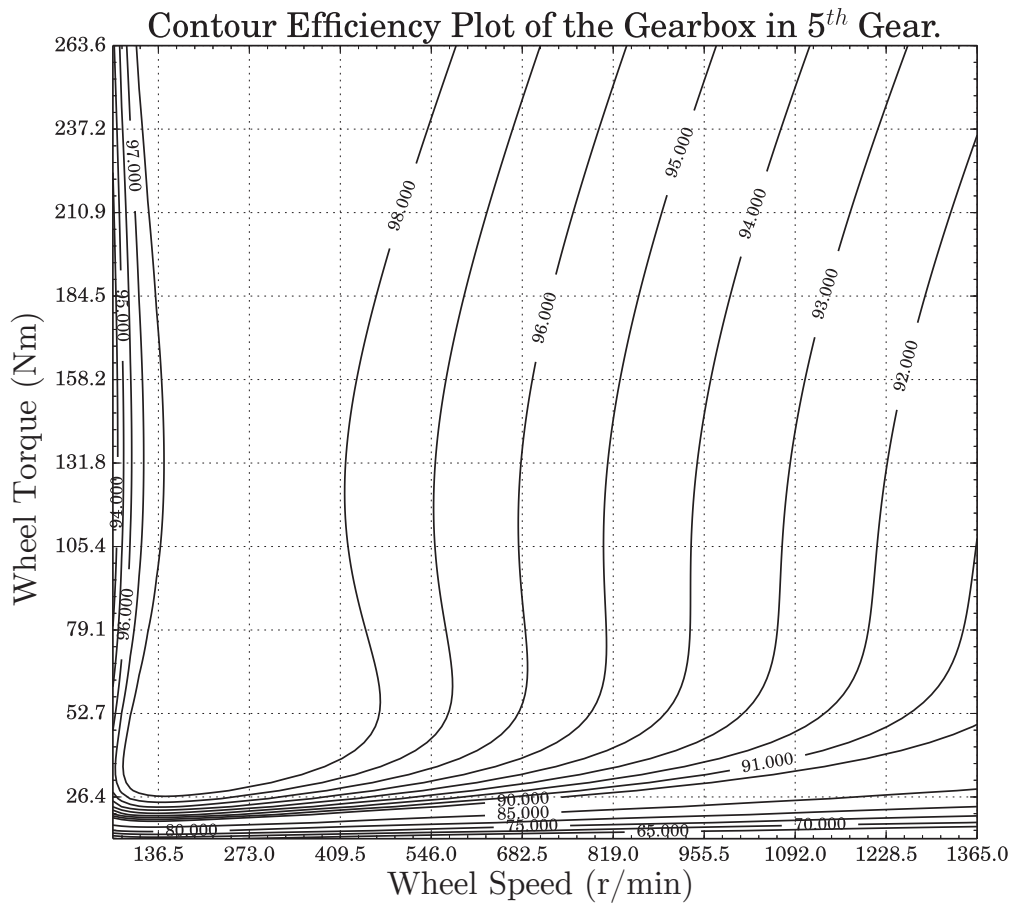


Figure 8.3: Contour efficiency map for the gearbox in 5th gear.

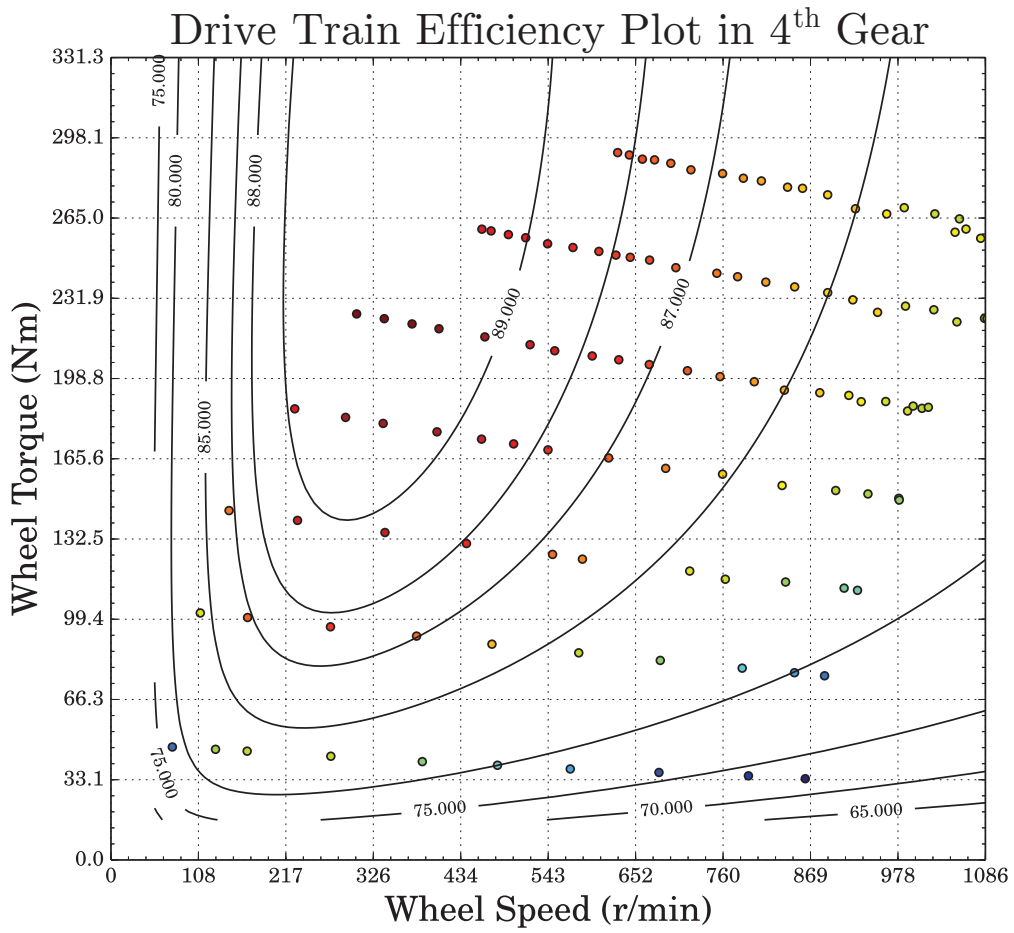


Figure 8.4: Contour efficiency map for system in 4th gear for torque over speed.

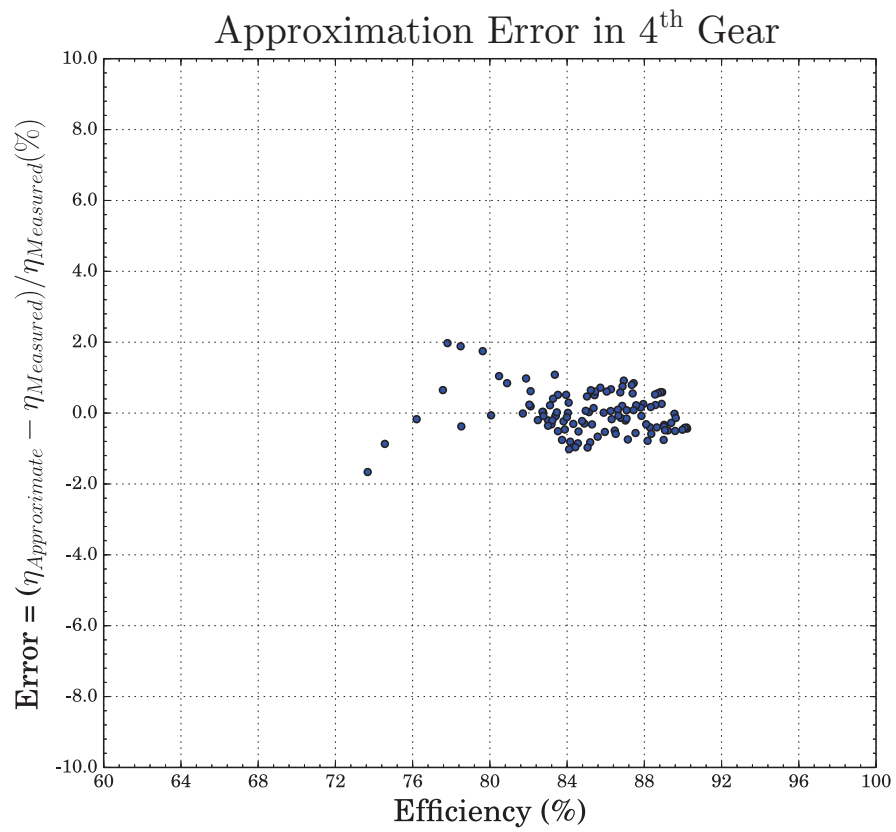


Figure 8.5: Error in the approximation for the system in 4th gear.

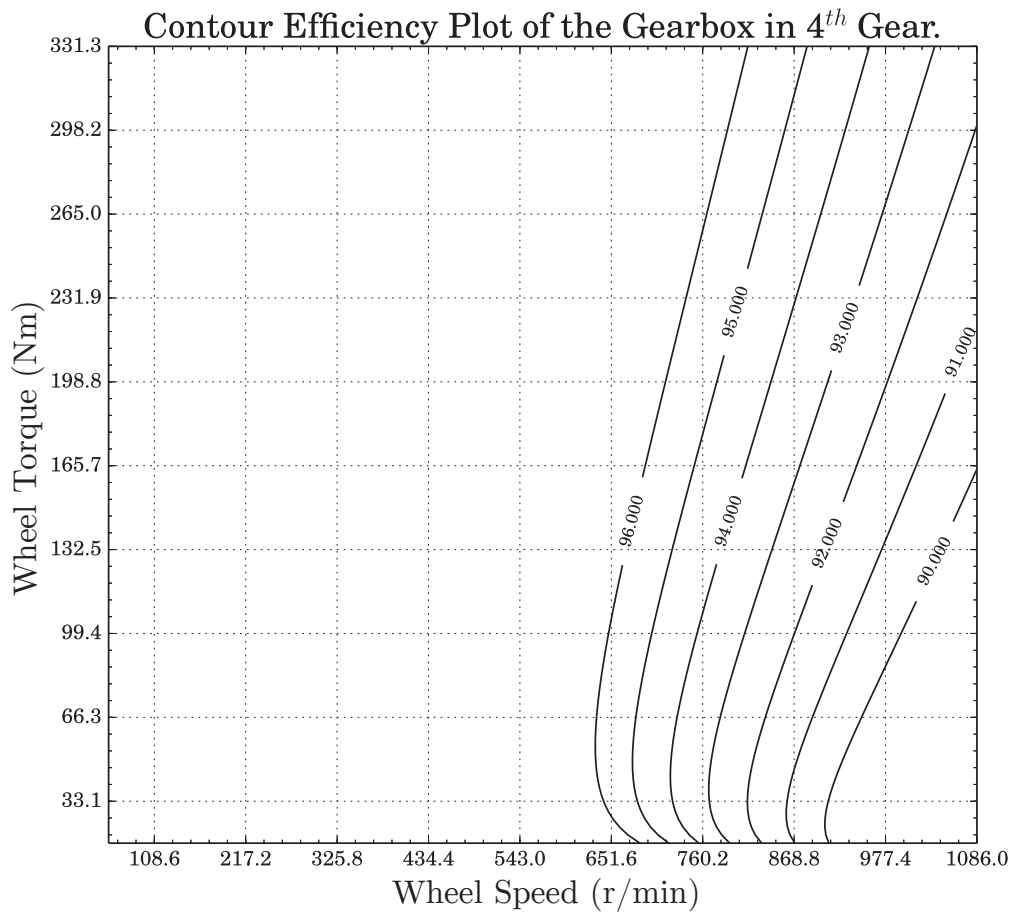


Figure 8.6: Contour efficiency map for the gearbox in 4th gear.



## Chapter 9

# Conclusions and recommendations

The aim of the thesis is to design a RSM as a traction motor for a EV with a multi speed gearbox. Thus the RSM has to meet the design specification and the efficiency of the power train should be measured to see whether it is feasible to implement a RSM with multi speed gearbox for EV application.

### 9.1 Conclusions

- The powertrain of EVs that are directly driven are more efficient than a geared drives, when the assumption is made that the motor efficiency is the same. The drawback of such a system is the number of drives and motors needed that increase both cost and complexity.
- It is evident that most EVs have an electric motor with a single speed gearbox. Most vehicles have PMS motors, but induction and field-wound rotor motors are also used.
- Multi-speed gearboxes offer benefits over a single speed gearboxes such as a smaller motor, no field weakening and lower operation speed. This advantages make the RSM motor a perfect candidate to use in conjunction with a multi speed gearbox.
- Simple methods that are not computationally expensive are investigated to calculate the efficiency of the RSM. The proposed ironloss equation is simple however from the case study done it is inconclusive whether the ironloss method is an accurate approximation.
- The optimised motor achieved the desired design specifications.
- The rotor of the optimised motor was changed by removing the webs. This increased the saliency, but the change to the torque and torque

ripple was insignificant. The rotor was still mechanically sound and able to operate at the rated condition.

- The laminations of the rotor was changed from NO20 to M530-65A. This increased the ironloss. There is another motor built with only M530-65A laminations on the rotor and the stator. The ironloss of the motor with the M530-65A motor is higher.
- The measured efficiency of the two motors is high throughout the speed and torque spectrum. The efficiency of the motor with the NO20 laminations are higher, because of the better laminations. The NO20 stator showed a very high efficiency of above 90% and the M530 stator above 88%.
- There is too much error in the measurements and not enough tests are done to derive accurate parameters for the simple ironloss equation given in Chapter 3.
- The RSM can definitely be considered as traction motor for EV application.
- The most practical measurement of the drive train was in 5<sup>th</sup> and 4<sup>th</sup> gear. The highest measured efficiency of the power train system was above 85% for 5<sup>th</sup> gear and 89% for 4<sup>th</sup> gear. The approximated efficiency of both 4<sup>th</sup> and 5<sup>th</sup> gear are between 90-96%. The multi speed gearbox is definitely a viable option for EVs from a performance and efficiency point of view. The efficiency of the inverter still needs to be taken into account to get the overall efficiency and performance of the system.

## 9.2 Recommendations

The test bench for the measuring of the power train needs improved and calibrated sensors. The EMC problem with the power analyser needs to be sorted out. This can be done by using a serial opto-coupler or grounding the cables. All the gears should be tested, this would make it possible to simulate a drive cycle on the test bench.

The motor test bench needs to be improved to more accurately measure the input and output power. Thermocouples should be added to the coils to measure the temperature and therefore the copper loss. The windage and friction loss should be measured. This would make the calculation of the ironloss possible and the results would be more conclusive.

There are a variety of commercial inverters available, Sevcon, Kollmorgen, Brusa, LTI and should be considered for the test bench and the EV.

The vehicle power train system can be modelled and then simulated in either Modelica or Simulink and then tested on the test bench to see how well the model and reality compare. This can lead to an improvement of the overall system, shorter development times and quicker fault finding in the system.

The possibility of field weakening can be considered to use the inverter more effectively.

The mechanical design of the rotor and the stator can be improved by considering the mechanical design analysis, vibration and heat transfer. The overall performance of the motor can be improved if the the quality of the manufacturing is improved.

The efficiency of the system can be compared to the efficiency of the single speed power train so compare the performance and efficiency of both systems.

# Appendices

# Appendix A

## Specifications and performance tests of the Corsa 140i.

Table A.1: Specifications of the Opel Corsa 140i 3-dr.

### SPECIFICATIONS

<b>ENGINE</b>	
Cylinders	four in-line, traverse
Fuel supply	multipoint injection
Bore/stroke	77,6/77,4 cm
Cubic capacity	1389 cm <sup>3</sup>
Compression ratio	9,5:1
Valve gear	s-o-h-c
Ignition	DIS electronic
Main bearings	five
Fuel Requirement	leaded/unleaded
<b>ENGINE OUTPUT</b>	
Max power ISO (kW)	65
Power peak (r/min)	6400
Max useable r/min	6600
Max torque (N.m)	112
Torque peak (r/min)	2800
<b>TRANSMISSION</b>	
Forward speeds	five
Low gear	3,727 to 1
2 <sup>nd</sup>	2,136 to 1
3 <sup>rd</sup>	1,414 to 1
4 <sup>th</sup>	1,121 to 1
5 <sup>th</sup>	0,892 to 1
Reverse gear	3,920 to 1
Final drive	3,940 to 1

Table A.1 – continued from previous page

Drive wheels	front
<b>WHEELS AND TYRES</b>	
Road wheels	13x5J alloy
Tyre make	Continental Contact
Tyre size	155/80 TR13
Tyre Pressure (front)	200-210 kPa
Tyre Pressure (rear)	180-230 kPa
<b>BRAKES</b>	
Front	ventilated discs
Rear	drum
Hydraulics	dual circuit
<b>STEERING</b>	
Steering	rack and pinion, power assisted
Lock to lock	2,8 turns
Turning circle	9,95 metres
<b>SUSPENSION</b>	
Front	MacPherson strut, anti-roll bar
Rear	compound link, trailing arms
<b>CAPACITIES</b>	
Seating	4/5
Fuel tank	45 litres
Boot space	168 dm <sup>3</sup>
Utility space	824 dm <sup>3</sup>
<b>WARRANTY AND SERVICE INTERVALS</b>	
3 years/100 000 km	
Service every 15 000 km	

Table A.2: Test results for the Opel Corsa 140i 3-dr.

**TEST RESULTS****MAXIMUM SPEED (km/h)**

True speed	178 at 5958 r/min in top gear			
Speedometer reading	187 km			
Calibration	60	80	100	120
True Speed	51	71	91	111
Odometer error	0,7 percent over			
	(Average of runs both ways on a level road)			

**ACCELERATION (seconds)**

0-60	5,18
0-80	8,20
0-100	12,47
0-120	17,71
1 km sprint	33,88
Terminal speed	150,9 km/h

**OVERTAKING ACCELERATION (seconds)**

	3 <sup>rd</sup>	4 <sup>th</sup>	Top
40-60	4,24	6,18	8,68
60-80	4,50	5,57	8,72
80-100	4,88	6,98	8,41
100-120	5,00	7,79	12,21
120-60		9,84	17,30

**FUEL CONSUMPTION (liters/100 km)**

60	5,17
80	5,87
100	7,10
120	8,27
Fuel index*	9,94/100 km
	10,06 km/litre
Estimated tank range	452 km

(\*Calculated overall consumption)

**BRAKING TEST****From 100 km/h**

Best stop	3,0
Worst stop	3,4
Average of 10 stops	3,22

(Measured in seconds with stops from true speeds at 30 second intervals on a good bituminous surface.)

Table A.2 – continued from previous page

<b>RESERVE POWER (in top)</b>			
Speed	kW available	kW used	Total kW
80	17	10	27
100	21	15	36
120	16	24	40
140	13	35	48
<b>GEARED SPEEDS (km/h)</b>			
Low gear			46* 47
2 <sup>nd</sup>			80* 82
3 <sup>rd</sup>			121* 124
4 <sup>th</sup>			152* 157
5 <sup>th</sup>			191* 197
(Calculated at engine power peak* 6400 r/min and at max usable r/min - 6600 r/min.)			
<b>INTERIOR NOISE LEVELS (db. A-weighted)</b>			
	Mech	Road	
Idling	50		
60	61		
80	63	69	
100	66	72	
120	71	75	
<b>PERFORMANCE FACTORS</b>			
Power/mass net (W/kg)			66,19
Frontal area (m <sup>2</sup> )			2,28
km/h per 1000 r/min(top)			29,88
Mass as tested (kg)			928
(Calculated on "mass as tested", gross frontal area, gearing, and ISO power output)			
<b>TEST CONDITIONS</b>			
Altitude	at sea level		
Weather	warm, clear, light air		
Fuel Used	97 octane leaded		
Test car's odometer	1603		



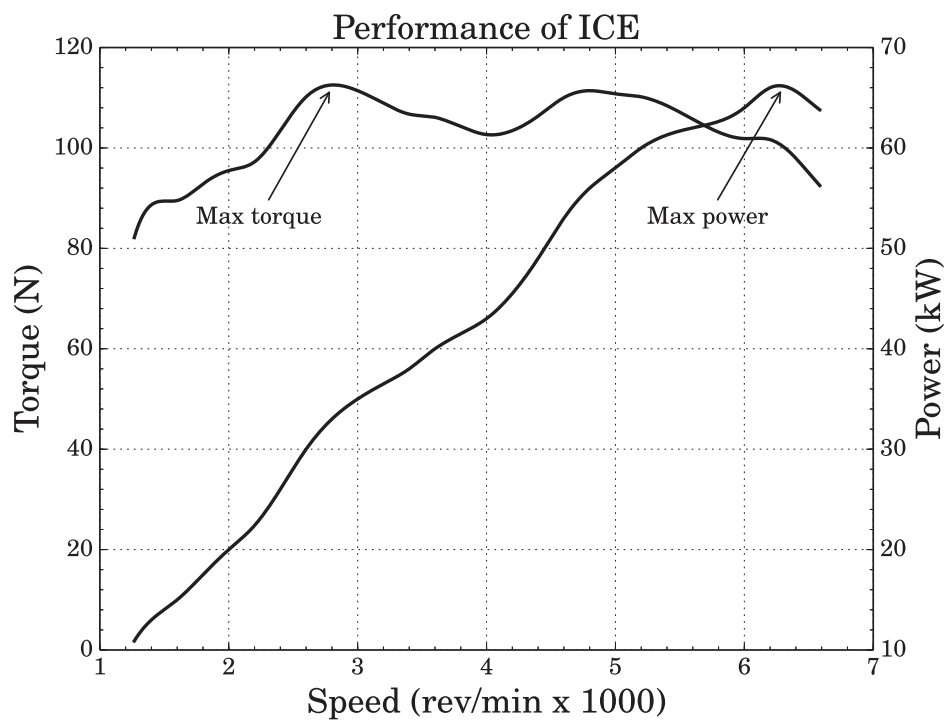


Figure A.1: Engine speed vs. Torque and Power.

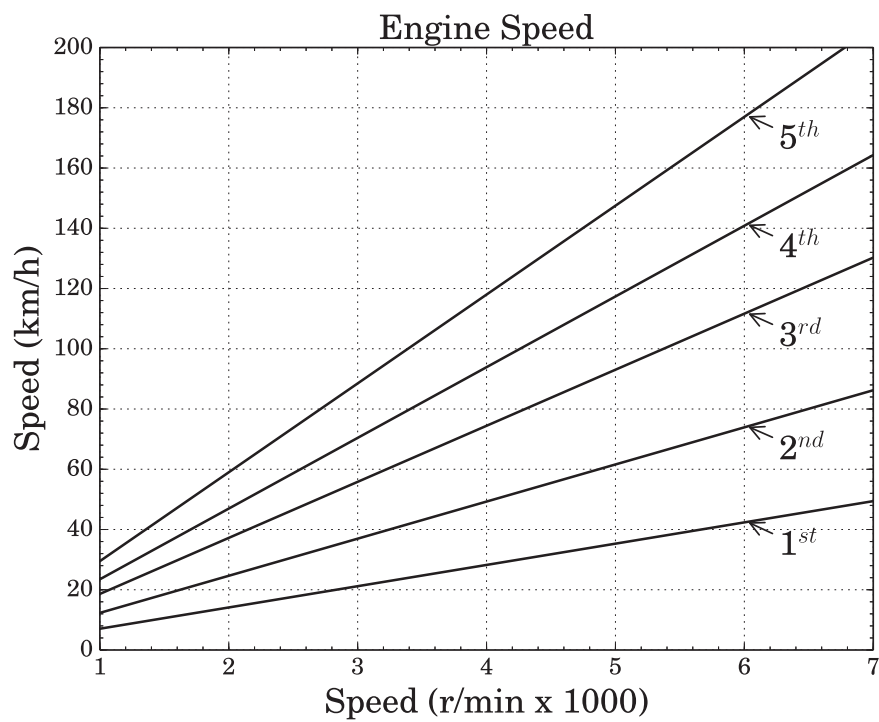


Figure A.2: Engine speed vs. vehicle speed .

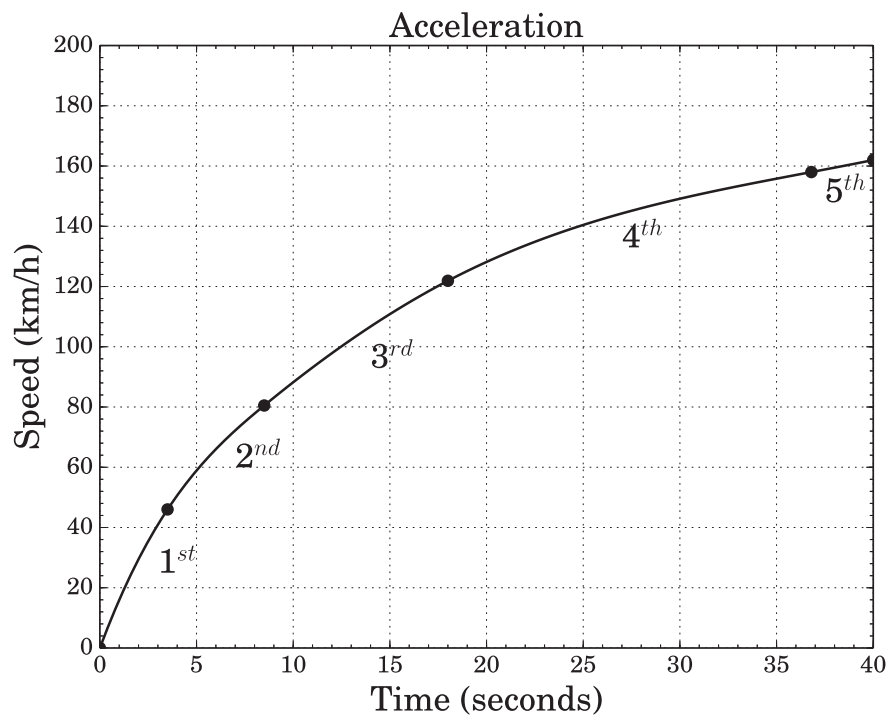


Figure A.3: Acceleration of the vehicle vs time.

# Appendix B

## Vehicle modelling

### B.1 Vehicle modelling

The basic understanding of vehicle modelling is important to determine proper design specifications. The force that moves the vehicle is called the tractive force,  $F_t$ . This is an important factor in the design of the primemover because it will determine the performance and the acceleration of the vehicle. The expected driving resistance is important to calculate as the primemover has to overcome the total resistance to move the vehicle. The driving resistances are a sum of the following:

- wheel resistance  $F_r$
- air resistance  $F_w$
- gradient resistance  $F_g$
- acceleration resistance  $F_a$

#### B.1.1 Wheel resistance

The wheel resistance is the sum of the rolling resistance, road surface resistance and slip resistance. It is determined as follow

$$F_r = fG = fmg\cos(\alpha) \quad (\text{B.1.1})$$

#### B.1.2 Air Resistance

Air resistance is the aerodynamic drag force exerted of the body of the vehicle.

$$F_w = 0.5\rho_Lc_dAv^2 \quad (\text{B.1.2})$$

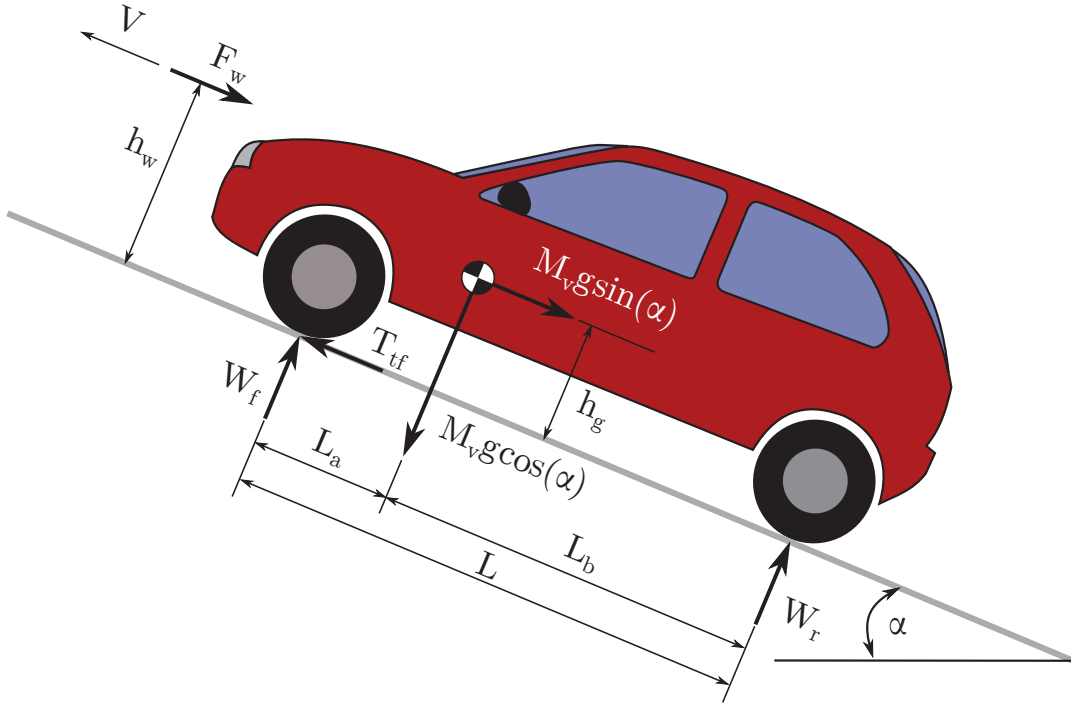


Figure B.1: Forces acting on a vehicle.

### B.1.3 Gradient Resistance

The gradient resistance force is the force that is due to the weight of the car and the slope of the road. The force is shown in Fig. B.1

$$F_{St} = mgsin(\alpha) \quad (B.1.3)$$

### B.1.4 Acceleration Resistance

$$F_a = m_{red,i}a, \text{ with} \quad (B.1.4)$$

$$m_{red,i} = m + \frac{\sum J_{red,i}}{r_{dyn}^2} \quad (B.1.5)$$

$$F_a = \lambda \cdot m \cdot a \quad (B.1.6)$$

### B.1.5 Total driving resistance

The traction requirement at the wheels, due to the above mentioned forces can be summed as

$$F_Z = F_R + F_{St} + F_L F_a \quad (B.1.7)$$

substituting equations ... gives

$$F_Z = mg(f \cos(\alpha) + \sin(\alpha)) + 0.5 \rho_L c_d A v^2 + m \lambda a. \quad (\text{B.1.8})$$

When the vehicle is driving at steady-state ( $a=0$ ) and approximating  $\cos(\alpha) \approx 1$  and  $\sin(\alpha) \approx \tan(\alpha)$  the equation simplifies to

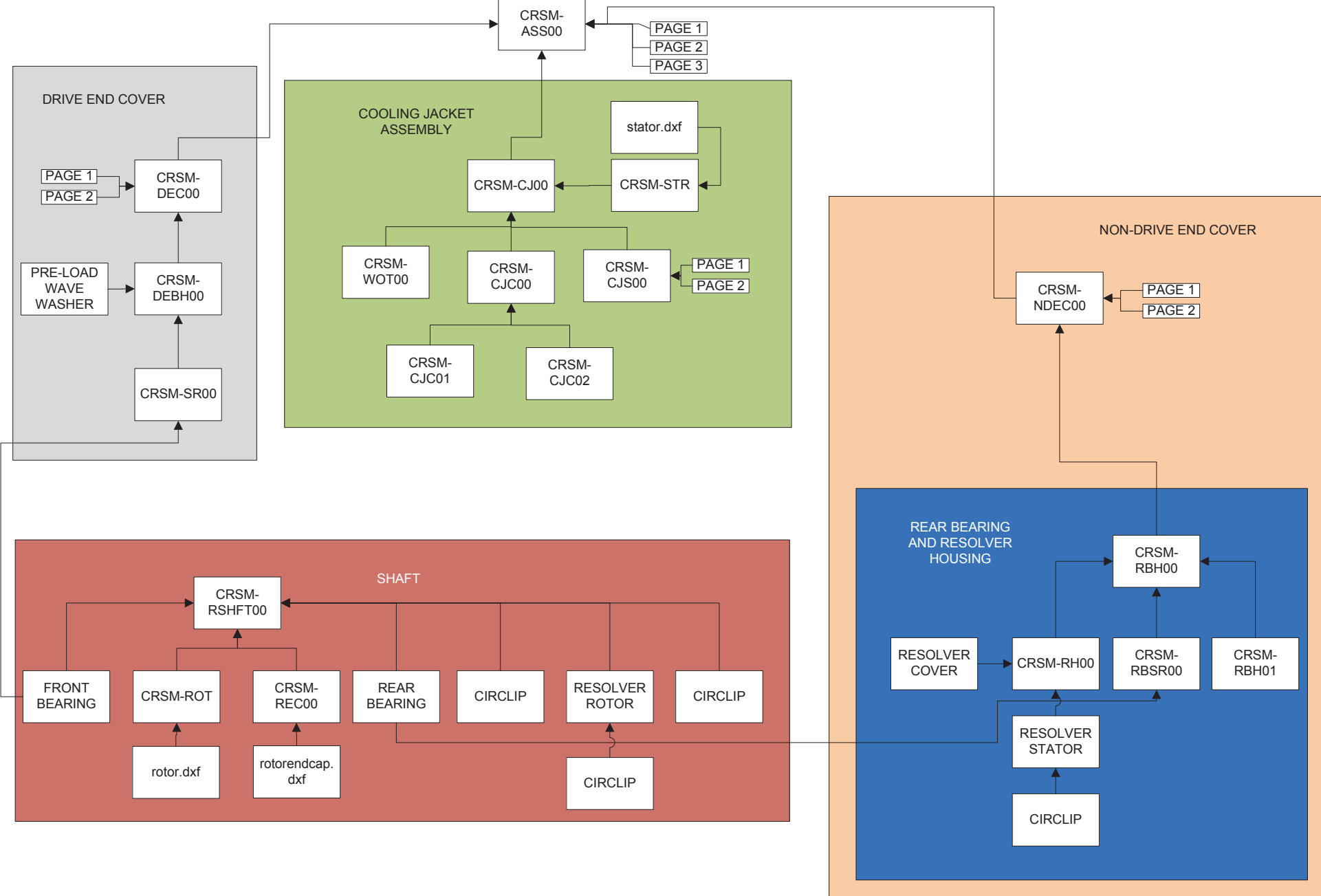
$$F_Z = mg(f + \tan(\alpha)) + 0.5 \rho_L c_d A v^2. \quad (\text{B.1.9})$$

The required wheel traction can be obtained from this at different inclinations.

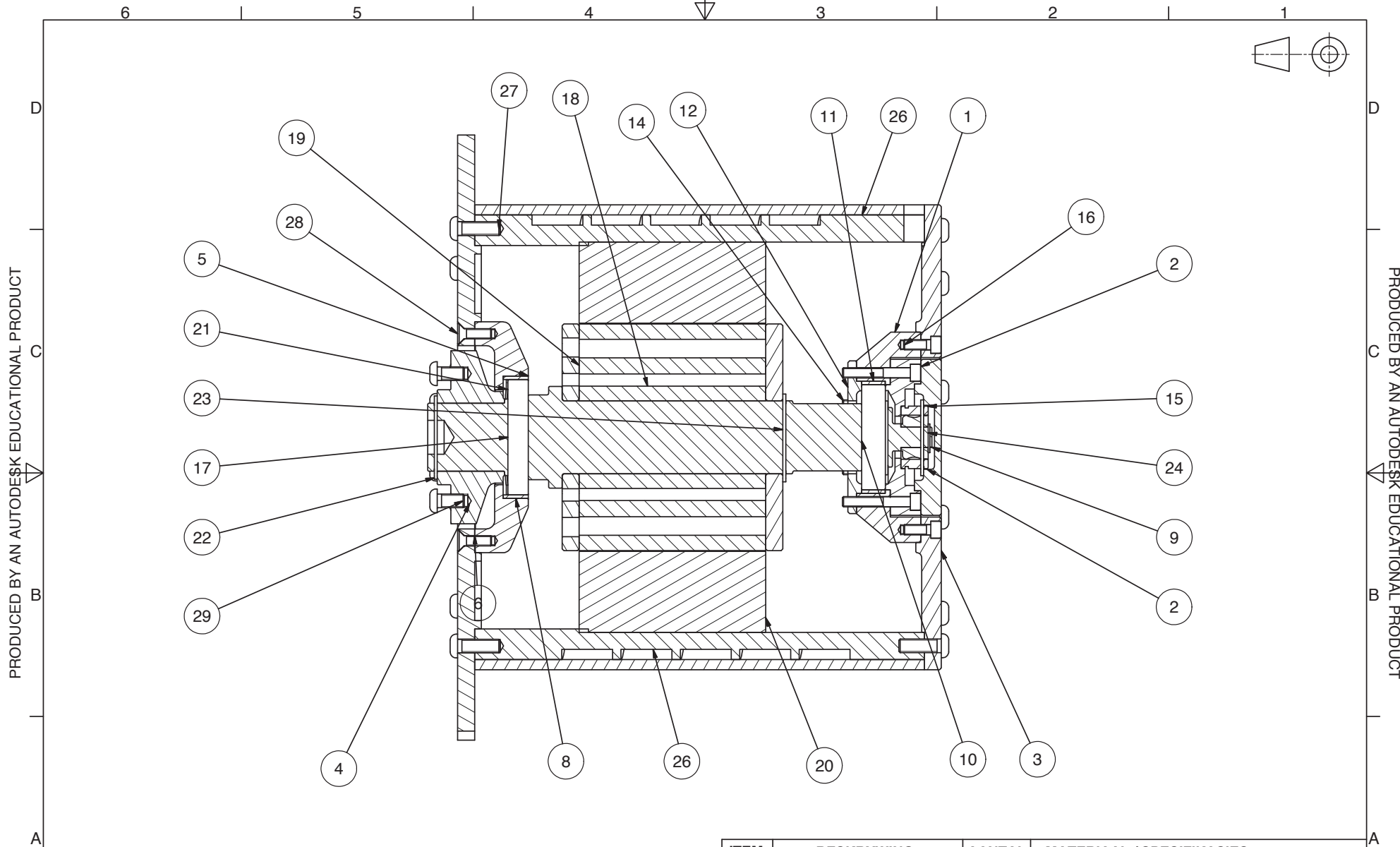
## Appendix C

# Mechanical Design for RSM with water cooled jacket.

# DRAWING TREE FOR CORSA RSM



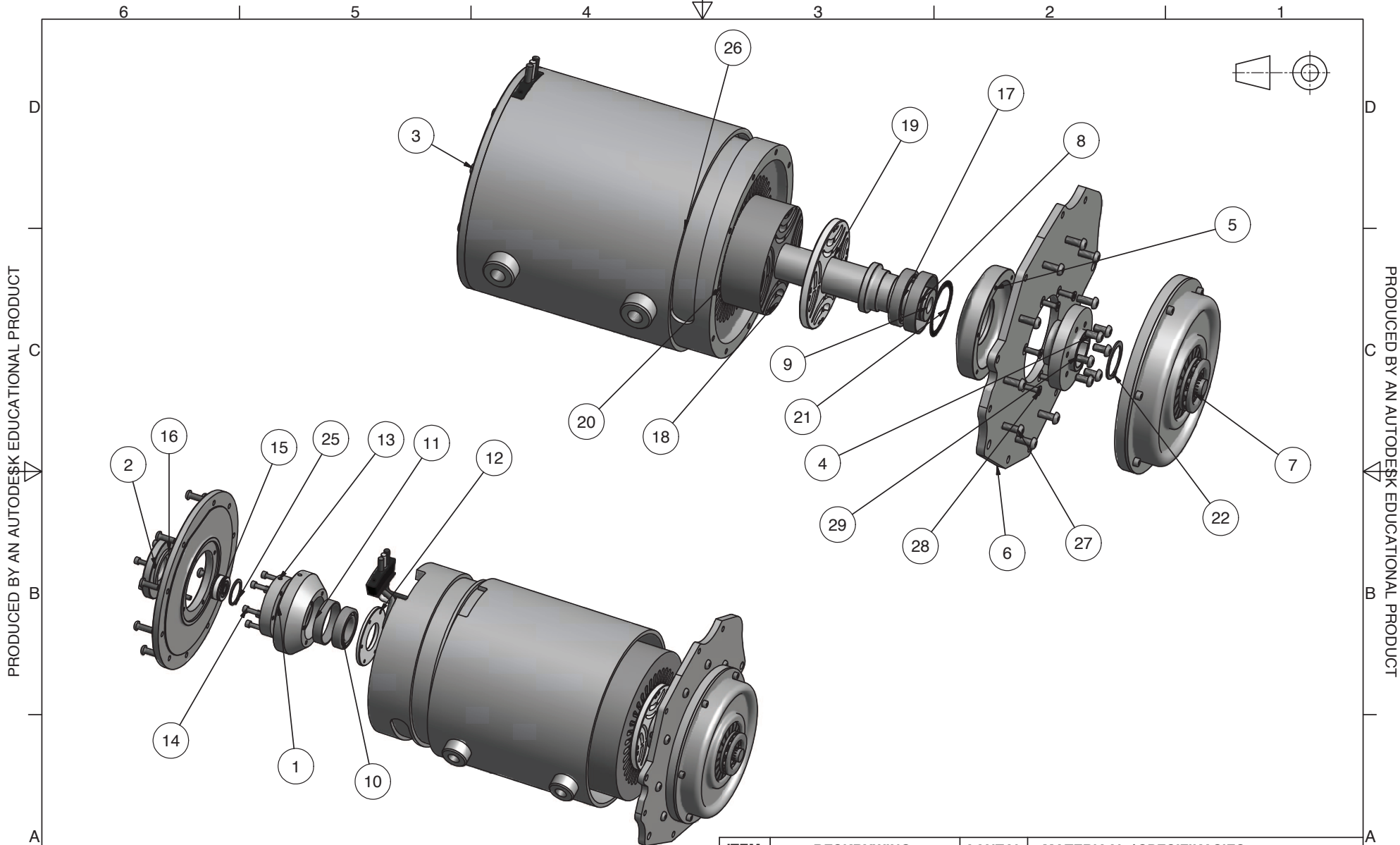




PRODUCED BY AN AUTODESK EDUCATIONAL PRODUCT

PRODUCED BY AN AUTODESK EDUCATIONAL PRODUCT

<b>UNIVERSITEIT VAN STELLENBOSCH</b>				ITEM	BESKRYWING	AANTAL	MATERIAAL / SPESIFIKASIES
				SKAAL OP A 3 1:2		TITEL: MOTOR ASSEMBLY	
STUDENTE No. 14827891		TEKENAAR CW VORSTER	NAGESIEN	DATUM 27/08/2012	VEL No. VAN VELLE	No. CRSM-ASS00	



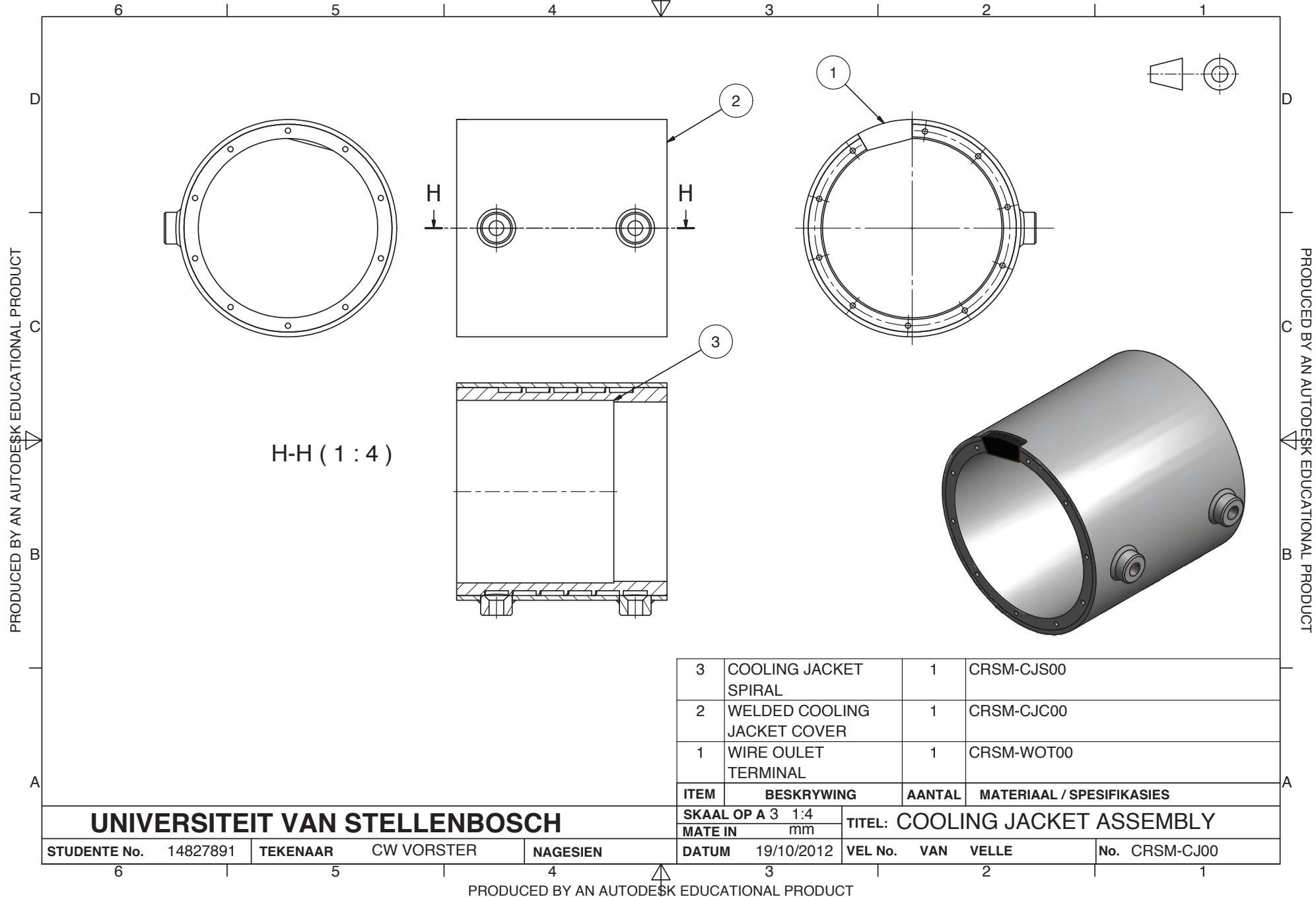
ITEM	BESKRYWING	AANTAL	MATERIAAL / SPESIFIKASIES
SKAAL OP A NOT TO SCALE		TITEL: MOTOR ASSEMBLY	
MATE IN mm			
DATUM	25/10/2012	VEL No. 2 VAN 3 VELLE	No. CRSM-ASS00

**UNIVERSITEIT VAN STELLENBOSCH**

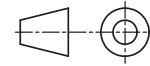
STUDENTE No. 14827891 | TEKENAAR CW VORSTER | NAGESIEN

6 | 5 | 4 | 3 | 2 | 1

UNIVERSITEIT VAN STELLENBOSCH				SKAAL OP A		TITEL: MOTOR ASSEMBLY		
				MATE IN mm				
STUDENTE No.	TEKENAAR	NAGESIEN	DATUM	VEL No. 3 VAN 3 VELLE		No. CRSM-ASS00		
15	RESOLVER	1	LTN 2005 RE - 15 -1 K01	31	CIRCLIP	1	CRSM-SHFT-C03	
14	SOCKET HEAD CAP SCREW	6	M6X40 (GRADE 8.8)	32	COUPLING KEY	1	CRSM-SHFT-K00	
13	RESOLVER HOUSING	1	CRSM-RH00	31	ROTOR KEY	1	CRSM-SHFT-K01	
12	NON-DRIVE END FRONT BEARING LOCATOR	1	CRSM-RBH01	30	CIRCLIP	1	CRSM-SHFT-CO4	
11	STEELRING	1	CRSM-SR00	29	BUTTON HEAD CAP SCREW	6	M8X16	
10	SKF- SINGLE ROW DEEP GROOVE BALL BEARING	1	6007-2RZ	28	COUNTERSUNK HEAD CAP SCREW	6	M6X20	
9	SHAFT	1	CRSM-SHFT00	27	BUTTON HEAD CAP SCREW	20	M8X25 (GRADE 8.8)	
8	STEELRING	1	CRSM-SR00	26	COOLING JACKET ASSEMBLY	1	CRSM-CJ00	
7	CLUTCH ASSEMBLY	1	-	24	CIRCLIP	1	CRSM-SHFT-C00	
6	DRIVE END COVER	1	CRSM-DEC00	23	CIRCLIP	1	CRSM-SHFT-C01	
5	DRIVE END BEARING HOUSING	1	CRSM-DEBH00	22	CIRCLIP	1	CRSM-SHFT-C02	
4	SHAFT FLYWHEEL COUPLING	1	CRSM-SFC00	21	PRELOAD WASHER	1	SSB-0268(SMALLEY STEEL RING CO. USA)	
3	NON-DRIVE END COVER	1	CRSM-NDEC00	20	STATOR	1	CRSM-STR	
2	RESOLVER COVER	1	CRSM-RC00	19	ROTOR END CAPS	2	CRSM-REC00	
1	NON-DRIVE END BEARING HOUSING	1	CRSM-RBH00	18	ROTOR	1	CRSM-RTR	
				17	SKF- SINGLE ROW DEEP GROOVE BALL BEARING	1	61909-2RZ	
				16	SOCKET HEAD CAP SCREW	7	M6X15 (GRADE8.8)	
					ITEM	BESKRYWING	AANTAL	MATERIAAL / SPESIFIKASIES

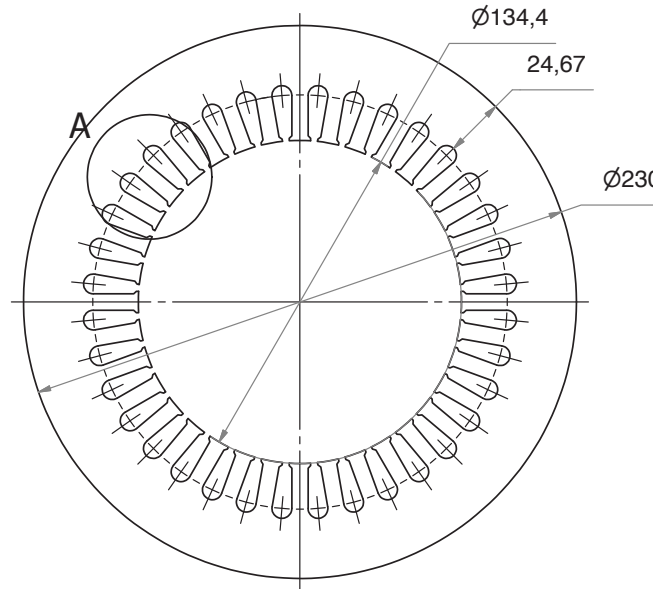
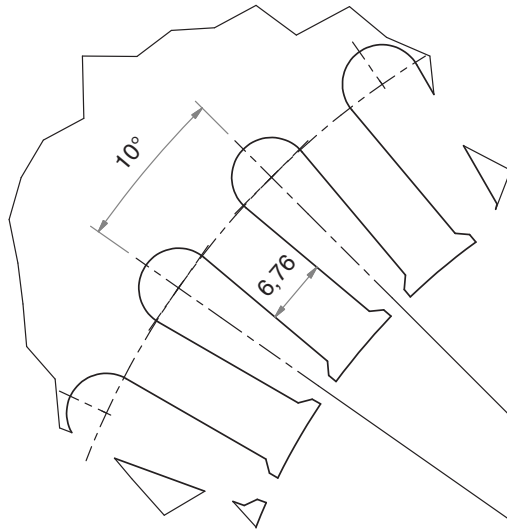


6 | 5 | 4 | 3 | 2 | 1



NOTE: DXF FILE FOR LASER CUTTING AVAILABLE.  
STACKLENGHT = 110mm, THUS +570 LAMINATIONS REQUIRED.

A (2:1)



PRODUCED BY AN AUTODESK EDUCATIONAL PRODUCT

PRODUCED BY AN AUTODESK EDUCATIONAL PRODUCT

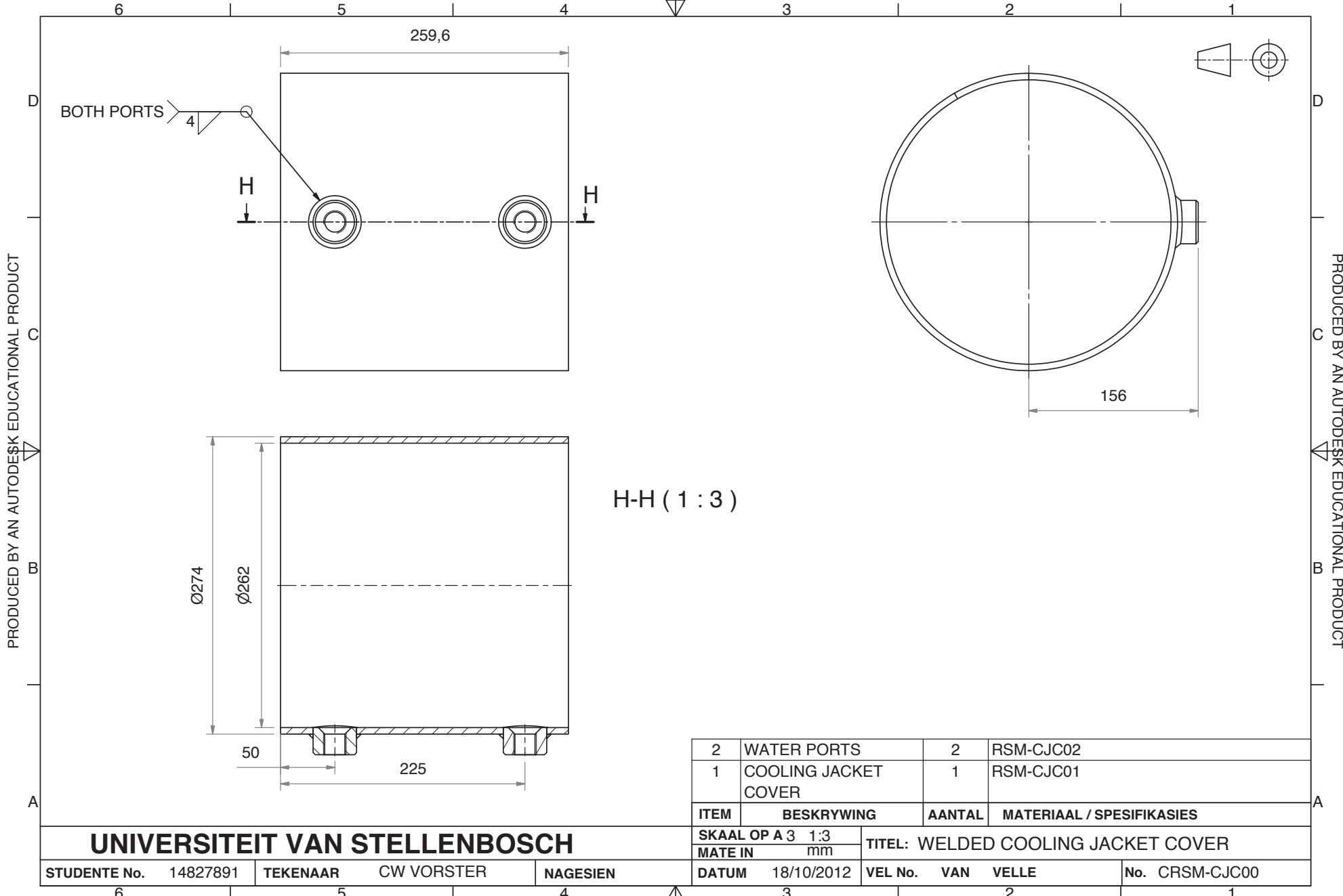
A | B | C | D

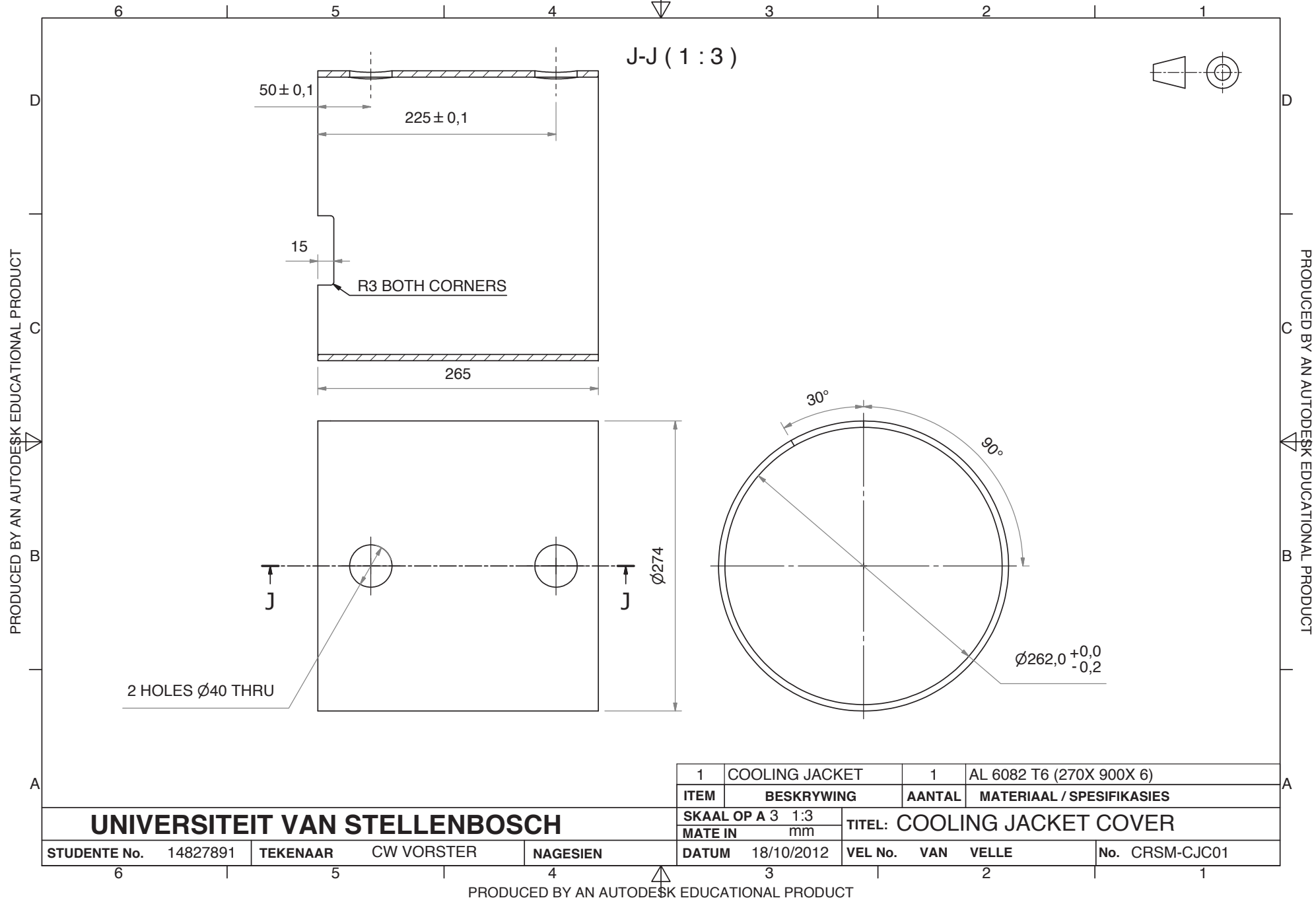
1	STATOR LAMINATION	1	NO20 STACKLENGT = 110mm
ITEM	BESKRYWING	AANTAL	MATERIAAL / SPESIFIKASIES
SKAAL OP A 3 1:1		TITEL: STATOR	
MATE IN mm			
DATUM	25/10/2012	VEL No.	VAN VELLE
			No. CRSM-STR

**UNIVERSITEIT VAN STELLENBOSCH**

STUDENTE No. 14827891 | TEKENAAR CW VORSTER | NAGESIEN

6 | 5 | 4 | 3 | 2 | 1

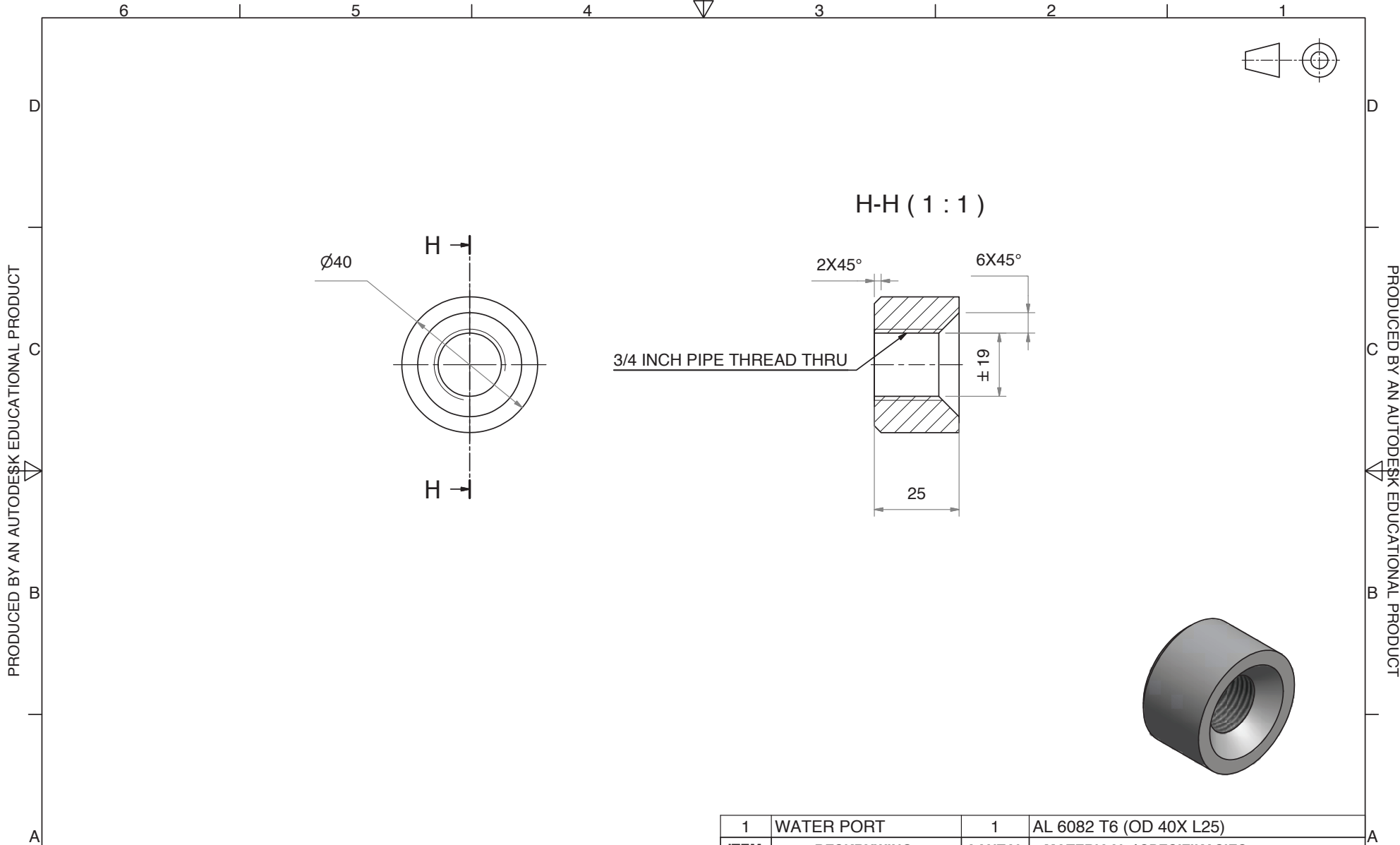




1	COOLING JACKET	1	AL 6082 T6 (270X 900X 6)
ITEM	BESKRYWING	AANTAL	MATERIAAL / SPESIFIKASIES
SKAAL OP A 3 1:3		TITEL: COOLING JACKET COVER	
MATE IN mm			
DATUM	18/10/2012	VEL No. VAN VELLE	No. CRSM-CJC01

**UNIVERSITEIT VAN STELLENBOSCH**

STUDENTE No. 14827891 | TEKENAAR CW VORSTER | NAGESIEN



1	WATER PORT	1	AL 6082 T6 (OD 40X L25)
ITEM	BESKRYWING	AANTAL	MATERIAAL / SPESIFIKASIES
SKAAL OP A 3 1:1		TITEL: WATER PORT	
MATE IN mm			
DATUM	17/10/2012	VEL No.	VAN VELLE
			No. CRSM-CJC02

**UNIVERSITEIT VAN STELLENBOSCH**

STUDENTE No. 14827891    TEKENAAR CW VORSTER    NAGESIEN

6

5

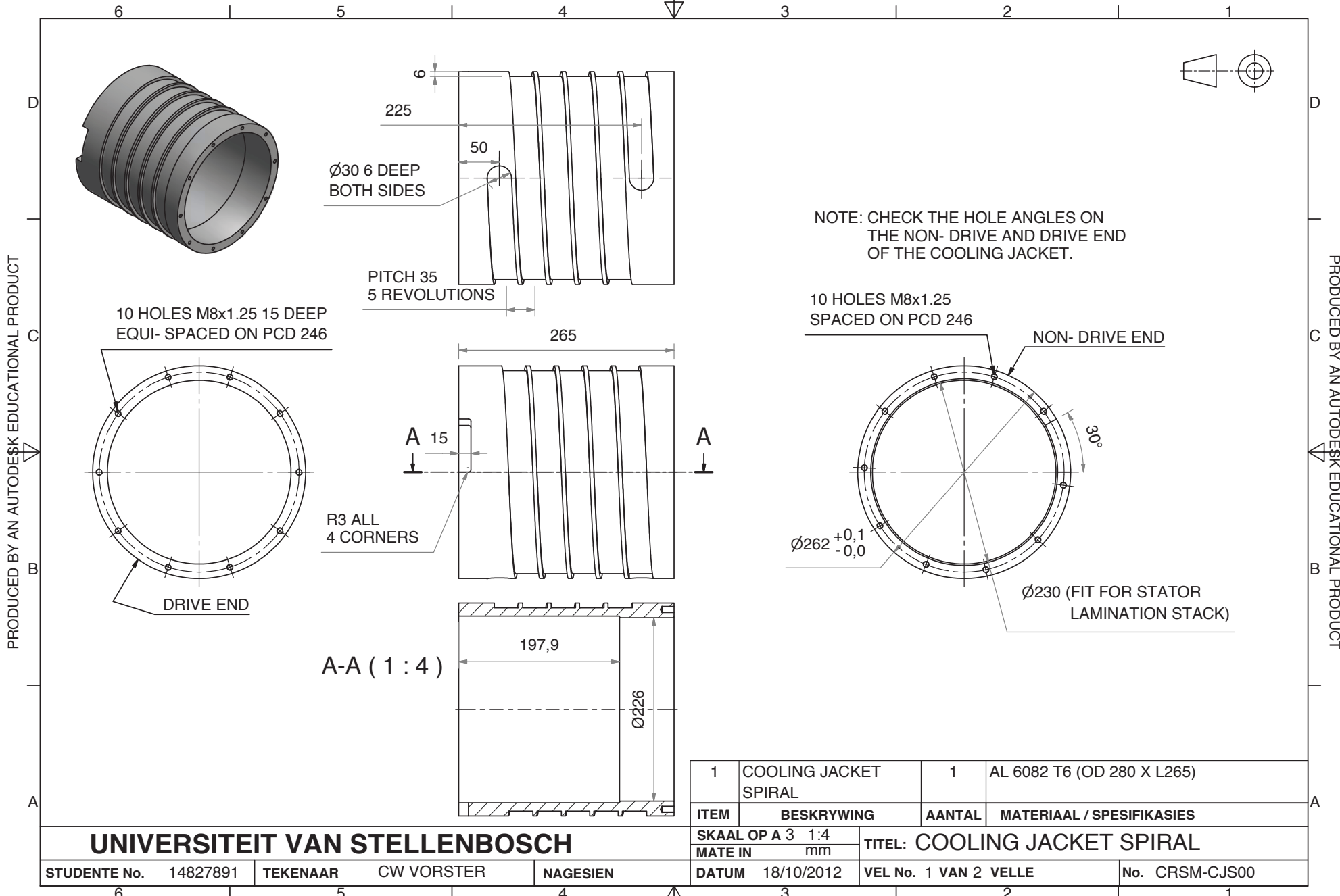
4

3

2

1





UNIVERSITEIT VAN STELLENBOSCH

STUDENTE No. 14827891 TEKENAAR CW VORSTER NAGESIEN

SKAAL OP A 3 1:4

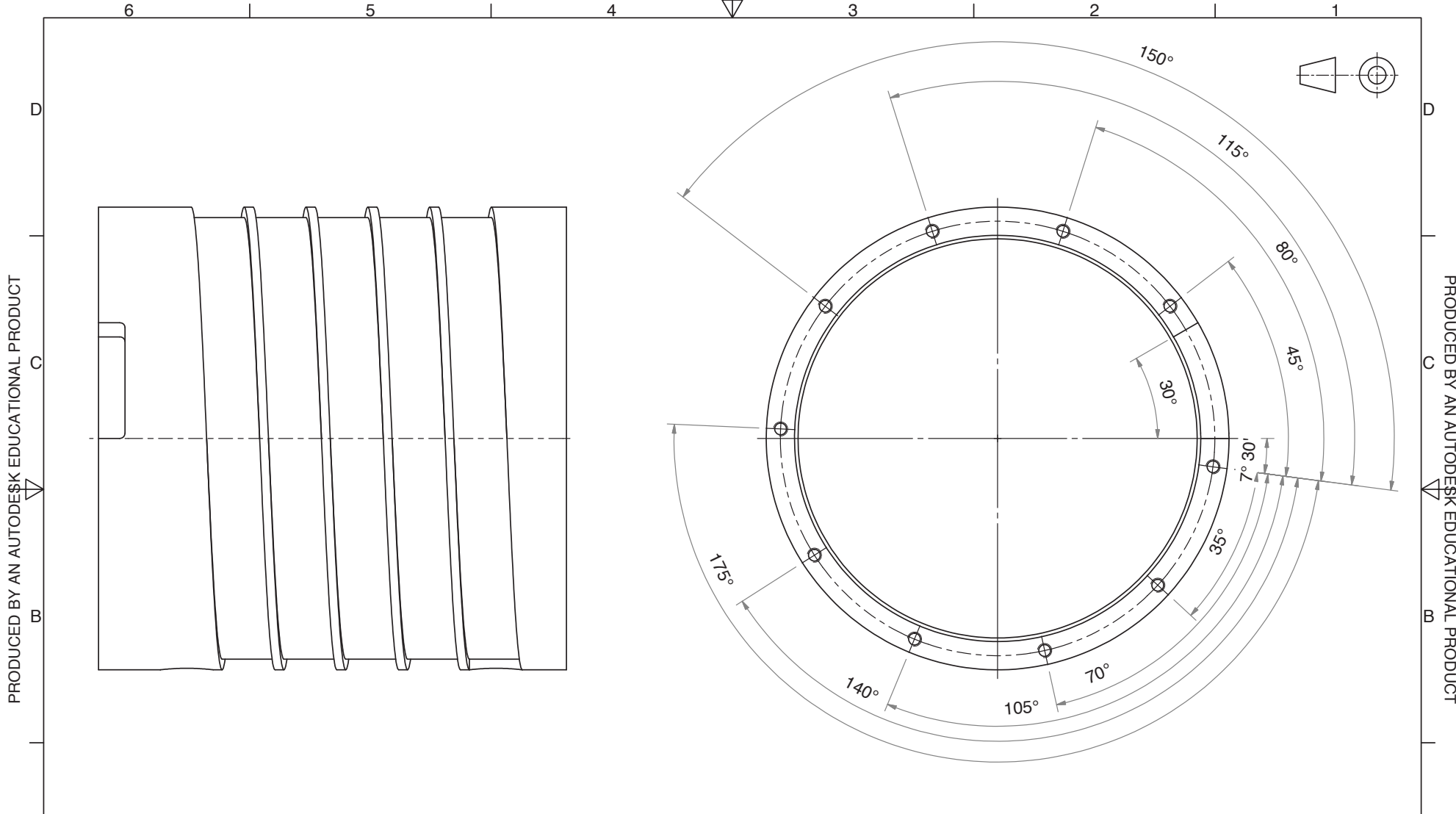
MATE IN mm

TITEL: COOLING JACKET SPIRAL

DATUM 18/10/2012

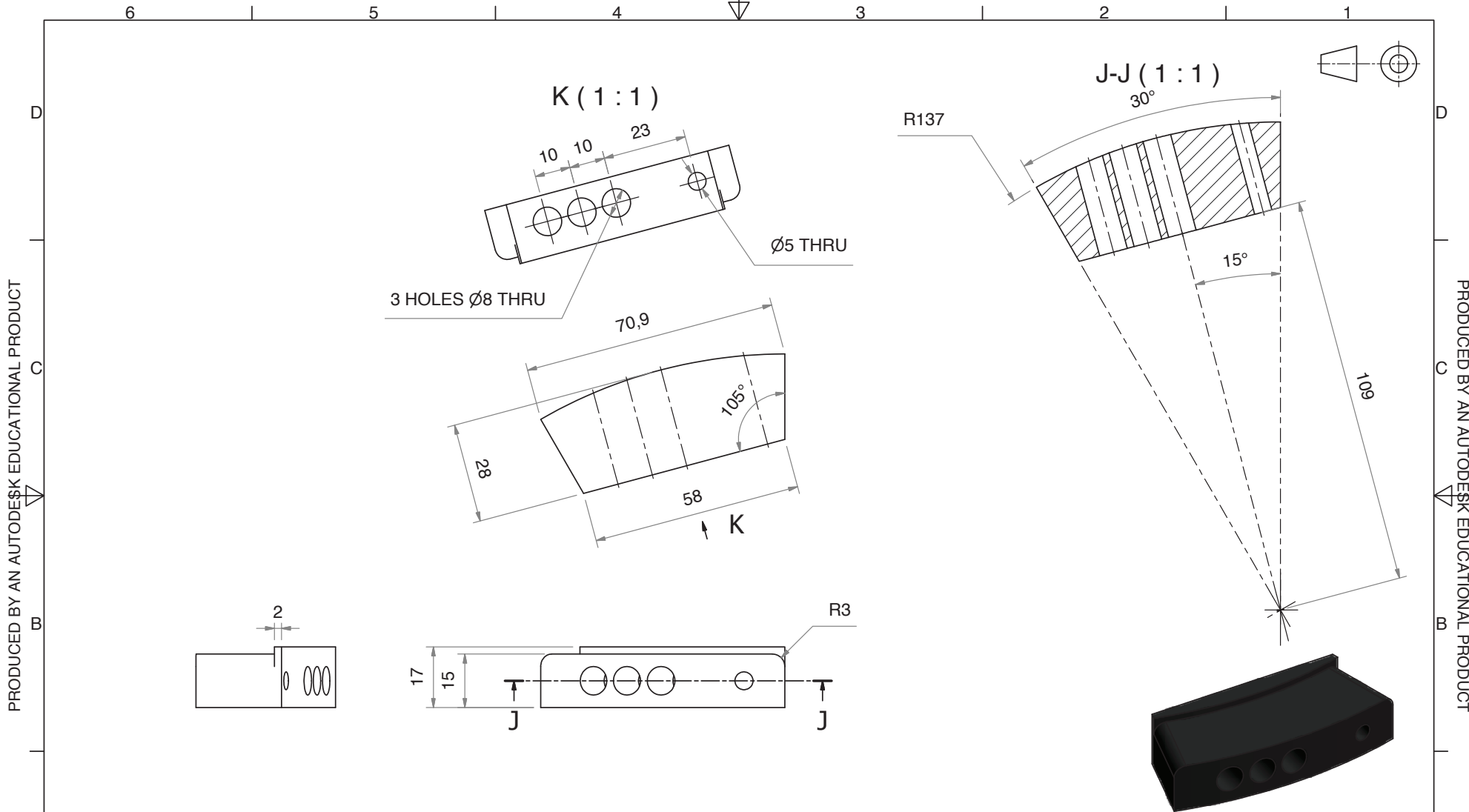
VEL No. 1 VAN 2 VELLE

No. CRSM-CJS00



1	COOLING JACKET SPIRAL	1	AL 6082 T6 (OD 280 X L265)
ITEM	BESKRYWING	AANTAL	MATERIAAL / SPESIFIKASIES

UNIVERSITEIT VAN STELLENBOSCH		SKAAL OP A 3 1:2	TITEL: COOLING JACKET SPIRAL
		MATE IN mm	
STUDENTE No. 14827891	TEKENAAR CW VORSTER	NAGESIEN	DATUM 18/10/2012
		VEL No. 2 VAN 2 VELLE	
			No. CRSM-CJS00



PRODUCED BY AN AUTODESK EDUCATIONAL PRODUCT

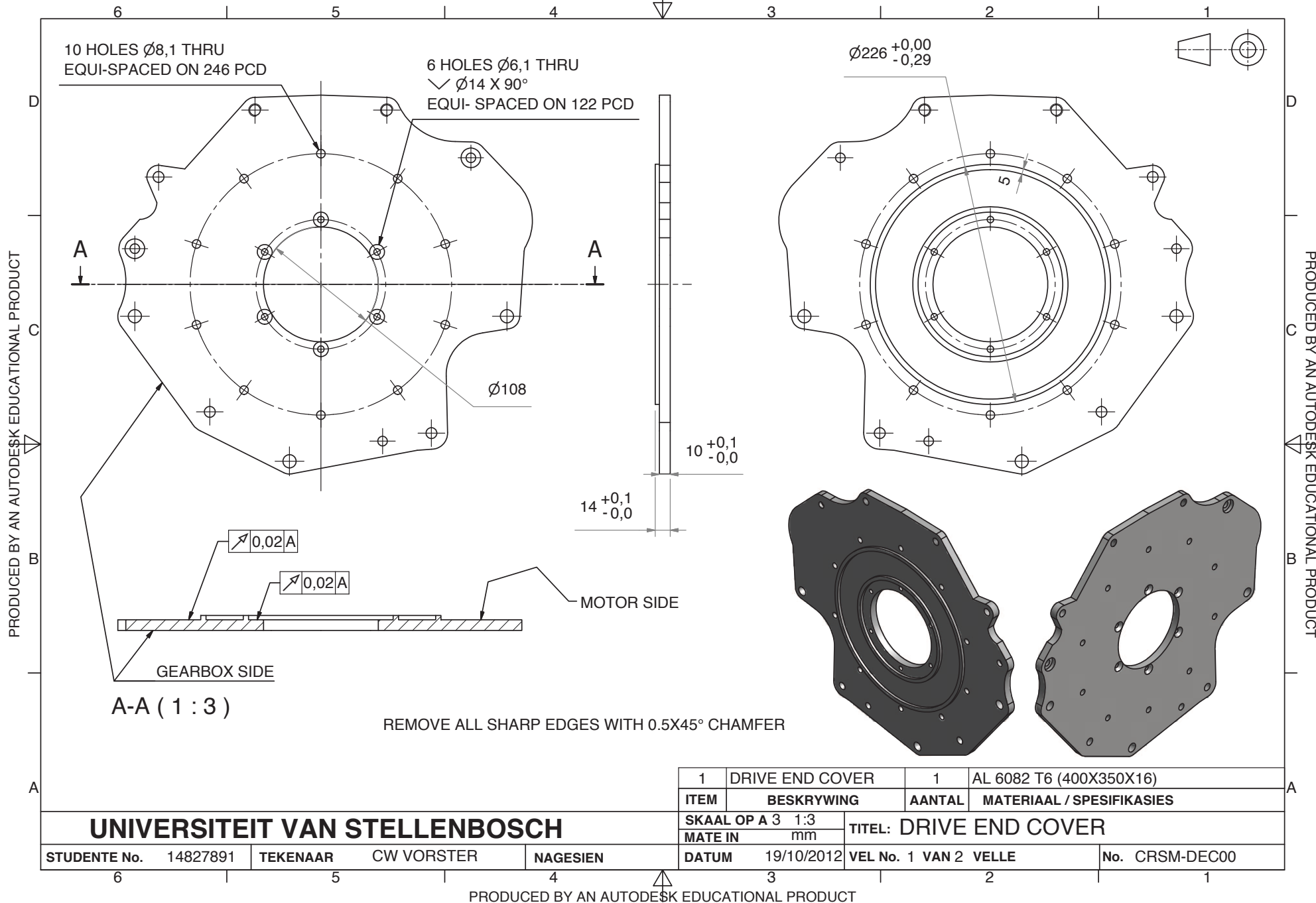
PRODUCED BY AN AUTODESK EDUCATIONAL PRODUCT

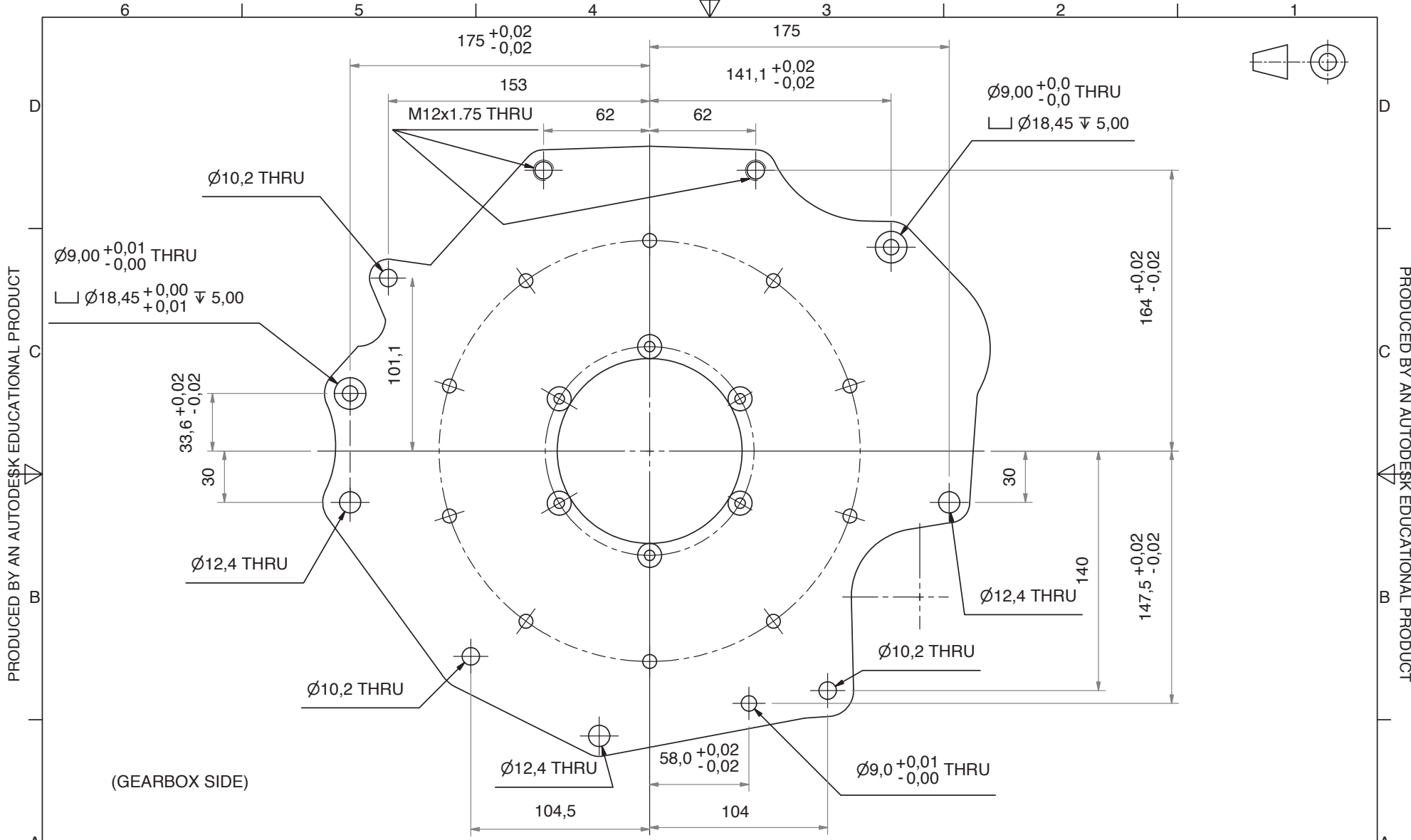
1	WIRE OULET TERMINAL	1	SUSTARIN C (80 X30 X20) BLACK
ITEM	BESKRYWING	AANTAL	MATERIAAL / SPESIFIKASIES
SKAAL OP A 3 1:1		TITEL: WIRE OULET TERMINAL	
MATE IN mm			
DATUM	19/10/2012	VEL No.	VAN VELLE
			No. CRSM-WOT00

**UNIVERSITEIT VAN STELLENBOSCH**

STUDENTE No. 14827891    TEKENAAR CW VORSTER    NAGESIEN

DATUM 19/10/2012    VEL No. VAN VELLE    No. CRSM-WOT00

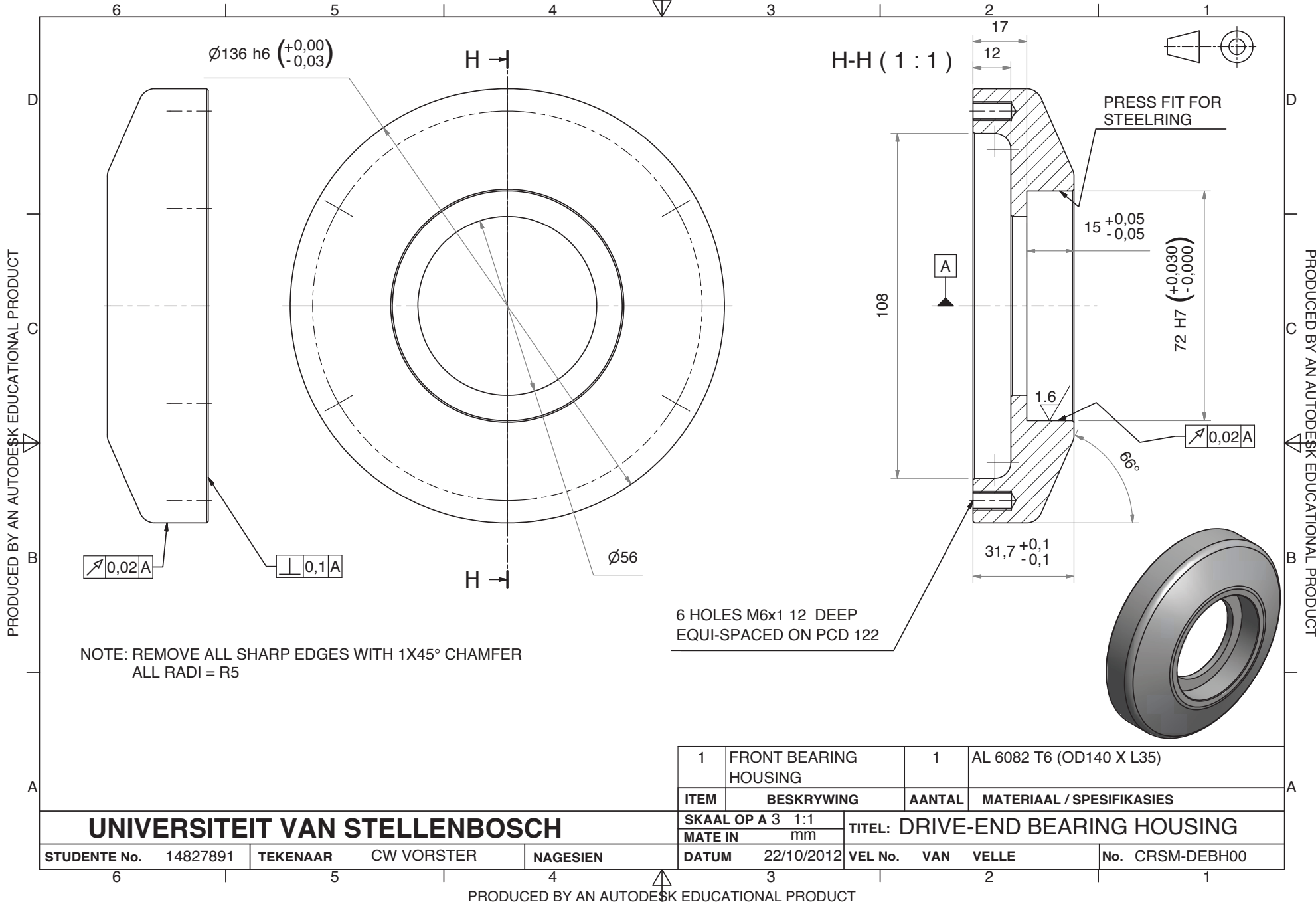


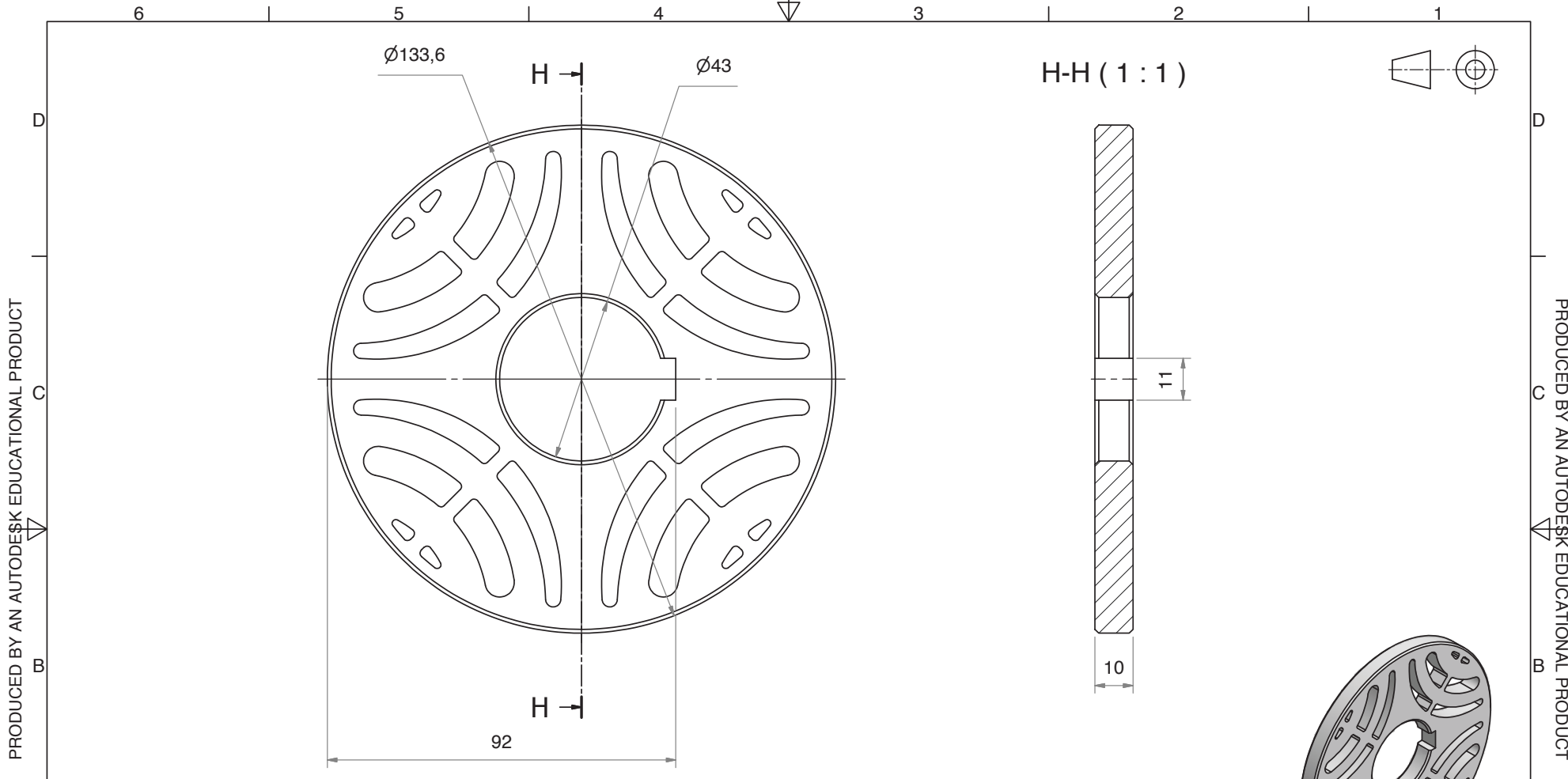


**UNIVERSITEIT VAN STELLENBOSCH**

ITEM	BESKRYWING	AANTAL	MATERIAAL / SPESIFIKASIES
SKAAL OP A3 1:2		TITEL: DRIVE END COVER	
MATE IN mm			
DATUM	19/10/2012	VEL No. 2 VAN 2 VELLE	No. CRSM-DEC00

STUDENTE No. 14827891	TEKENAAR CW VORSTER	NAGESIEN
-----------------------	---------------------	----------





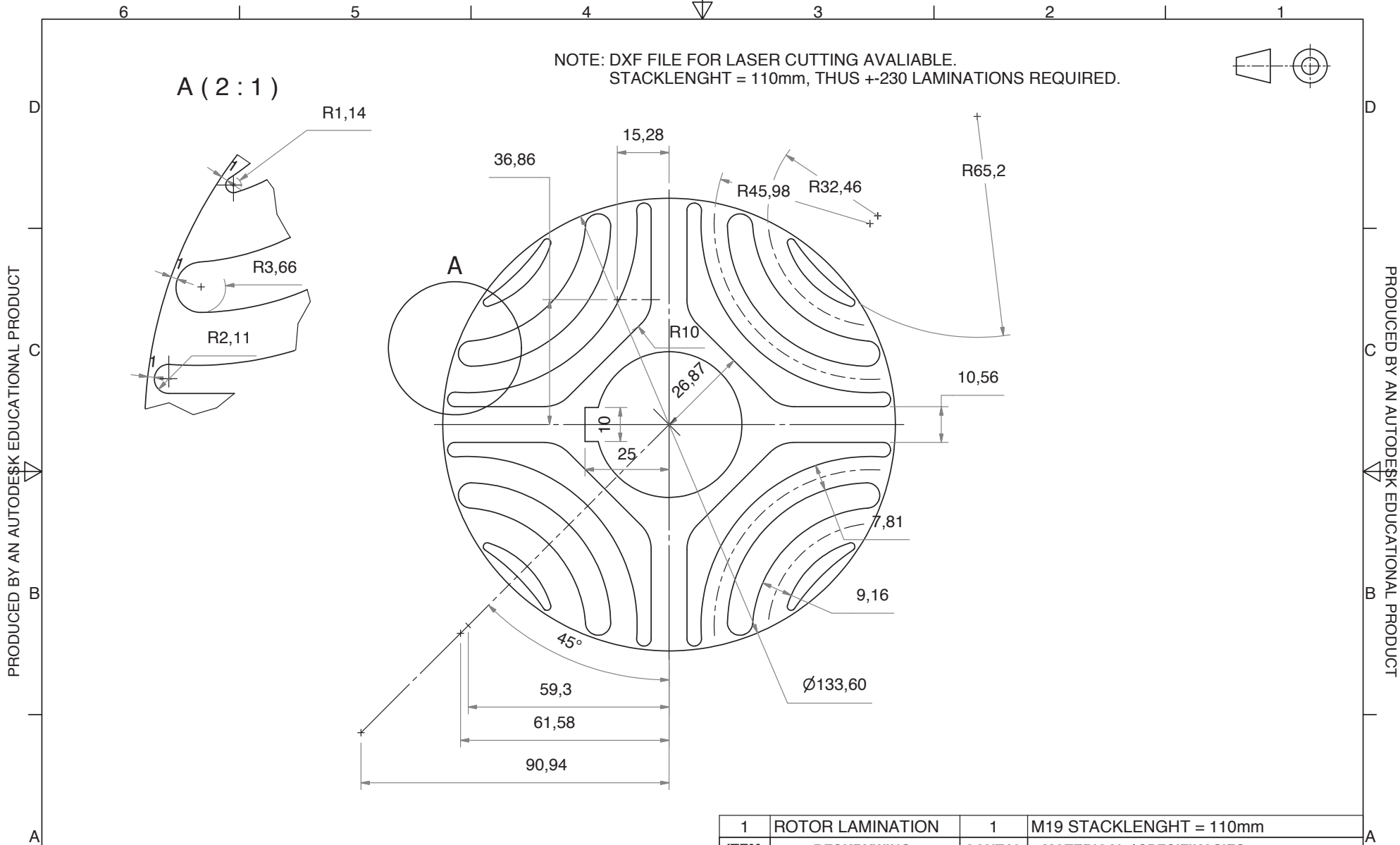
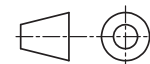
NOTE: DXF FILE WILL BE ATTACT FOR LASER  
OR WATERJET CUTTING.  
REMOVE SHARP EDGES WITW 1X45° CHAMFER

1	ROTOR END-CAPS	1	AL 6082 T6 (OD135 X L12)
ITEM	BESKRYWING	AANTAL	MATERIAAL / SPESIFIKASIES
SKAAL OP A 3 1:1		TITEL: ROTOR END CAPS	
MATE IN mm			
DATUM	22/10/2012	VEL No.	VAN VELLE
			No. CRSM-REC00

**UNIVERSITEIT VAN STELLENBOSCH**

STUDENTE No. 14827891    TEKENAAR CW VORSTER    NAGESIEN

NOTE: DXF FILE FOR LASER CUTTING AVAILABLE.  
STACKLENGHT = 110mm, THUS +-230 LAMINATIONS REQUIRED.

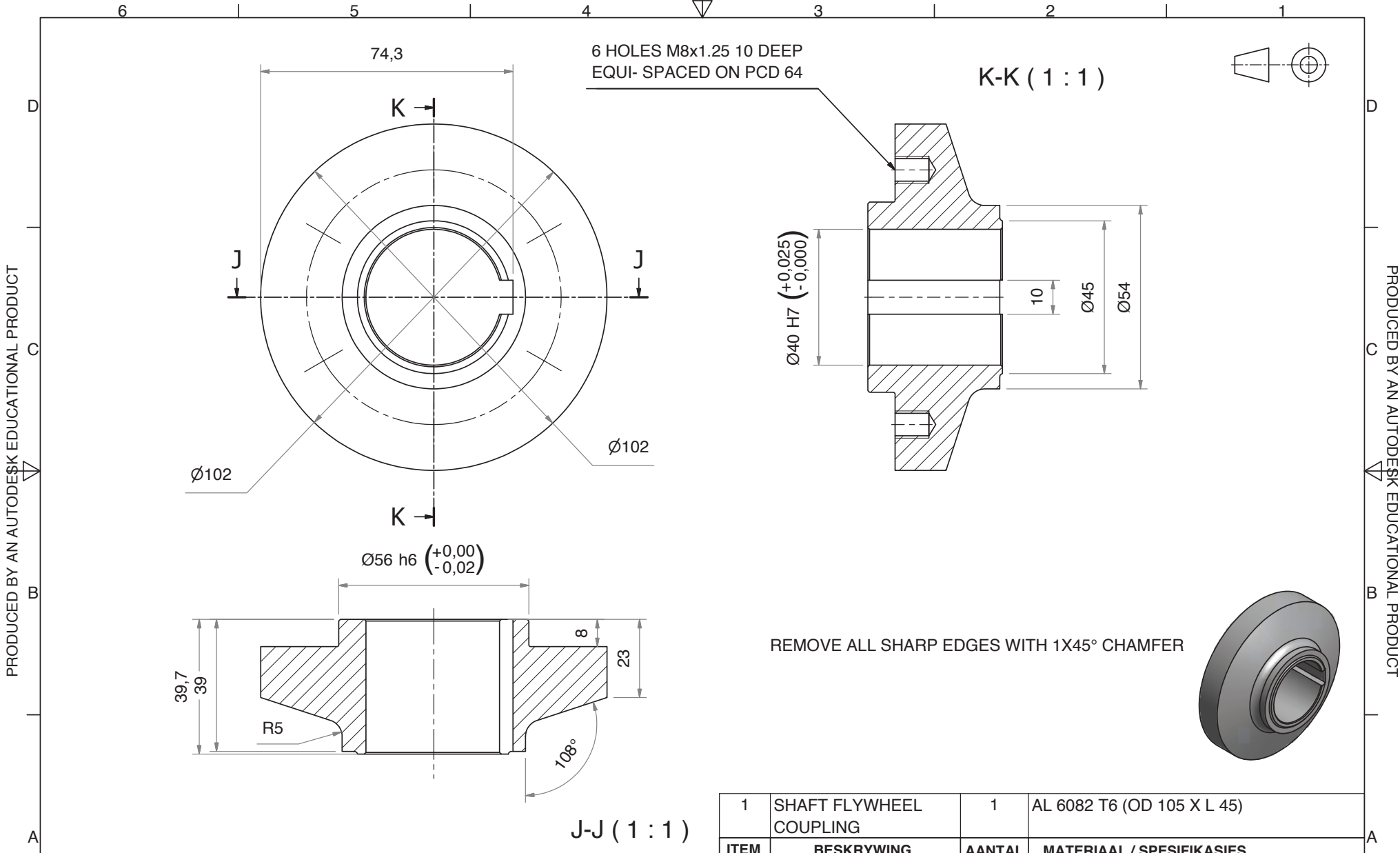


1	ROTOR LAMINATION	1	M19 STACKLENGHT = 110mm
ITEM	BESKRYWING	AANTAL	MATERIAAL / SPESIFIKASIES
SKAAL OP A 3	1:1	TITEL: ROTOR	
MATE IN	mm		
DATUM	25/10/2012	VEL No.	VAN VELLE
		No. CRSM-RTR	

**UNIVERSITEIT VAN STELLENBOSCH**

STUDENTE No. 14827891 | TEKENAAR CW VORSTER | NAGESIEN

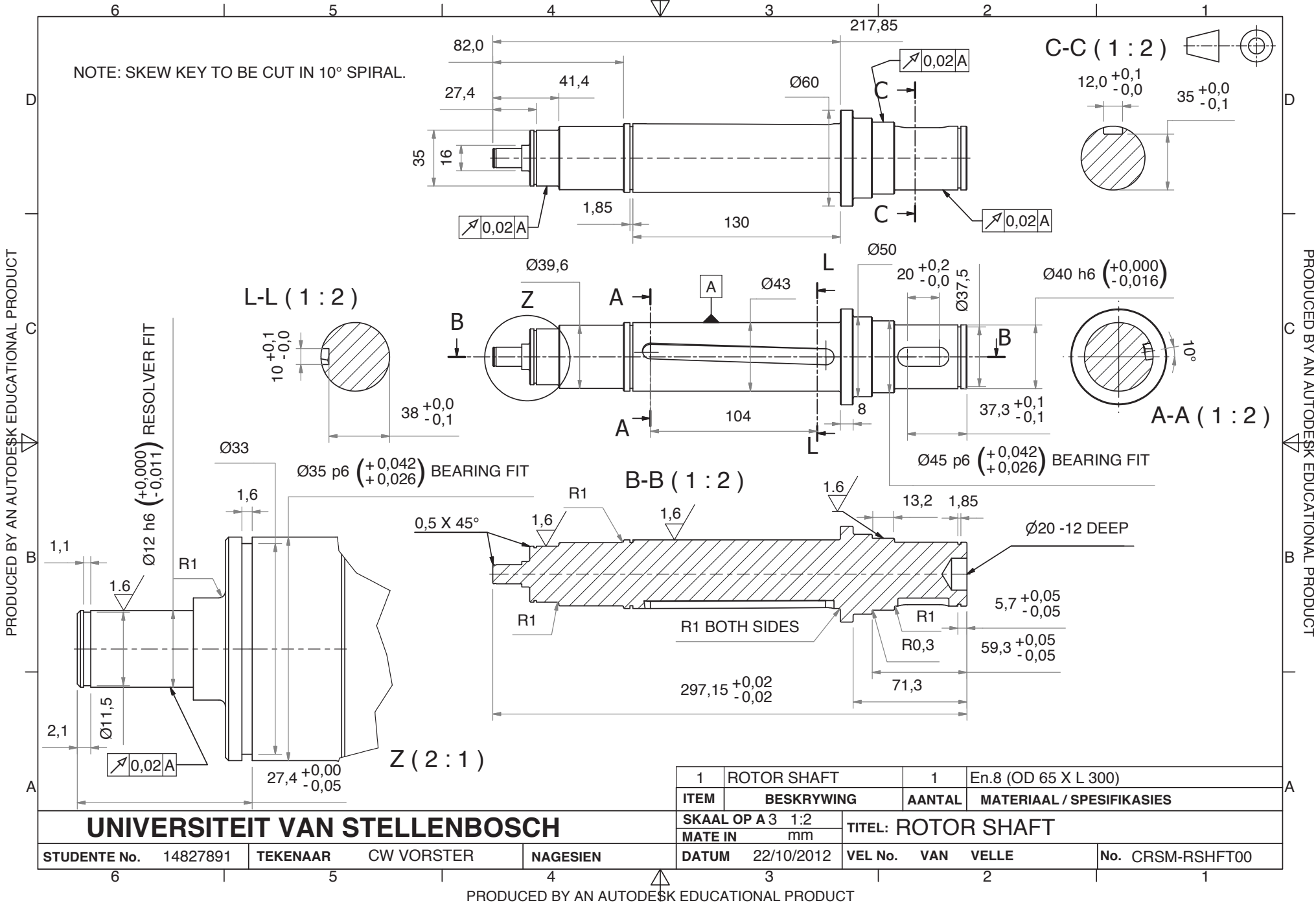


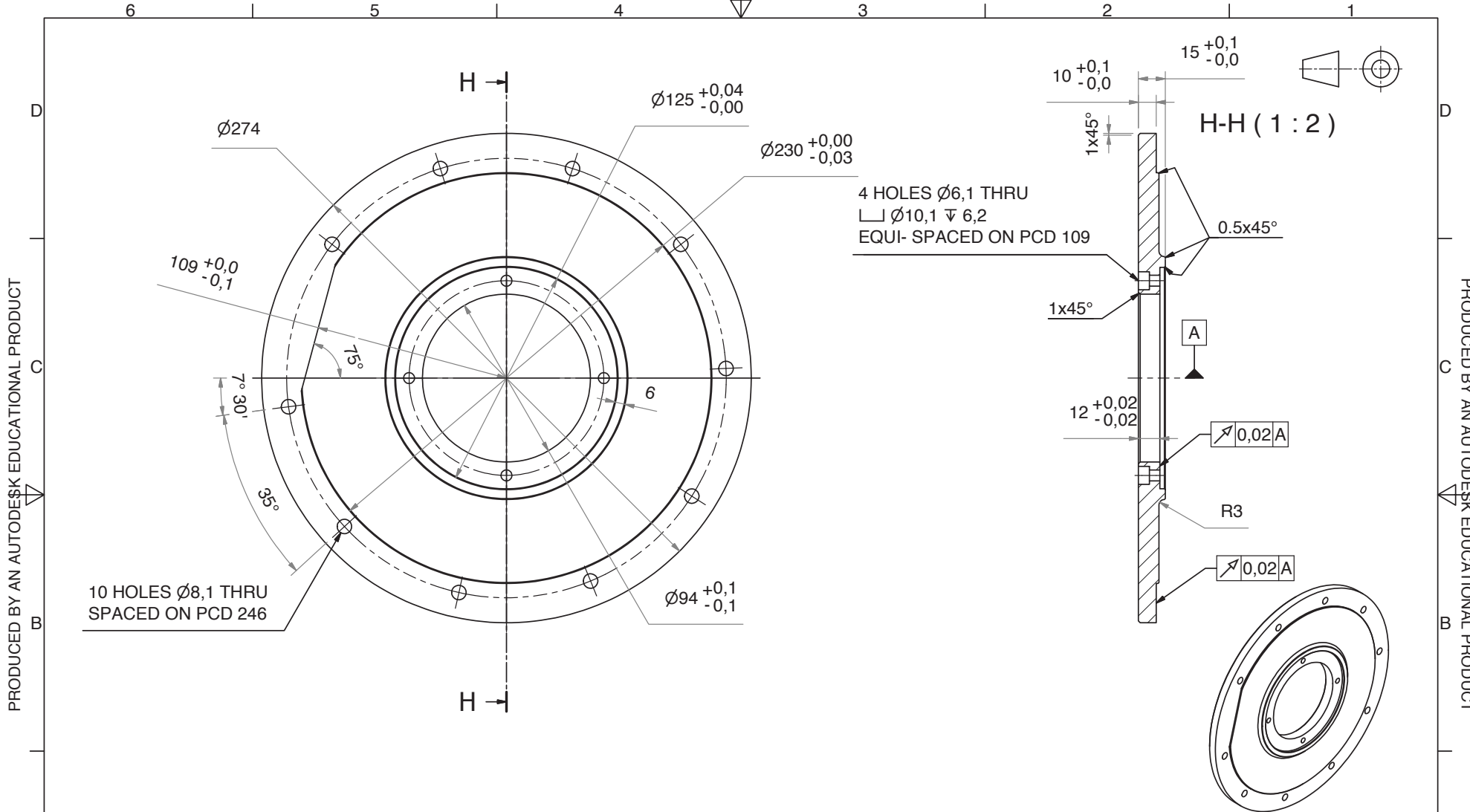


1	SHAFT FLYWHEEL COUPLING	1	AL 6082 T6 (OD 105 X L 45)
ITEM	BESKRYWING	AANTAL	MATERIAAL / SPESIFIKASIES
SKAAL OP A 3 1:1		TITEL: SHAFT FLYWHEEL COUPLING	
MATE IN mm			
DATUM	22/10/2012	VEL No.	VAN VELLE
			No. CRSM-SFC00

**UNIVERSITEIT VAN STELLENBOSCH**

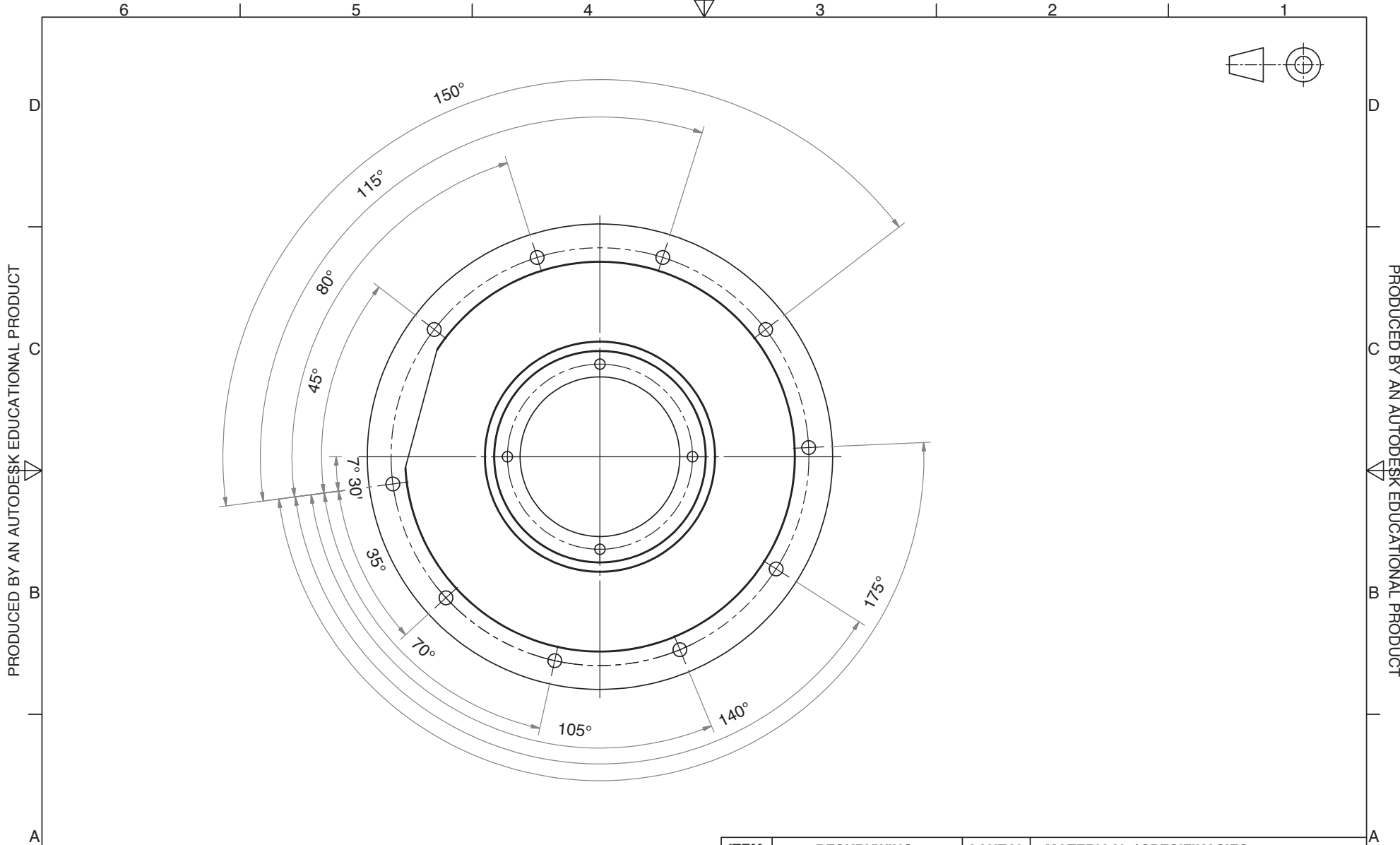
STUDENTE No. 14827891    TEKENAAR CW VORSTER    NAGESIEN





1	NON- DRIVE END COVER	1	AL 6082 T6 (OD275 X L16)
ITEM	BESKRYWING	AANTAL	MATERIAAL / SPESIFIKASIES

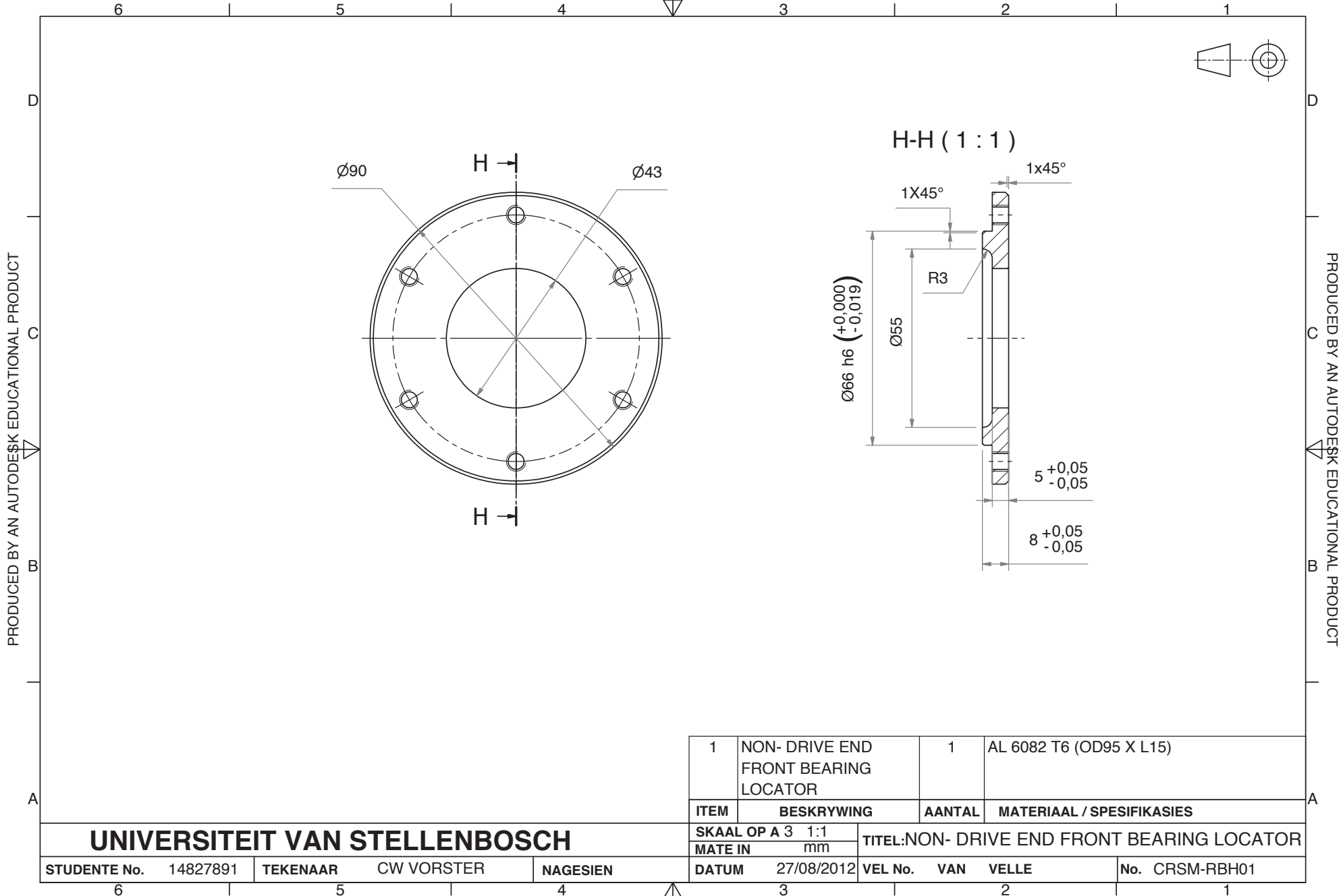
<b>UNIVERSITEIT VAN STELLENBOSCH</b>				SKAAL OP A 3 1:2		TITEL: NON- DRIVE END COVER	
				MATE IN mm			
STUDENTE No. 14827891	TEKENAAR CW VORSTER	NAGESIEN	DATUM 18/10/2012		VEL No. 1 VAN 2 VELLE		No. CRSM-NDEC00



PRODUCED BY AN AUTODESK EDUCATIONAL PRODUCT

PRODUCED BY AN AUTODESK EDUCATIONAL PRODUCT

<b>UNIVERSITEIT VAN STELLENBOSCH</b>				ITEM	BESKRYWING	AANTAL	MATERIAAL / SPESIFIKASIES
				SKAAL OP A 3 1:2		TITEL: NON- DRIVE END COVER	
STUDENTE No. 14827891		TEKENAAR CW VORSTER	NAGESIEN	DATUM 18/10/2012	VEL No. 2 VAN 2 VELLE	No. CRSM-NDEC00	

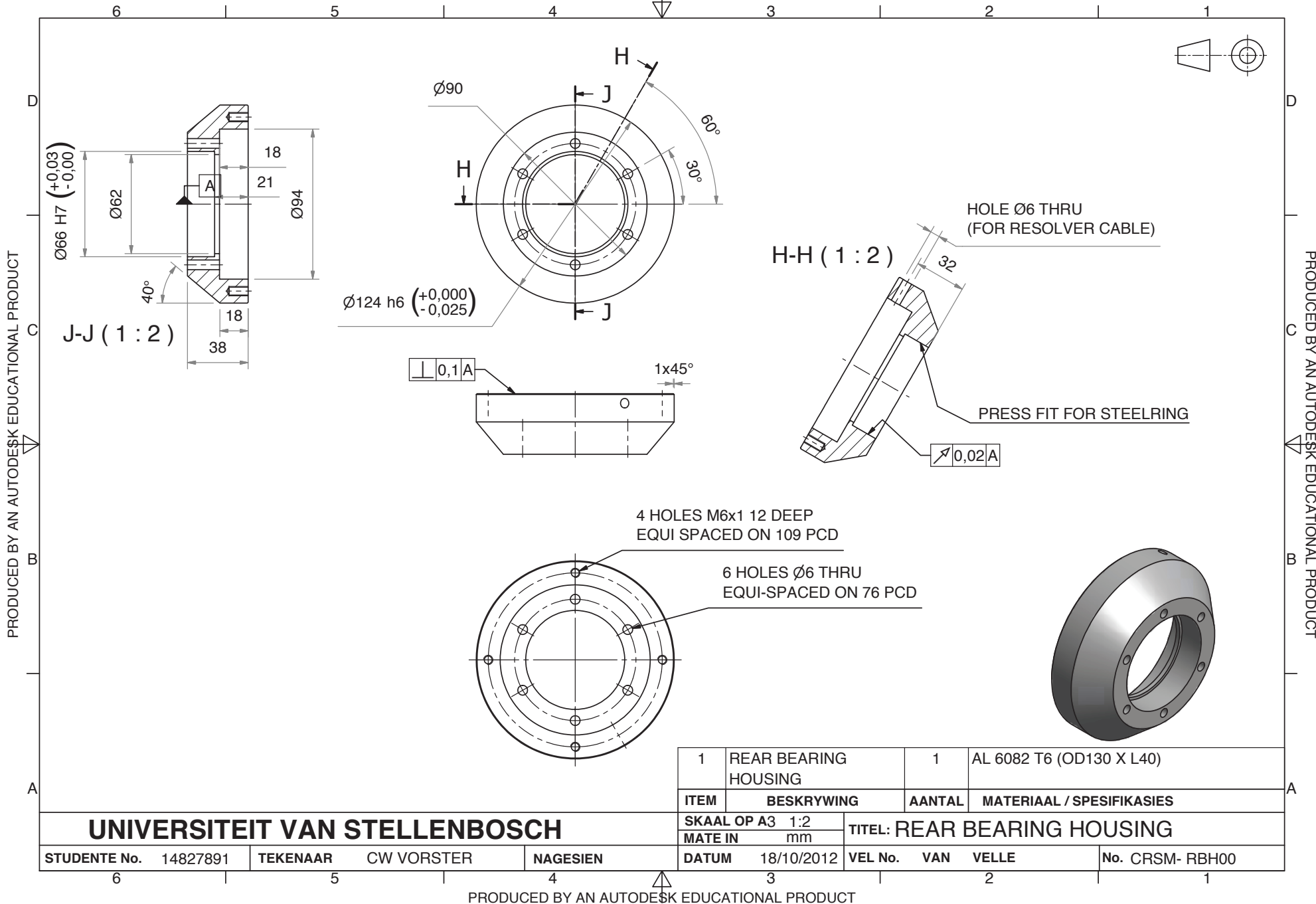


1	NON- DRIVE END FRONT BEARING LOCATOR	1	AL 6082 T6 (OD95 X L15)
ITEM	BESKRYWING	AANTAL	MATERIAAL / SPESIFIKASIES
SKAAL OP A 3 1:1		TITEL:NON- DRIVE END FRONT BEARING LOCATOR	
MATE IN mm			
STUDENTE No.	14827891	TEKENAAR	CW VORSTER
NAGESIEN		DATUM	27/08/2012
VEL No.		VAN	VELLE
No.		CRSM-RBH01	

**UNIVERSITEIT VAN STELLENBOSCH**

STUDENTE No. 14827891    TEKENAAR CW VORSTER    NAGESIEN

DATUM 27/08/2012    VEL No. VAN VELLE    No. CRSM-RBH01

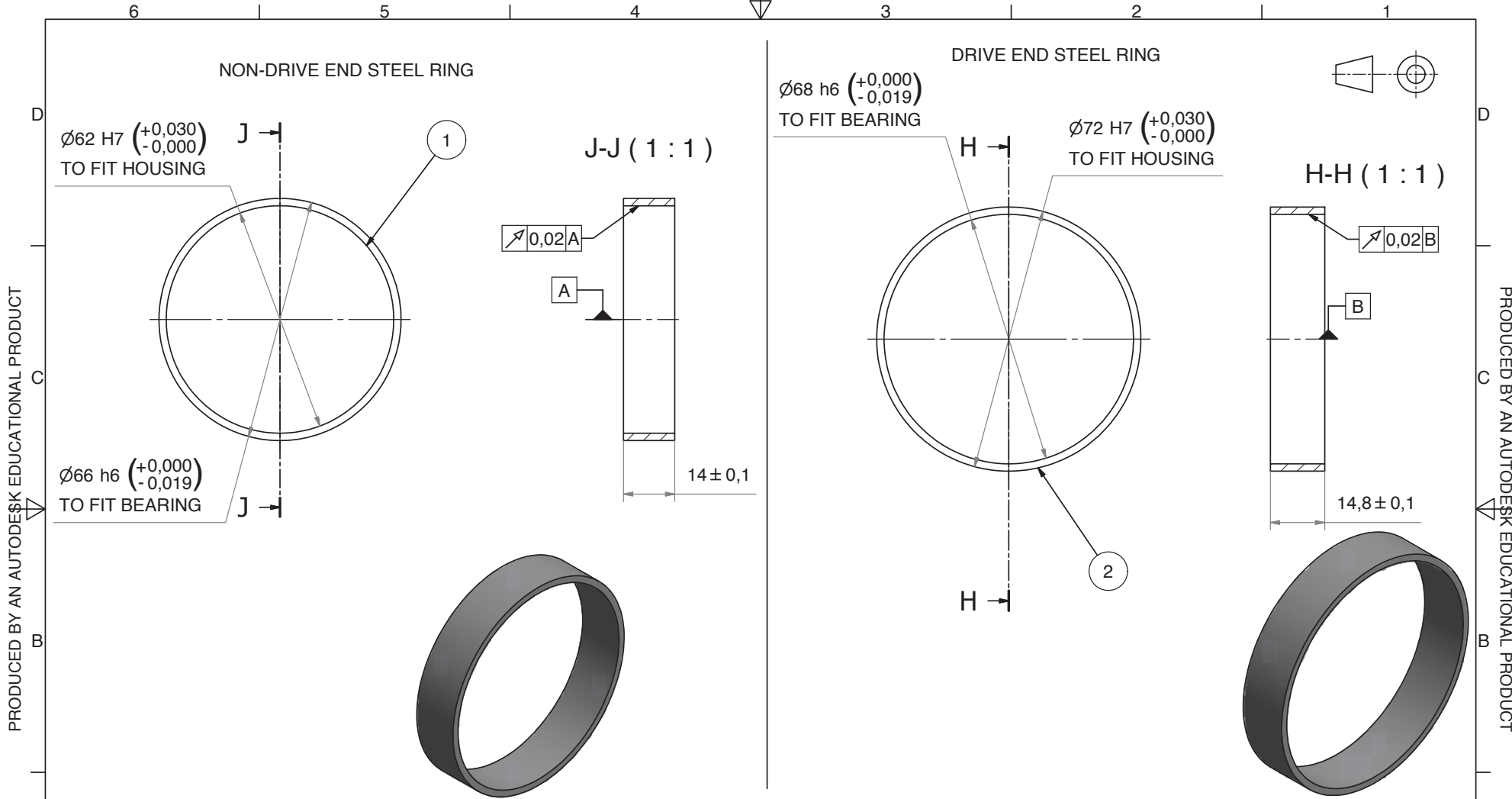


1	REAR BEARING HOUSING	1	AL 6082 T6 (OD130 X L40)
ITEM	BESKRYWING	AANTAL	MATERIAAL / SPESIFIKASIES
SKAAL OP A3 1:2		TITEL: REAR BEARING HOUSING	
MATE IN mm			
DATUM	18/10/2012	VEL No.	VAN VELLE
			No. CRSM- RBH00

**UNIVERSITEIT VAN STELLENBOSCH**

STUDENTE No. 14827891    TEKENAAR CW VORSTER    NAGESIEN

PRODUCED BY AN AUTODESK EDUCATIONAL PRODUCT



2	DRIVE END STEEL RING	1	STEEL 300WA ( OD72 X ID68 X L15)
1	NON-DRIVE END STEEL RING	1	STEEL 300WA ( OD66 X ID62 X L14)
ITEM	BESKRYWING	AANTAL	MATERIAAL / SPESIFIKASIES

**UNIVERSITEIT VAN STELLENBOSCH**

SKAAL OP A 3 1:1  
MATE IN mm

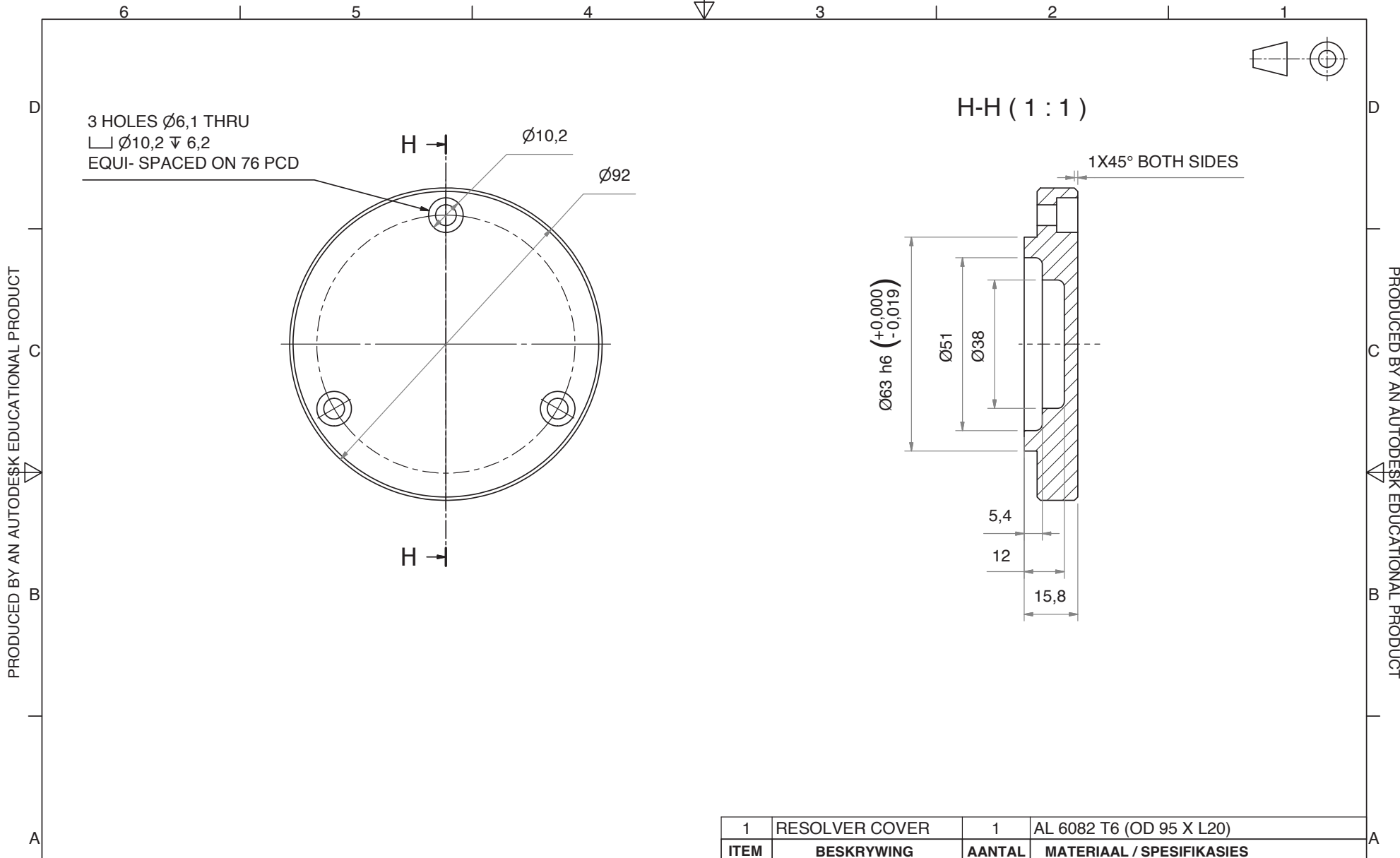
TITEL: STEEL RINGS

STUDENTE No. 14827891 | TEKENAAR CW VORSTER | NAGESIEN

DATUM 18/10/2012

VEL No. VAN VELLE

No. CRSM-SR00

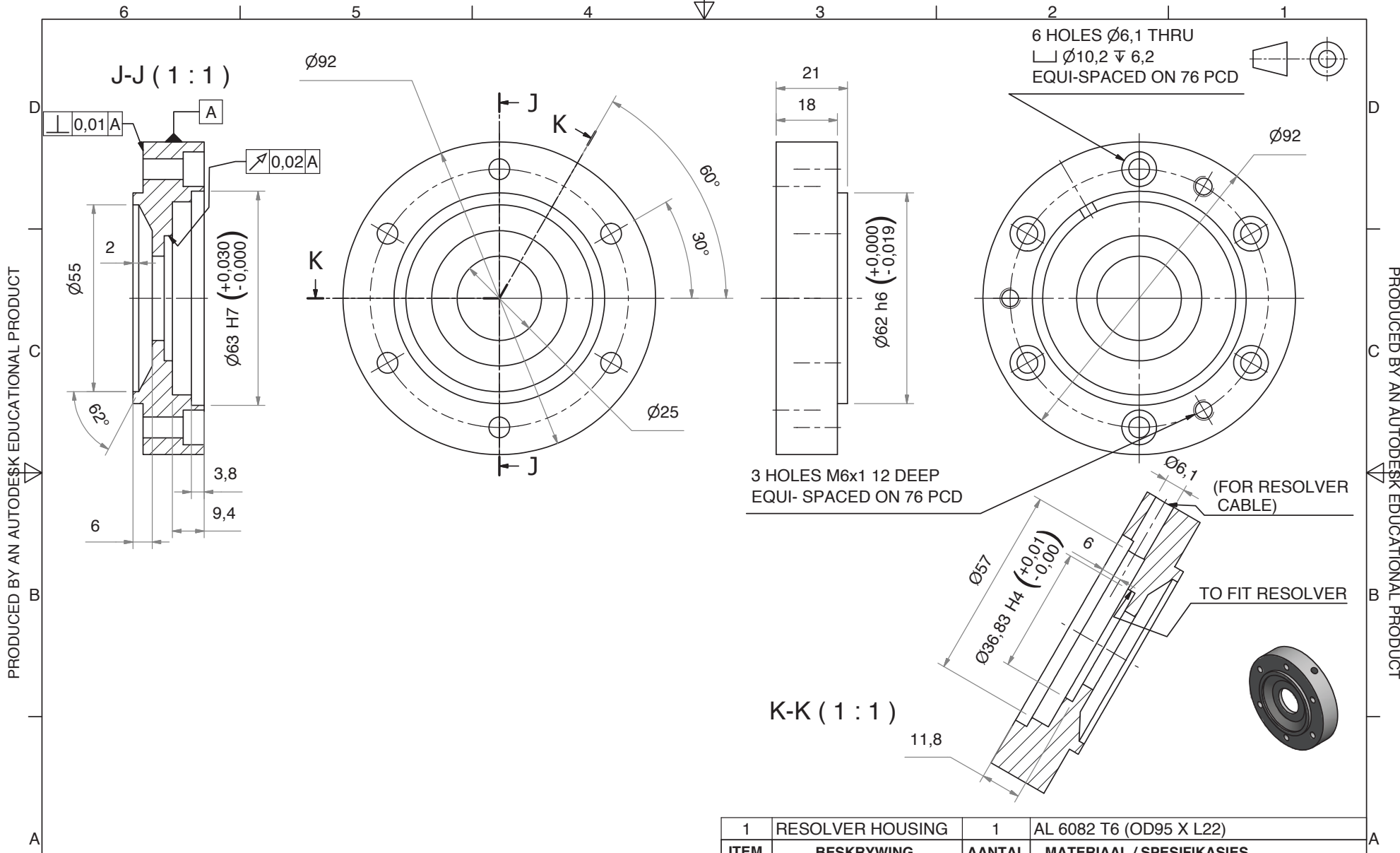


1	RESOLVER COVER	1	AL 6082 T6 (OD 95 X L20)
ITEM	BESKRYWING	AANTAL	MATERIAAL / SPESIFIKASIES
SKAAL OP A3 1:1		TITEL: MOTOR ASSEMBLY	
MATE IN mm			
DATUM	18/10/2012	VEL No.	VAN VELLE
			No. CRSM-RBC00

**UNIVERSITEIT VAN STELLENBOSCH**

STUDENTE No. 14827891    TEKENAAR CW VORSTER    NAGESIEN





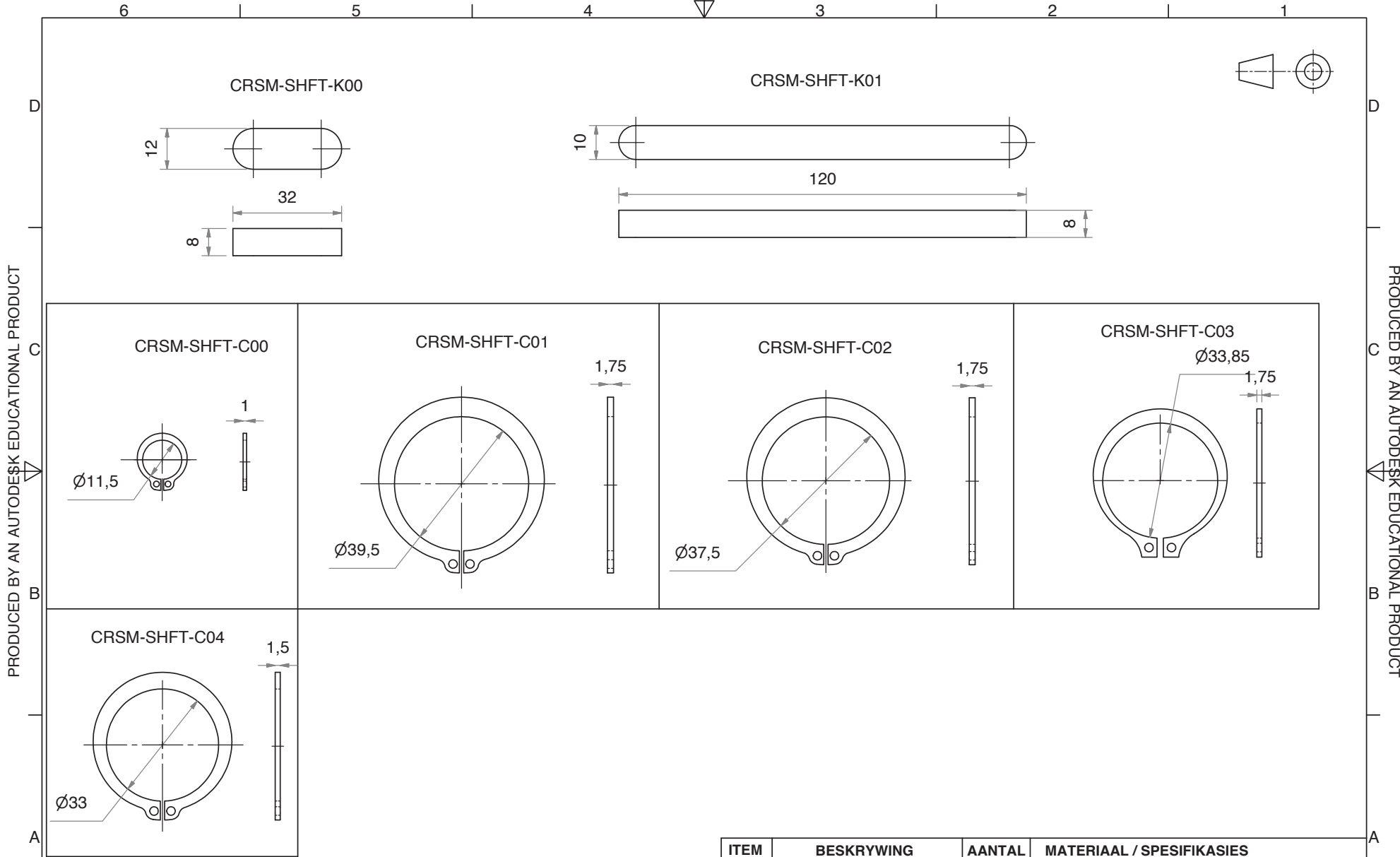
PRODUCED BY AN AUTODESK EDUCATIONAL PRODUCT

PRODUCED BY AN AUTODESK EDUCATIONAL PRODUCT

1	RESOLVER HOUSING	1	AL 6082 T6 (OD95 X L22)
ITEM	BESKRYWING	AANTAL	MATERIAAL / SPESIFIKASIES
SKAAL OP A3 1:2		TITEL: RESOLVER HOUSING	
MATE IN mm		VEL No. VAN VELLE	
DATUM	18/10/2012	No. CRSM-RH00	

**UNIVERSITEIT VAN STELLENBOSCH**

STUDENTE No. 14827891    TEKENAAR CW VORSTER    NAGESIEN



**UNIVERSITEIT VAN STELLENBOSCH**

ITEM	BESKRYWING	AANTAL	MATERIAAL / SPESIFIKASIES
SKAAL OP A 3 1:1		TITEL: SHAFT COMPONENTS	
MATE IN mm			
DATUM	25/10/2012	VEL No.	VAN VELLE
			No. CRSM-SHFT

STUDENTE No.	14827891	TEKENAAR	CW VORSTER	NAGESIEN
--------------	----------	----------	------------	----------

# Bibliography

- [1] Kamper, M.: *Design Optimization of Cageless Flux Barrier Rotor Reluctance Synchronous Machine*. Ph.D. thesis, University of Stellenbosch, December 1996.
- [2] Tesla: Motor. <http://www.teslamotors.com/blog/induction-versus-dc-brushless-motors>, 03 2014.
- [3] Tesla: Features and Specs. Available at: [http://www.teslamotors.com/en\\_GB/models/features/performance](http://www.teslamotors.com/en_GB/models/features/performance), [2014, March 18], 03 2014.
- [4] Chevrolet: 2014 Spark EV Models and Specs - Powertrain. <http://www.chevrolet.com/spark-ev-electric-vehicle/specs/powertrain.html>, 03 2014.
- [5] Nissan USA: Features and Specs. <http://www.nissanusa.com/electric-cars/leaf/versions-specs/>, 03 2014.
- [6] BMW: TECHNICAL DATA. [http://www.bmw.com/com/en/newvehicles/i/i3/2013/showroom/technical\\_data.html](http://www.bmw.com/com/en/newvehicles/i/i3/2013/showroom/technical_data.html), [Online; accessed 19-March-2014], 03 2014.
- [7] EV's, I.: TECHNICAL DATA. <http://insideevs.com/wp-content/uploads/2013/07/bmw-i3-and-REx-specs.png>, 03 2014.
- [8] Volkswagen: Electric motor. <http://www.volkswagen.co.uk/technology/electric-technology/electric-motor>, 03 2014.
- [9] Volkswagen: Engines and performance. <http://www.volkswagen.co.uk/new/e-up-nf/which-model/engines/overview>, 03 2014.
- [10] Renault: ELECTRIC MOTOR 5A. <http://www.renault.com/en/innovation/gamme-mecanique/pages/moteur-electrique-5a.aspx>, 03 2014.
- [11] Renault: Renault ZOE. [http://www.renault.co.uk/cars/electric-vehicles/zoe/zoe/prices/index.jsp?modelKey=W10&versions=VEC010\\_GRBR](http://www.renault.co.uk/cars/electric-vehicles/zoe/zoe/prices/index.jsp?modelKey=W10&versions=VEC010_GRBR), 03 2014.
- [12] Nerg, J., Rilla, M., Ruuskanen, V., Pyrhonen, J. and Ruotsalainen, S.: Direct-driven interior magnet permanent-magnet synchronous motors for a full electric sports car. *Industrial Electronics, IEEE Transactions on*, vol. 61, no. 8, pp. 4286–4294, Aug 2014. ISSN 0278-0046.

- [13] Tesla: Motor. <http://www.teslamotors.com/roadster/technology/motor>, 03 2014.
- [14] Hofman, T. and Dai, C.: Energy efficiency analysis and comparison of transmission technologies for an electric vehicle. In: *Vehicle Power and Propulsion Conference (VPPC), 2010 IEEE*, pp. 1 –6. Sept 2010.
- [15] Ren, Q., Crolla, D. and Morris, A.: Effect of transmission design on electric vehicle (ev) performance. In: *Vehicle Power and Propulsion Conference, 2009. VPPC '09. IEEE*, pp. 1260 –1265. sept 2009.
- [16] Sornioti, A., Boscolo, M., Turner, A. and Cavallino, C.: Optimization of a multi-speed electric axle as a function of the electric motor properties. In: *Vehicle Power and Propulsion Conference (VPPC), 2010 IEEE*, pp. 1 –6. Sept 2010.
- [17] Roberts, S.: Multi-Speed Transmissions for Electric Vehicle Applications. *ATZ Worldwide*, vol. 114, no. 4, pp. 8–11, 2012.
- [18] SAE: Oerlikon Graziano unveils new 4-speed transmission for EVs. <http://articles.sae.org/11499/>, 04 19-Oct-2012.
- [19] ZEROSHIFT: Zeroshift transmission for electric vehicles. <http://www.zeroshift.com/pdf/ZeroshiftElectricVehicleTransmissions.pdf>, 2012.
- [20] Straubel, J.: An Engineering Update on Powertrain 1.5. <http://www.teslamotors.com/blog/engineering-update-powertrain-15>, 27-May-2008.
- [21] eO, D.: OSCar eO becomes the first electric vehicle to finish the Dakar rally. <http://osc.lv/blog/1539-oscar-eo-first-electric-vehicle-finish-dakar-rally/>, 27-May-2008.
- [22] Groenewald, D.: *Evaluation of a Radial Flux Air-cored Permanent Magnet Machine Drive with Manual Transmission Drivetrain for Electric Vehicles*. Master's thesis, Stellenbosch University, 2010.
- [23] Malan, J., Kamper, M. and Williams, P.: Reluctance synchronous machine drive for hybrid electric vehicle. In: *Industrial Electronics, 1998. Proceedings. ISIE '98. IEEE International Symposium on*, vol. 2, pp. 367–372 vol.2. Jul 1998.
- [24] Malan, J. and Kamper, M.: Performance of a hybrid electric vehicle using reluctance synchronous machine technology. *Industry Applications, IEEE Transactions on*, vol. 37, no. 5, pp. 1319–1324, Sep 2001. ISSN 0093-9994.
- [25] IEC: IEC International Standard IEC 60034-1. <http://www.nostop.cn/1com1net/webeditor/UploadFile/200922717728626.pdf>, 2004.

- [26] BorgWarner: eGearDrive Electric Drive Transmission. <http://www.borgwarner.com/en/torqtransfer/products/Literature/BW\%20TTS\%20-\%20eGear\%2031-03.pdf>, 04 2012.
- [27] Kuchle, A., Naunheimer, H., Bertsche, B., Ryborz, J., Novak, W. and Fietkau, P.: *Automotive Transmissions: Fundamentals, Selection, Design and Application*. Springer, 2010. ISBN 9783642162145.  
Available at: <http://books.google.de/books?id=AffNYW-3yZYC>
- [28] ABB: Synchronous Reluctance Motor-Drive Packages. <http://www.abb.co.za/product/us/9AAC171953.aspx>, 2014.
- [29] REEL: REEL Synchronous reluctance motors. Efficient, compact and leading-edge. [http://www.ksb.com/REEL-en/Product\\_and\\_services/Product\\_catalogue\\_\\_\\_/Products\\_by\\_category/Synchronous\\_reluctance\\_motors/](http://www.ksb.com/REEL-en/Product_and_services/Product_catalogue___/Products_by_category/Synchronous_reluctance_motors/), 2014.
- [30] MotorBrain: Motorbrain Project. <http://www.motorbrain.eu/>, 2014.
- [31] <http://www.jmag-international.com/>, 2014.
- [32] Bomela, X. and Kamper, M.: Effect of machine design on performance of reluctance synchronous machine. In: *Industry Applications Conference, 2000. Conference Record of the 2000 IEEE*, vol. 1, pp. 515–522 vol.1. 2000. ISSN 0197-2618.
- [33] Pyrhonen, J., Jokinen, T. and Hrabovcova, V.: *Design of Rotating Electrical Machines*. Wiley, 2009. ISBN 9780470740088.  
Available at: <http://books.google.de/books?id=tFBm63puVssC>
- [34] SKF: Power loss and bearing temperature. <http://www.skf.com/group/products/bearings-units-housings/ball-bearings/principles/friction/power-loss-bearing-temperature/index.html>, 04 2014.
- [35] SKF: Estimating the frictional moment. <http://www.skf.com/group/products/bearings-units-housings/ball-bearings/principles/friction/estimating-frictional-moment/index.html>, 04 2014.
- [36] Saari, J.: *Thermal Modelling of High-Speed Induction Machines*. Ph.D. thesis, Acta Polytechnica Scandinavica, Helsinki University of Technology, 1998.
- [37] Corporation, J.: User's manual solver. Tech. Rep., October 2014.
- [38] AK Steel: AK Steel electrical steels. [http://www.aksteel.com/markets\\_products/electrical.aspx](http://www.aksteel.com/markets_products/electrical.aspx), 2014.
- [39] Autodesk: 3D CAD software for mechanical design. <http://www.autodesk.com/products/inventor/overview>, 2014.
- [40] Arora, J.: *Introduction to Optimum Design*. MATLAB examples. Academic Press, 2011. ISBN 9780123813756.  
Available at: <http://books.google.de/books?id=Qhpdh9xDsa4C>

- [41] der Plaats, V.: *Numerical optimization techniques for engineering design, V. Research and D. Incorporation*. 4th edn. Eds. Mcgraw Hill, 2005.
- [42] VisualDOC: *User Manual*. VANDERPLAATS RESEARCH AND DEVELOPMENT INC., 2011.
- [43] Jones, E., Oliphant, T., Peterson, P. *et al.*: SciPy: Open source scientific tools for Python. 2001–.  
Available at: <http://www.scipy.org/>
- [44] VisualDOC: *Theory Manual*. VANDERPLAATS RESEARCH AND DEVELOPMENT INC., 2011.
- [45] Villet, W.: *Critical Evaluation and Application of Position Sensorless Control Techniques for Reluctance Synchronous Machines*. PhD, Stellenbosch University, 2014.
- [46] James R. Phillips: ZunZun.com Online Curve Fitting and Surface Fitting Web Site. <http://zunzun.com/>, 2014.